Appendix

PLOS | PATHOGENS

RESEARCH ARTICLE

Molecular Mechanisms for Drug Hypersensitivity Induced by the Malaria Parasite's Chloroquine Resistance Transporter

Sashika N. Richards☯, Megan N. Nash☯, Eileen S. Baker, Michael W. Webster¤, Adele M. Lehane, Sarah H. Shafik, Rowena E. Martin*

Research School of Biology, Australian National University, Canberra, Australia

☯ These authors contributed equally to this work.
¤ Current address: Medical Research Council Laboratory of Molecular Biology, University of Cambridge, Cambridge CB2 0QH, UK
* rowena.martin@anu.edu.au

CrossMark
click for updates

OPEN ACCESS

Citation: Richards SN, Nash MN, Baker ES, Webster MW, Lehane AM, Shafik SH, et al. (2016) Molecular Mechanisms for Drug Hypersensitivity Induced by the Malaria Parasite's Chloroquine Resistance Transporter. PLoS Pathog 12(7): e1005725. doi:10.1371/journal.ppat.1005725

Editor: Akhil B. Vaidya, Drexel University College of Medicine, UNITED STATES

Received: February 16, 2016

Accepted: June 3, 2016

Published: July 21, 2016

Copyright: © 2016 Richards et al. This is an open access article distributed under the terms of the Creative Commons Attribution License, which permits unrestricted use, distribution, and reproduction in any medium, provided the original author and source are credited.

Data Availability Statement: All relevant data are within the paper and its Supporting Information files.

Funding: This work was supported by the Australian National Health and Medical Research Council (grant 1007035 and fellowship 1053082 to REM and fellowship 585519 to AML) and the L'Oréal Australia For Women in Science program (REM). The funders had no role in study design, data collection and analysis, decision to publish, or preparation of the manuscript.

Abstract

Mutations in the *Plasmodium falciparum* 'chloroquine resistance transporter' (PfCRT) confer resistance to chloroquine (CQ) and related antimalarials by enabling the protein to transport these drugs away from their targets within the parasite's digestive vacuole (DV). However, CQ resistance-conferring isoforms of PfCRT ($PfCRT^{CQR}$) also render the parasite hypersensitive to a subset of structurally-diverse pharmacons. Moreover, mutations in $PfCRT^{CQR}$ that suppress the parasite's hypersensitivity to these molecules simultaneously reinstate its sensitivity to CQ and related drugs. We sought to understand these phenomena by characterizing the functions of $PfCRT^{CQR}$ isoforms that cause the parasite to become hypersensitive to the antimalarial quinine or the antiviral amantadine. We achieved this by measuring the abilities of these proteins to transport CQ, quinine, and amantadine when expressed in *Xenopus* oocytes and complemented this work with assays that detect the drug transport activity of PfCRT in its native environment within the parasite. Here we describe two mechanistic explanations for PfCRT-induced drug hypersensitivity. First, we show that quinine, which normally accumulates inside the DV and therewithin exerts its antimalarial effect, binds extremely tightly to the substrate-binding site of certain isoforms of $PfCRT^{CQR}$. By doing so it likely blocks the normal physiological function of the protein, which is essential for the parasite's survival, and the drug thereby gains an additional killing effect. In the second scenario, we show that although amantadine also sequesters within the DV, the parasite's hypersensitivity to this drug arises from the $PfCRT^{CQR}$-mediated transport of amantadine from the DV into the cytosol, where it can better access its antimalarial target. In both cases, the mutations that suppress hypersensitivity also abrogate the ability of $PfCRT^{CQR}$ to transport CQ, thus explaining why rescue from hypersensitivity restores the parasite's sensitivity to this antimalarial. These insights provide a foundation for understanding clinically-relevant observations of inverse drug susceptibilities in the malaria parasite.

Competing Interests: The authors have declared that no competing interests exist.

Author Summary

In acquiring resistance to one drug, many pathogens and cancer cells become hypersensitive to other drugs. This phenomenon could be exploited to combat existing drug resistance and to delay the emergence of resistance to new drugs. However, much remains to be understood about the mechanisms that underlie drug hypersensitivity in otherwise drug-resistant microbes. Here, we describe two mechanisms by which the *Plasmodium falciparum* 'chloroquine resistance transporter' (PfCRT) causes the malaria parasite to become hypersensitive to structurally-diverse drugs. First, we show that an antimalarial drug that normally exerts its killing effect within the parasite's digestive vacuole is also able to bind extremely tightly to certain forms of PfCRT. This activity will block the natural, essential function of the protein and thereby provide the drug with an additional killing effect. The second mechanism arises when a cytosolic-acting drug that normally sequesters within the digestive vacuole is leaked back into the cytosol via PfCRT. In both cases, mutations that suppress hypersensitivity also abrogate the ability of PfCRT to transport chloroquine, thus explaining why rescue from hypersensitivity restores the parasite's sensitivity to this antimalarial. These insights provide a foundation for understanding and exploiting the hypersensitivity of chloroquine-resistant parasites to several of the current antimalarials.

Introduction

Originally identified as the protein responsible for conferring resistance to the 'wonder-drug' chloroquine (CQ) [1, 2], the *Plasmodium falciparum* 'chloroquine resistance transporter' (PfCRT) has become a key player in the malaria parasite's steadily expanding resistance to drugs [3–5]. The isoforms of PfCRT that confer CQ resistance ($PfCRT^{CQR}$) render the parasite less susceptible to many other compounds [6–10], but also simultaneously induce hypersensitivity to a subset of structurally-diverse molecules [6, 10–18]. This phenomenon, whereby resistance to one drug causes hypersensitivity to another, is known as 'inverse susceptibility' or 'collateral sensitivity' and has been observed in a wide range of pathogens and cancer cells [19–22]. The growing awareness of the propensity of drug-resistant pathogens to exhibit hypersensitivity to one or more other drugs has sparked interest in the potential for exploiting this Achilles' heel to combat existing drug resistance and to delay the emergence of resistance to new drugs [19]. However, it is not known how $PfCRT^{CQR}$ isoforms induce hypersensitivity to certain drugs and, more generally, much remains to be understood about the molecular mechanisms that underpin collateral sensitivity in pathogens and cancer cells [20–22].

The ability of PfCRT to affect the activity of so many compounds is likely to be a product of its location at the membrane of the parasite's digestive vacuole (DV) [1, 11]; an acidic compartment in which many types of antimalarials accumulate and/or act. The parasite takes up hemoglobin and digests it within this compartment in order to grow within its host erythrocyte. This process releases heme monomers that are detoxified via conversion into the inert crystal hemozoin. Quinoline-type antimalarial drugs, including CQ, quinine, and quinidine, concentrate within the DV via 'weak-base trapping' [23], where they exert an antimalarial effect by binding to heme and arresting its detoxification [24–27]. Resistance to these quinolines is associated with reductions in the accumulation of the drugs within the DV [8, 11, 28] and we have previously obtained direct evidence of this phenomenon being due, at least in part, to the ability of $PfCRT^{CQR}$ isoforms to efflux CQ, quinine, and quinidine from this compartment. This was achieved by expressing a $PfCRT^{CQR}$ isoform from Dd2 parasites ($PfCRT^{Dd2}$) and the wild-type protein (PfCRT^{3D7}) in *Xenopus laevis* oocytes. PfCRT^{Dd2} was found to possess significant CQ, quinine, and quinidine transport activity, whereas PfCRT^{3D7} did not [29–31]. These findings were consistent with a number of biochemical studies that had provided indirect evidence of drug transport via PfCRT^{CQR} isoforms. For example, PfCRT^{CQR} isoforms had been linked to the efflux of CQ and quinine from parasite-infected red blood cells [32, 33], and PfCRT^{CQR} was also implicated in the quinoline-induced efflux of protons from the DV of CQ-resistant parasites [34–36]. Moreover, the expression of PfCRT^{Dd2} at endosomal membranes within *Dictyostelium discoideum* reduced the accumulation of CQ and quinine within these vesicles, consistent with the mutant protein mediating the transport of these two drugs [37, 38]. Aside from modulating the parasite's susceptibility to diverse pharmacons, PfCRT fulfills an essential [39, 40] but currently unresolved physiological function in the parasite.

In this study, we investigated the mechanistic basis of PfCRT-induced drug hypersensitivity by characterizing the isoforms of PfCRT carried by nine different parasite lines (Table 1). These lines were generated by Cooper, Johnson, and colleagues [11, 12, 14, 15] and were produced by applying CQ, quinine, and/or amantadine pressure to either the CQ-sensitive strain 106/1 or the CQ-resistant strain K1. CQ-resistant strains, including K1, are hypersensitive to amantadine [13, 15]—a weak-base antiviral drug that is thought to accumulate in acidic organelles [41]. Like all PfCRT^{CQR} isoforms identified to date, the K1 variant of PfCRT (PfCRT^{K1}) contains a mutation at position 76, where a positively-charged lysine (K) residue is replaced by an uncharged residue (usually threonine; T) (S1 Fig). The K76T mutation is necessary (but not sufficient) to enable PfCRT to mediate the transport of protonated CQ [30, 42]. The version of PfCRT carried by 106/1 retains 76K but is otherwise identical to PfCRT^{K1}. Pressuring 106/1 parasites with CQ resulted in the CQ-resistant lines 106/1^{76T}, 106/1^{76I}, and 106/1^{76N}, which carried either PfCRT^{K1} or PfCRT^{K1} with an isoleucine (I) or an asparagine (N) at position 76 (76I-PfCRT^{K1} and 76N-PfCRT^{K1}, respectively) [11]. The latter two lines displayed unexpected drug responses: 106/1^{76I} was hypersensitive to quinine and 106/1^{76N} was sensitive to quinidine [11, 12]. The subsequent selection of 106/1^{76I} parasites with quinine resulted in the reintroduction of a positively-charged residue (C72R, Q352K, or Q352R) into 76I-PfCRT^{K1} that suppressed the parasite's hypersensitivity to quinine but also re-sensitized it to CQ [12]. This 'reciprocal collateral sensitivity' was also observed when K1 parasites or the 106/1^{76I} line were pressured with amantadine [14, 15]; the resulting parasites gained mutations in PfCRT (including S163R and V369F), were no longer hypersensitive to amantadine, but were rendered sensitive to CQ.

We compared the abilities of these PfCRT^{K1} variants to transport CQ, quinine, quinidine, and amantadine when expressed in *Xenopus* oocytes and complemented the amantadine work with assays that detected the PfCRT-mediated transport of the drug in the parasite. Our findings indicate that the hypersensitivity of the 106/1^{76I} line to quinine arises from the drug exerting two antiplasmodial effects—its normal anti-hemozoin activity as well as potent inhibition of PfCRT^{CQR}, which likely kills the parasite by blocking the normal function of the transporter. By contrast, the hypersensitivity of CQ-resistant parasites to amantadine is due to its PfCRT^{CQR}-mediated efflux from the DV into the cytosol, where it appears to gain better access to its antiplasmodial target. In both cases, the mutations that suppress hypersensitivity cause a substantial or complete reduction in the capacity of PfCRT^{CQR} for CQ transport, thus explaining why rescue from hypersensitivity reinstates the parasite's sensitivity to CQ.

Results

Expression of PfCRT^{K1} isoforms at the oocyte plasma membrane

We used a previously-described version of the PfCRT^{K1} coding sequence [42] to generate the isoforms of *pfcrt* carried by the 106/1 and K1 parasite lines (Table 1). This version of the *pfcrt*

Table 1. The origins, drug susceptibilities, and PfCRT haplotypes of different 106/1 and K1 *P. falciparum* lines.

Line or isolate[a]	Origin or drug selection	PfCRT variant	Drug susceptibility[b] (*In vitro* resistance index)			Amino acid changes in PfCRT[c]											
			CQ	QN	QD	72	74	75	76	163	220	271	326	352	369	356	371
HON	Africa	PfCRT[3D7]	1	1	1	C	M	N	K	S	A	Q	N	Q	V	I	R
Dd2	Indochina/ Laos	PfCRT[Dd2]	11.78 ± 0.18	1.82 ± 0.31	2.88 ± 0.46	C	***I***	***E***	***T***	S	***S***	***E***	***S***	Q	V	***T***	***I***
106/1	Sudan	76K-PfCRT[K1]	1.10 ± 0.06	1.08 ± 0.06	1.01 ± 0.01	C	***I***	***E***	K	S	***S***	***E***	***S***	Q	V	I	***I***
106/1[76T]	CQ	PfCRT[K1]	12.95 ± 0.95	1.69 ± 0.19	1.95 ± 0.05	C	***I***	***E***	***T***	S	***S***	***E***	***S***	Q	V	I	***I***
106/1[76N]	CQ	76N-PfCRT[K1]	8.60 ± 0.90	1.56 ± 0.16	1.08 ± 0.08	C	***I***	***E***	***N***	S	***S***	***E***	***S***	Q	V	I	***I***
106/1[76I]	CQ	76I-PfCRT[K1]	15.66 ± 2.20	0.11 ± 0.04	1.72 ± 0.13	C	***I***	***E***	***I***	S	***S***	***E***	***S***	Q	V	I	***I***
106/1[72R,76I]	CQ then QN	72R,76I-PfCRT[K1]	1.13 ± 0.07	0.76 ± 0.07	0.87 ± 0.06	***R***	***I***	***E***	***I***	S	***S***	***E***	***S***	Q	V	I	***I***
106/1[76I,352K]	CQ then QN	76I,352K-PfCRT[K1]	0.91 ± 0.09	0.93 ± 0.25	1.28 ± 0.07	C	***I***	***E***	***I***	S	***S***	***E***	***S***	***K***	V	I	***I***
106/1[76I,352R]	CQ then QN	76I,352R-PfCRT[K1]	1.58 ± 0.02	0.99 ± 0.16	0.88 ± 0.02	C	***I***	***E***	***I***	S	***S***	***E***	***S***	***R***	V	I	***I***
106/1[76I,369F]	CQ then AMT[d]	76I,369F-PfCRT[K1]	3.53	0.28	0.98	C	***I***	***E***	***I***	S	***S***	***E***	***S***	Q	***F***	I	***I***
K1AM	CQ then AMT	163R,356V-PfCRT[K1]	0.95	0.72	n.d.	C	***I***	***E***	***T***	***R***	***S***	***E***	***S***	Q	V	***V***	***I***

[a]The 106/1-derived lines were generated by Cooper and colleagues [11, 12, 14] and the K1AM line was produced by Johnson et al. [15].

[b]The susceptibilities of the parasite lines to CQ, quinine (QN), and quinidine (QD) were collated from Cooper et al. [11, 12, 14] and Johnson et al. [15]. The drug resistance index is the IC_{50} for a drug in a given strain or line divided by the IC_{50} determined in the same study in a drug-sensitive reference strain (i.e., 106/1, HON, or GC03). The indices were calculated from a single study or are the mean of values from two (± range/2) or ≥ three (± SEM) studies.

[c]Residues that differ from the wild-type amino acid sequence (e.g., the PfCRT sequence carried by 3D7, D10, and HON parasites) are shown in bold italics.

[d]CQ-resistant parasites are hypersensitive to amantadine [13, 15].

doi:10.1371/journal.ppat.1005725.t001

sequence has been codon-harmonized for expression in *Xenopus* oocytes and encodes a retention motif-free form of PfCRT that expresses in a functional form at the oocyte plasma membrane [42]. We conducted immunofluorescence assays (Fig 1A) to confirm the localization of each of the PfCRT[K1] variants to the oocyte plasma membrane and used a semiquantitative western blot analysis [42] to establish that they were present at comparable levels in the oocyte membrane (Fig 1B). Hence, any differences in drug transport activity between these isoforms of PfCRT can be attributed to differences in their transport properties rather than differences in expression.

Quinoline transport via PfCRT largely correlates with quinoline resistance

To understand the mechanisms underlying the inverse drug susceptibilities of the 106/1- and K1-derived lines, we characterized the transport properties of the respective PfCRT[K1] variants in *Xenopus* oocytes. A key advantage of the oocyte system is that it allows the transport activity of PfCRT to be studied directly and in isolation, without confounding effects such as the binding of drugs to heme or interactions of the compound with other parasite targets or transporters. The direction of [^{3}H]drug transport in this system is from the acidic extracellular medium (pH 5.0–6.0) into the oocyte cytosol (pH 7.1–7.2 [30]), which corresponds to the efflux of protonated drug from the acidic DV (pH 5.0–5.5 [43, 44]) into the parasite cytosol (pH 7.3 [45]). Noninjected oocytes take up [^{3}H]CQ, [^{3}H]quinine, and [^{3}H]quinidine to low levels via simple diffusion of the neutral species of the drug (Fig 2A–2C); this represents the background level of [^{3}H]drug accumulation [29, 30]. We found that none of the PfCRT[K1] isoforms carried by CQ-sensitive exhibited CQ transport activity when expressed in oocytes (Fig 2A). By contrast, the

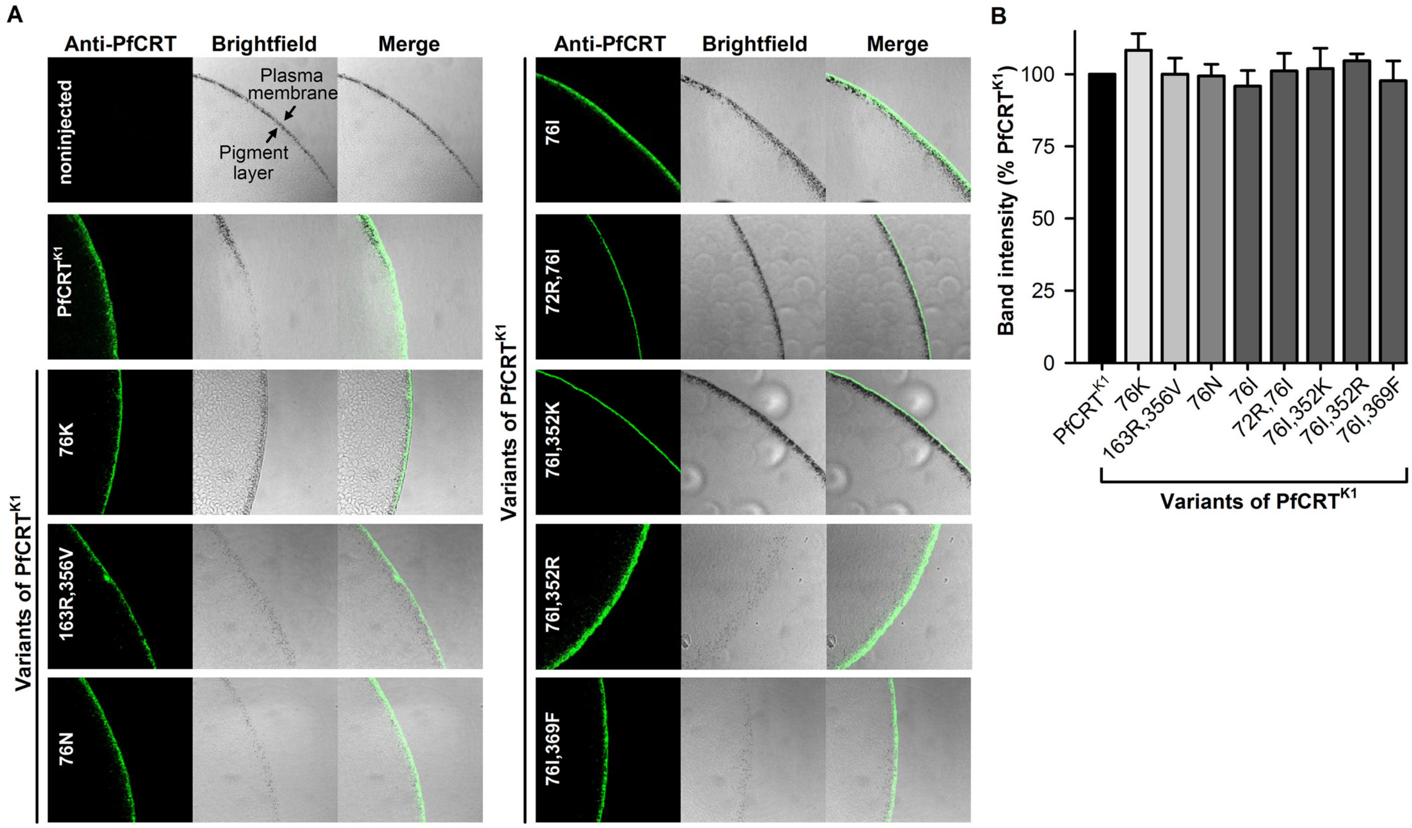

Fig 1. Isoforms of PfCRT^{K1} localize to the surface of *Xenopus* oocytes. (A) Immunofluorescence microscopy was used to localize PfCRT in the oocyte. In each case, the expression of the PfCRT variant resulted in a fluorescent band external to the pigment layer, indicating that the protein was expressed in the oocyte plasma membrane. The band was not present in noninjected oocytes. The images are representative of at least two independent experiments (performed using oocytes from different frogs), within which images were obtained from a minimum of three oocytes per oocyte type. (B) The level of PfCRT protein in the oocyte membrane was semiquantified using a western blot method [42]. The analysis included PfCRT^{K1} as a positive control, to which the other band intensity values were normalized. The data are the mean + SEM of at least five independent experiments (performed using oocytes from different frogs), within which measurements were averaged from two independent replicates. There were no significant differences in expression levels between constructs ($P > 0.05$; one-way ANOVA); hence, all of the PfCRT variants were present at similar levels in the oocyte membrane.

doi:10.1371/journal.ppat.1005725.g001

expression of PfCRT^{K1} variants from CQ-resistant parasites caused significant increases in the accumulation of CQ. Indeed, we observed a positive correlation between the ability of a PfCRT^{K1} variant to transport CQ and the magnitude of *in vitro* CQ resistance exhibited by the respective parasite line (R^2 value of 0.856; S2A Fig). We conclude that the mutations which suppress the quinine-hypersensitivity of the 106/1^{76I} line (C72R, Q352K, or Q352R) simultaneously re-sensitize the parasite to CQ by abrogating the protein's capacity to efflux CQ from the DV. Likewise, a mutation that suppresses the hypersensitivity of 106/1^{76I} parasites to amantadine (V369F), also caused a marked reduction in the ability of 76I-PfCRT^{K1} to transport CQ, which explains why the 106/1^{76I,369F} line displayed a relatively low level of resistance to CQ.

Similar results were obtained when we examined the uptake of [^{3}H]quinine and [^{3}H]quinidine (Fig 2B and 2C and S2 Fig). That is, the capacities of the different PfCRT^{K1} isoforms to transport quinine or quinidine generally correlated with the *in vitro* responses of the parasite lines to these drugs. Key exceptions included the quinine hypersensitivities of the 106/1^{76I} and 106/1^{76I,369F} lines, which were not readily reconciled with the low quinine transport activity of 76I-PfCRT^{K1} and the lack of quinine transport via 76I,369F-PfCRT^{K1}, respectively. The modest capacity of 76I-PfCRT^{K1} for quinine transport was nonetheless abolished by the

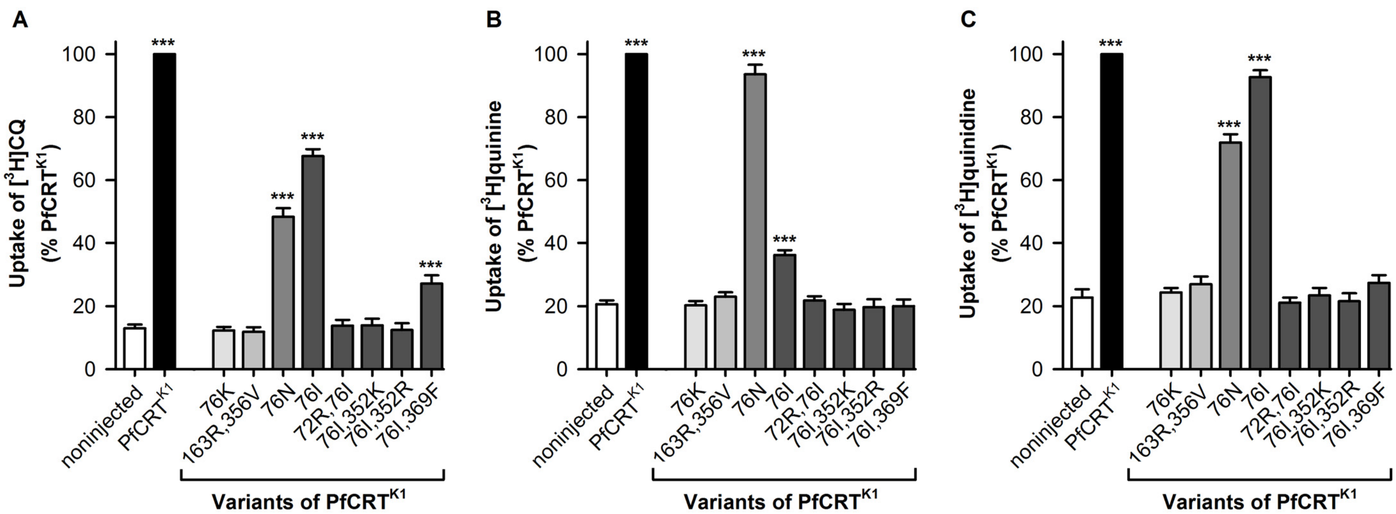

Fig 2. CQ, quinine, and quinidine transport activities differ significantly between isoforms of PfCRT^{K1}. Noninjected oocytes accumulate low levels of CQ, quinine, and quinidine via simple diffusion of the neutral species of the drug [29, 30]. This represents the background level of drug accumulation. In all cases, the concentration of the [^{3}H]drug under study was 0.25 μM. (A) The uptake of [^{3}H]CQ was measured at pH 6.0 and in the presence of 15 μM unlabeled CQ. The rates of CQ uptake (pmol per oocyte/h) in noninjected oocytes and oocytes expressing PfCRT^{K1} were 0.98 ± 0.13 and 6.75 ± 0.94, respectively. (B, C) The uptake of [^{3}H]quinine or [^{3}H]quinidine was measured at pH 5.0 and in the presence of 1 μM of the respective unlabeled drug. The rates of uptake (pmol per oocyte/h) in noninjected oocytes and oocytes expressing PfCRT^{K1} were 0.10 ± 0.01 and 0.55 ± 0.03, respectively, for quinine and 0.063 ± 0.010 and 0.38 ± 0.08, respectively, for quinidine. Note that the relatively low total concentration of quinine and quinidine (1.25 μM) used in these assays enabled the detection of [^{3}H]quinine transport via the 76I-PfCRT^{K1} isoform. However, this low drug concentration also resulted in rates of quinine and quinidine transport that were 10–15 times lower than those measured for CQ (a difference which corresponds well with the ~12-fold reduction in the total concentration of quinine or quinidine relative to the total concentration of CQ). In all panels, drug uptake is expressed relative to that measured in oocytes expressing PfCRT^{K1} and the data are the mean + SEM of at least five independent experiments (performed using oocytes from different frogs), within which measurements were made from 10 oocytes per treatment. The asterisks denote a significant difference in drug uptake between the noninjected treatment and that measured in oocytes expressing a variant of PfCRT: *P < 0.05; **P < 0.01; ***P < 0.001 (one-way ANOVA).

doi:10.1371/journal.ppat.1005725.g002

introduction of C72R, Q352K, or Q352R. Another exception was the moderate ability of 76N-PfCRT^{K1} to transport quinidine, which was at odds with the sensitivity of 106/1^{76N} parasites to this drug.

Together, these findings revealed a strong relationship between the magnitude of CQ, quinine, or quinidine resistance exhibited by a given 106/1 or K1 parasite and the capacity of its PfCRT protein for mediating the efflux of the respective drug from the DV. However, the mechanism underpinning the quinine-hypersensitivity caused by the introduction of T76I into PfCRT^{K1}, and why the subsequent addition of C72R, Q352K, or Q352R negates this response, remained unclear.

High-affinity binding of quinine to 76I-PfCRT^{K1} causes hypersensitivity to quinine

We undertook experiments to determine whether the kinetics of 76I-PfCRT^{K1}- and 76N-PfCRT^{K1}-mediated transport could explain why these proteins cause unexpected responses to quinine and quinidine, respectively. All of the PfCRT^{K1} isoforms we had identified as possessing significant CQ, quinine, or quinidine transport activity (Fig 2A–2C) were included for study. The resulting Michaelis-Menten plots (S3 Fig) yielded a Michaelis–Menten constant (K_m) and maximum velocity (V_{max}) for each drug and PfCRT isoform (Table 2). Across all three drugs, the K_m values increased in the order 76I-PfCRT^{K1} < PfCRT^{K1} < 76N-PfCRT^{K1}, whereas the V_{max} values increased in the order 76I-PfCRT^{K1} < 76N-PfCRT^{K1} ≤ PfCRT^{K1}. Thus, we conclude that T76I increases the affinity of PfCRT^{K1} for its quinoline substrates, but

Table 2. Kinetic parameters for the transport of CQ, quinine, and quinidine via variants of $PfCRT^{K1}$.

PfCRT variant	Apparent K_m (μM)[a,b]			Apparent V_{max} (pmol per oocyte/h)		
	CQ	Quinine	Quinidine	CQ	Quinine	Quinidine
$PfCRT^{K1}$	282 ± 5 *(9)*	28.8 ± 2.7 *(7)*	84 ± 1 *(6)*	72 ± 3 *(9)*	10.3 ± 0.8 *(7)*	24.4 ± 1.6 *(7)*
$76N\text{-}PfCRT^{K1}$	303 ± 5[e,f] *(7)*	41.0 ± 2.6[f] *(6)*	94 ± 4[c,f] *(6)*	48.0 ± 4.5[c,f] *(7)*	13.0 ± 1.0[d,f] *(6)*	14.1 ± 0.9[e,g] *(6)*
$76I\text{-}PfCRT^{K1}$	247 ± 7[c,f] *(5)*	0.42 ± 0.04[c,f] *(4)*	24.1 ± 3.0[f] *(6)*	29.3 ± 7.2[c,f] *(5)*	0.09 ± 0.01[c,f] *(4)*	7.2 ± 0.5[e,g] *(6)*
$76I,369F\text{-}PfCRT^{K1}$	415 ± 25[c] *(5)*	n.d.	n.d.	13.8 ± 1.3[c] *(5)*	n.d.	n.d.

[a]PfCRT-mediated transport was calculated by subtracting the uptake of drug measured in the control oocytes (oocytes expressing $76K\text{-}PfCRT^{K1}$) from that in oocytes expressing $PfCRT^{K1}$, $76N\text{-}PfCRT^{K1}$, $76I\text{-}PfCRT^{K1}$, or $76I,369F\text{-}PfCRT^{K1}$. The data are shown in S3 Fig.

[b]All values are the mean ± SEM of multiple independent experiments (performed using oocytes from different frogs), within which measurements were made from 10 oocytes per treatment. The exact *n* values are indicated in parentheses.

The *P* values determined from an ANOVA were less than [c]0.001, [d]0.01, or [e]0.05 for comparisons with $PfCRT^{K1}$ within the same drug treatment and kinetic parameter.

The *P* values determined from an ANOVA were less than [f]0.001 or [g]0.01 for comparisons between $76N\text{-}PfCRT^{K1}$ and $76I\text{-}PfCRT^{K1}$ within the same drug treatment and kinetic parameter.

doi:10.1371/journal.ppat.1005725.t002

that this change is accompanied by a significant decrease in its maximum rate of transport. By contrast, T76N consistently decreased the affinity of $PfCRT^{K1}$ for its quinoline substrates, and either had little effect on the V_{max} (quinine) or caused a marked reduction in the V_{max} (CQ and quinidine). Interestingly, the introduction of V369F into $76I\text{-}PfCRT^{K1}$ significantly reduced the protein's affinity for CQ (from 247 to 415 μM) and further reduced its maximum rate for CQ transport (from 29.3 to 13.8 pmol per oocyte/h), while also abrogating its ability to transport quinine and quinidine (Fig 2B and 2C). Our finding that 76I,369F $PfCRT^{K1}$ is a very low-affinity and low-capacity transporter of CQ is again consistent with the modest level of CQ resistance exhibited by the $106/1^{76I,369F}$ parasite line.

Remarkably, we found that $76I\text{-}PfCRT^{K1}$ possesses an extraordinarily high affinity for quinine and an extraordinarily low V_{max} for quinine transport; its K_m was ~70 times lower, and its V_{max} ~115 times lower, than the value obtained for $PfCRT^{K1}$. This combination of kinetic properties indicates that $76I\text{-}PfCRT^{K1}$ binds extremely tightly to quinine and only occasionally translocates the drug. Thus, quinine will clog the binding site of $76I\text{-}PfCRT^{K1}$, which should greatly diminish the ability of the protein to transport its natural substrate. These findings suggest that quinine-hypersensitivity results from quinine exerting two killing effects in $106/1^{76I}$ parasites—the inhibition of hemozoin formation and the inhibition of PfCRT's normal physiological role (which is essential for parasite survival [39, 40]). The low level of quinine transport mediated by $76I\text{-}PfCRT^{K1}$ was not detected following the introduction of C72R, Q352K, Q352R, or V369F (Fig 2B). Of these mutations, Q352R and Q352K each fully return $106/1^{76I}$ parasites to quinine-sensitive status, C72R causes a substantial but incomplete rescue from quinine-hypersensitivity, and V369F confers a modest but significant suppression of the parasite's hypersensitivity to quinine (Table 1). Taken together, our data indicate that the insertion of a positively-charged residue into the substrate-binding cavity of $76I\text{-}PfCRT^{K1}$ greatly diminishes or abolishes its interaction with quinine (and its ability to transport CQ and quinidine), thereby reversing the parasite's hypersensitivity to quinine (and simultaneously re-sensitizing it to CQ and quinidine). Our finding that these effects are achieved to a much lesser degree by V369F, which instead introduces a bulky hydrophobic residue into $76I\text{-}PfCRT^{K1}$, indicates that electrostatic repulsion is the key mechanism underpinning the dramatic decrease in the protein's ability to bind and translocate protonated quinolines.

Our kinetic analyses also revealed that 76N-PfCRT^{K1} is unique in being both a low-affinity and a low-capacity transporter of quinidine. By comparison, PfCRT^{K1} mediated the low-affinity but high-capacity transport of quinidine, and 76I-PfCRT^{K1} was a high-affinity, low-capacity transporter of quinidine. Thus, the sensitivity of 106/1^{76N} parasites to quinidine is likely due to the inability of 76N-PfCRT^{K1} to decrease the concentration of quinidine within the DV to sub-toxic levels.

I356T increases quinine transport via 76I-PfCRT^{K1}

We recently reported [42] that the CQ transport activity of PfCRT^{K1} is ~20% higher than that of PfCRT^{Dd2}, even though the two proteins differ only at position 356 (Table 1). However, the I356T mutation also demonstrated epistasis. That is, depending on the nature and number of the mutations already present, its introduction increased, decreased, or had no effect on the ability of PfCRT to transport CQ [42]. We therefore investigated whether the introduction of I356T decreases the ability of PfCRT^{K1} variants to transport quinine and quinidine. We measured the uptake of [^{3}H]quinine or [^{3}H]quinidine in oocytes expressing either a PfCRT^{K1} variant (PfCRT^{K1}, 76N-PfCRT^{K1}, or 76I-PfCRT^{K1}) or its I356T counterpart (PfCRT^{Dd2}, 76N-PfCRT^{Dd2}, or 76I-PfCRT^{Dd2}). Consistent with our previous observation with CQ transport, we found that the rate of quinine and quinidine uptake mediated by PfCRT^{K1} was 17–35% greater than that measured for PfCRT^{Dd2} (S4 Fig). Moreover, we observed the same relationship, only considerably more exaggerated, between the 76N variants of PfCRT^{K1} and PfCRT^{Dd2} and, in the case of quinidine transport, between 76I-PfCRT^{K1} and 76I-PfCRT^{Dd2}. The single exception to this pattern was quinine transport via 76I-PfCRT^{K1}, which showed a 30–40% decrease relative to its PfCRT^{Dd2} counterpart. Our findings establish a key role for position 356 in the attainment of a high level of quinoline transport activity, but also confirm the epistatic nature of this position.

Isoforms of PfCRT from amantadine-hypersensitive parasites transport amantadine

We next sought to understand why CQ-resistant parasites are hypersensitive to amantadine and how certain mutations in PfCRT (e.g., T76K, S163R, or V369F) countercheck this response. Given that we had already ascertained that the PfCRT^{K1} variants carrying T76K or S163R do not possess significant quinoline transport activity (Fig 2A–2C), we focused our initial investigations on 76I,369F-PfCRT^{K1}, as it mediates a detectable level of CQ transport. To test the possibility that hypersensitivity to amantadine is due to it clogging the substrate-binding cavity of PfCRT, and that this effect is alleviated by the addition of V369F, we compared the ability of unlabeled amantadine to inhibit the transport of [^{3}H]CQ via 76I-PfCRT^{K1} and 76I,369F-PfCRT^{K1} (Fig 3A). Somewhat surprisingly, there was little difference in the resulting half-maximum inhibitory concentrations (IC_{50}s; listed in Fig 3A). Moreover, these IC_{50}s were much higher than those obtained in the oocyte system for established inhibitors of PfCRT^{CQR}, such as the quinine dimer Q_2C (1.4 ± 0.2 μM [46]), saquinavir (13 ± 1 μM [47]), and verapamil (30 ± 3 μM [30]). Since amantadine is a relatively low-affinity inhibitor of both 76I-PfCRT^{K1} and 76I,369F-PfCRT^{K1}, it is unlikely that the hypersensitivity of CQ-resistant parasites to amantadine is due to it exerting an anti-PfCRT^{CQR} effect.

This result led us to examine whether amantadine hypersensitivity is instead a consequence of significant changes in the ability of PfCRT to transport amantadine. We found that oocytes expressing PfCRT^{K1} or 76I-PfCRT^{K1} showed a marked increase in [^{3}H]amantadine accumulation relative to noninjected oocytes (Fig 3B and 3C). By contrast, oocytes expressing 76K-PfCRT^{K1} or 163R,356V-PfCRT^{K1} failed to take up [^{3}H]amantadine above the background level

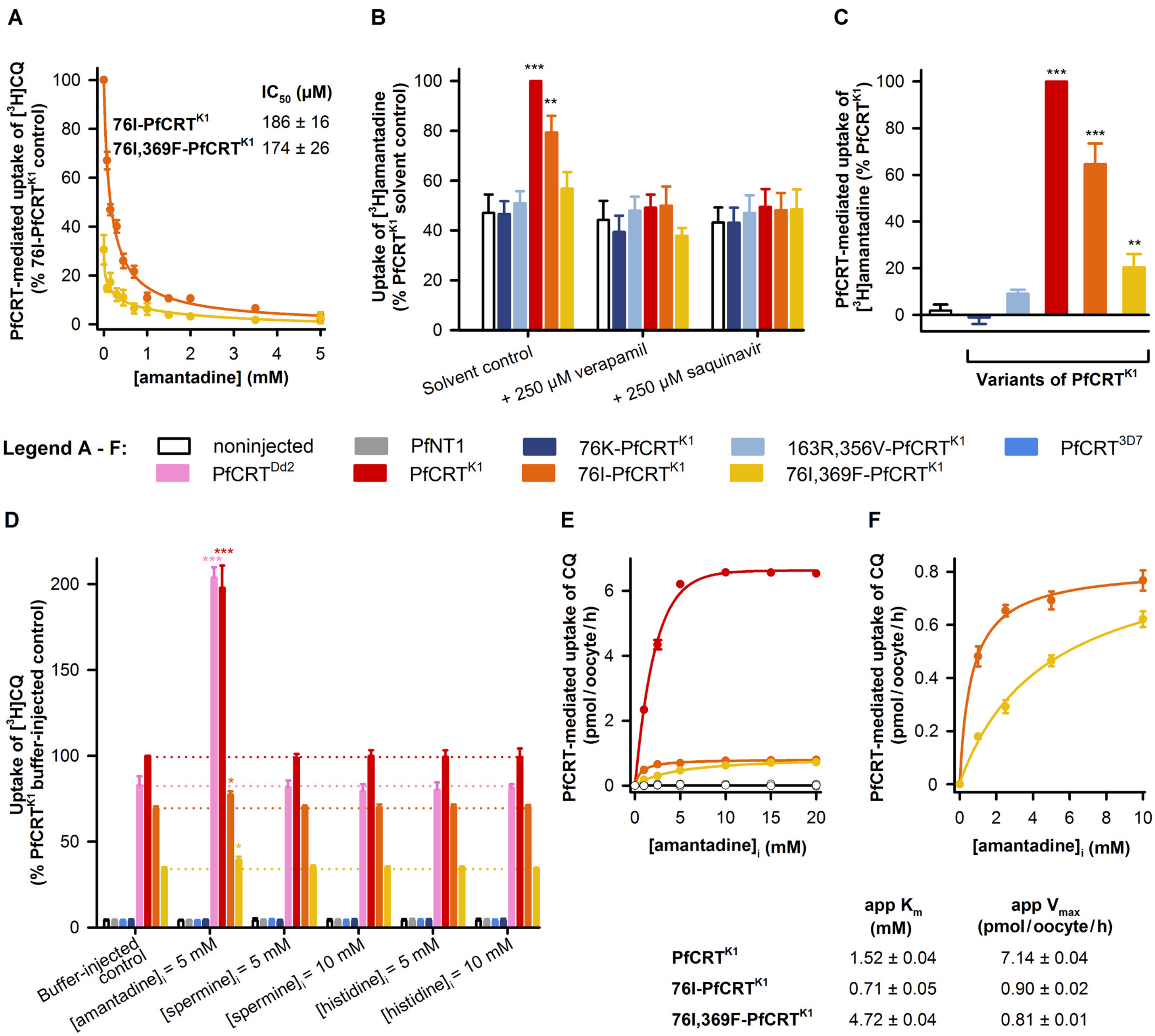

Fig 3. Isoforms of PfCRT^{K1} from amantadine-hypersensitive parasites transport amantadine. (A) Amantadine inhibits the transport of [^{3}H]CQ via 76I-PfCRT^{K1} and 76I,369F-PfCRT^{K1} in a concentration-dependent manner (IC$_{50}$s of 186 ± 16 and 174 ± 26 μM, respectively). (B) The uptake of [^{3}H]amantadine (0.146 μM) in the absence and presence of verapamil or saquinavir. The measurements were undertaken at pH 5.0 and in the presence of 50 μM unlabeled amantadine. (C) The PfCRT-mediated transport of [^{3}H]amantadine. Using the data shown for the solvent control in panel B, the component of [^{3}H]amantadine transport attributable to PfCRT was calculated by subtracting the background level of accumulation (i.e., the average of the uptake measured in noninjected oocytes and oocytes expressing 76K-PfCRT^{K1}) from that measured for each of the oocyte types. The rates of amantadine uptake (nmol per oocyte/h) in noninjected oocytes and PfCRT^{K1}-expressing oocytes were 5.4 ± 0.9 and 12 ± 2.8, respectively. The asterisks denote a significant difference from the noninjected control: **P* < 0.05; ***P* < 0.01; ****P* < 0.001 (one-way ANOVA). (D) *Trans*-stimulation of PfCRT-mediated [^{3}H]CQ transport by unlabeled amantadine. The oocytes were microinjected with a buffer control or with buffer containing amantadine, spermine, or histidine. The estimated intracellular concentrations ([compound]$_i$) are indicated. The asterisks denote a significant difference from the relevant buffer-injected control. (E) Concentration-dependence of the *trans*-stimulation of [^{3}H]CQ uptake by amantadine. The oocytes were microinjected with buffer containing amantadine to achieve an estimated [amantadine]$_i$ of 1 to 20 mM. The app K$_m$ and app V$_{max}$ values are the apparent kinetic parameters for the *trans*-stimulatory effect of amantadine. The data show CQ uptake above that measured in the relevant buffer-injected control; the total rates of CQ uptake are presented in S6 Fig. The noninjected data overlays the data obtained with oocytes expressing PfNT1, PfCRT^{3D7}, or 76K-PfCRT^{K1}. (F) A magnified plot of the 76I-PfCRT^{K1} and 76I,369F-PfCRT^{K1} data from panel E. In all panels, the data are the mean ± SEM of five independent experiments (performed using oocytes from different frogs), within which measurements were made from 10 oocytes per treatment. Where not shown, error bars fall within the symbols.

doi:10.1371/journal.ppat.1005725.g003

of accumulation, and 76I,369F-PfCRT^{K1} displayed only a very low (but statistically significant) level of amantadine transport activity. Moreover, [^{3}H]amantadine transport via PfCRT^{K1}, 76I-PfCRT^{K1}, and 76I,369F-PfCRT^{K1} was inhibited by the PfCRT^{CQR} inhibitors verapamil and saquinavir. These findings suggest that hypersensitivity to amantadine arises from the ability of PfCRT^{CQR} isoforms to transport amantadine, and that mutations such as T76K, S163R, and V369F reverse this response by substantially decreasing or abolishing amantadine transport activity.

The signal-to-background ratio we obtained for [^{3}H]amantadine transport in the oocyte system was around 2 (Fig 3B), which is relatively modest when compared with that obtained for quinine and quinidine transport (which typically produce ratios of 4–7; e.g., Fig 2B and 2C and S4 Fig) or CQ transport (which typically produces a ratio of 8–25; e.g., Figs 2A and 3D and S5 Fig). We therefore interrogated the amantadine transport properties of PfCRT further by conducting a series of *trans*-stimulation experiments. Many transporters reorientate more quickly from one face of the membrane to the other when a substrate is bound compared with when the transporter is empty. Transporters that display this characteristic can be *trans*-stimulated; in the case of PfCRT^{CQR}, the uptake of [3H]CQ from the external solution will be accelerated by the presence of an unlabeled substrate on the cytosolic face of the membrane. We therefore measured the uptake of [^{3}H]CQ into oocytes which had been microinjected with a buffer control or with buffer containing unlabeled amantadine, spermine, or histidine. Spermine (a polycation) and histidine (a weak base) do not appear to interact with PfCRT^{Dd2} (S5 Fig and Martin et al. [30]) and were therefore included as extra negative controls. In addition, oocytes expressing an unrelated *P. falciparum* transporter (the nucleoside transporter PfNT1 [48]) were included as a further negative control. We found that amantadine did not affect the accumulation of [^{3}H]CQ in noninjected oocytes or oocytes expressing 76K-PfCRT^{K1}, PfCRT^{3D7}, or PfNT1 (Fig 3D). Moreover, neither spermine nor histidine altered [^{3}H]CQ uptake in any of the oocyte types. By contrast, amantadine *trans*-stimulated the transport of [^{3}H]CQ into oocytes expressing PfCRT^{K1}, PfCRT^{Dd2}, 76I-PfCRT^{K1}, or 76I,369F-PfCRT^{K1}, albeit to different extents; the respective increases in the rate of CQ influx (in pmol per oocyte/h) were 6.4 ± 0.2, 6.7 ± 0.3, 0.68 ± 0.04, and 0.43 ± 0.02. We extended this analysis by measuring the concentration-dependence of the *trans*-stimulation of PfCRT^{K1}, 76I-PfCRT^{K1}, and 76I,369F-PfCRT^{K1} (Fig 3E and 3F and S6 Fig). A least-squares fit of the Michaelis-Menten equation to the data yielded apparent kinetic parameters for the *trans*-stimulatory effect of amantadine (listed in Fig 3). These results revealed that the addition of V369F to 76I-PfCRT^{K1} causes a 6.2- to 7.2-fold increase in the concentration of amantadine required for the half-maximal *trans*-stimulation of the transporter.

Taken together, our work shows that PfCRT variants from parasites that are hypersensitive to amantadine possess the ability to transport this drug, and that the introduction of mutations that suppress amantadine hypersensitivity either abolish (T76K and S163R) or substantially decrease (V369F) the protein's capacity for amantadine transport. These findings led us to propose that amantadine, which should sequester within the DV via weak-base trapping, exerts its main antiplasmodial effect outside of the DV and that the PfCRT-mediated leak of the drug back into the cytosol results in amantadine hypersensitivity. We therefore utilized a set of parasite assays to test this hypothesis *in situ*.

PfCRT effluxes amantadine from the DV of amantadine-hypersensitive parasites

The function of PfCRT can be investigated in its native environment by employing an assay that indirectly detects the movement of protonated drugs out of the DV [34–36]. This method uses a fluorescent pH-sensitive probe to measure an outward leak of protons, which manifests as an increase in the rate of alkalinization of the DV. A drug-induced proton leak arises when a weak-base drug enters the acidic DV in its unprotonated form and is effluxed in its protonated form. We applied this assay to a set of *P. falciparum* transfectants (the C2^{GC03}, C4^{Dd2}, and C6^{7G8} lines [2]) that are isogenic except for their *pfcrt* allele, which encodes either PfCRT^{3D7} (C2^{GC03}) or a PfCRT^{CQR} isoform of the protein (PfCRT^{Dd2} in C4^{Dd2} and PfCRT^{7G8} in C6^{7G8}). CQ was included as a positive control and consistent with previous observations [34–36, 46], it increased the rate of DV alkalinization in the CQ-resistant C4^{Dd2} and C6^{7G8} lines and was without effect in the CQ-sensitive C2^{GC03} line (Fig 4). We obtained similar results with amantadine and also showed that verapamil inhibits the amantadine-associated leak of protons from the DV of C4^{Dd2} and C6^{7G8} parasites. These findings confirm that amantadine accumulates within the DV

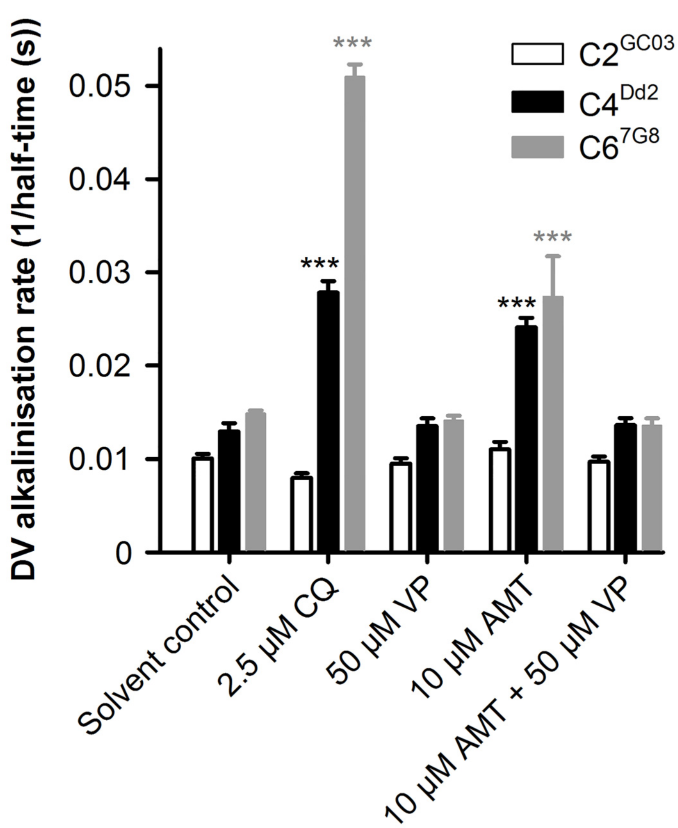

Fig 4. Amantadine is a substrate of PfCRT^{Dd2} and PfCRT^{7G8}, and not of wild-type PfCRT, *in situ*. The rate of concanamycin A-induced DV alkalization (expressed as the inverse of the half-time for DV alkalization) in the C2^{GC03} (CQ-sensitive, expressing PfCRT^{3D7}), C4^{Dd2} (CQ-resistant, expressing PfCRT^{Dd2}), and C6^{7G8} (CQ-resistant, expressing PfCRT^{7G8}) transfectant lines was measured in the absence and presence of amantadine (AMT), CQ, or verapamil (VP). The effect of amantadine on the DV alkalization rate was also measured in the presence of verapamil (final concentration of 50 µM). The drugs were added to suspensions of saponin-isolated trophozoite-stage parasites containing fluorescein-dextran in their DVs 4 min before the addition of concanamycin A (100 nM). CQ was added at a concentration of 2.5 µM and the concentration of amantadine was 10 µM. Consistent with previous studies, the addition of CQ elevated the rate of alkalinization in both of the CQ-resistant lines and had a small buffering effect in the C2^{GC03} parasites [34–36, 46]. The biological basis for the difference in the rate of CQ-dependent alkalinization between the two CQ-resistant lines is currently unclear, but could be due to differences in (1) the expression of PfCRT, (2) the transport properties of the two PfCRT isoforms, (3) the volume of the DV, and/or (4) the concentration of PfCRT's natural substrates within the DV. The data are the mean + SEM of five independent experiments (performed on different days). The asterisks denote a significant difference from the relevant solvent control: ***$P < 0.001$ (one-way ANOVA).

doi:10.1371/journal.ppat.1005725.g004

Table 3. ***In vitro*** **antiplasmodial activities of CQ and amantadine against CQ-sensitive and CQ-resistant *P. falciparum* parasites.**

Strain/line[b]	IC_{50}[a]					
	CQ (nM)[c]			Amantadine (μM)[c]		
	Control	+ 1 μM VP	+ 1 μM CP	Control	+ 1 μM VP	+ 1 μM CP
3D7	25 ± 1.1	24 ± 0.9	22 ± 0.7	344 ± 8.9	352 ± 9.1	351 ± 11
Dd2	151 ± 4.8[d]	25 ± 1.0[g]	11 ± 0.04[g]	11 ± 0.1[d]	55 ± 0.6[f]	64 ± 0.9[g]
$C2^{GC03}$	27 ± 1.6	26 ± 1.3	22 ± 3.1	335 ± 9.5	341 ± 11	348 ± 13
$C4^{Dd2}$	149 ± 4.6[d]	26 ± 0.09[g]	18 ± 0.01[g]	8.4 ± 0.06[d]	57 ± 0.6[g]	66 ± 1.0[g]
$C6^{7G8}$	87 ± 2.1[d]	25 ± 0.2[g]	20 ± 0.06[g]	43 ± 2.9[d]	78 ± 4.3[e]	88 ± 5.4[f]

[a]The IC_{50} values are the mean ± SEM of five independent experiments (performed on different days), within which measurements were averaged from 3 replicates.

[b]Field-derived strains: 3D7 (CQ-sensitive; Africa); Dd2 (CQ-resistant; Indochina/Laos). Isogenic *pfcrt* transfectant lines: $C2^{GCO3}$ (CQ-sensitive); $C4^{Dd2}$ (CQ-resistant); $C6^{7G8}$ (CQ-resistant).

[c]Measurements were made in the absence and presence of verapamil (VP) or chlorpheniramine (CP).

[d]The *P* values determined from a one-way ANOVA were less than 0.001 for comparisons with the relevant CQ-sensitive strain or line (and within either the CQ or amantadine treatment).

The *P* values determined from a one-way ANOVA were less than [e]0.001, [f]0.01, or [g]0.05 for comparisons between the control treatment and the relevant VP or CP treatment from the same strain or line.

doi:10.1371/journal.ppat.1005725.t003

via weak-base trapping and also provide *in situ* evidence of the ability of $PfCRT^{CQR}$ isoforms to transport amantadine back into the cytosol.

If amantadine hypersensitivity results from the PfCRT-mediated efflux of the drug from the DV, we would expect that inhibitors of $PfCRT^{CQR}$ would reduce this response. We tested this hypothesis by determining the susceptibility of the isogenic lines to amantadine in the absence and presence of verapamil or chlorpheniramine [49] (another established inhibitor of $PfCRT^{CQR}$). These experiments, which included CQ as a control as well as CQ-resistant (Dd2) and CQ-sensitive (3D7) reference strains, entailed using a fluorescence-based method to measure parasite growth in the presence of increasing concentrations of amantadine or CQ. The resulting IC_{50}s (Table 3) provided two salient findings. First, the data verified the striking hypersensitivity of CQ-resistant parasites to amantadine. Secondly, in all cases this hypersensitivity was partially suppressed by the PfCRT inhibitors. Thus, we conclude that the hypersensitivity of the $106/1^{76I}$ line, and of other CQ-resistant parasites, to amantadine arises from the $PfCRT^{CQR}$-mediated redistribution of the drug from the DV into the cytosol, where it gains better access to its main antiplasmodial target.

Discussion

Our work provides mechanistic explanations for the patterns of inverse susceptibility induced by PfCRT. First, we confirmed our previous observation [42] of there being a positive correlation between the capacity of a given PfCRT isoform for mediating CQ transport and the magnitude of CQ resistance achieved by the respective parasite (S7A Fig) and extended this relationship to include, with the notable exception of the QN-hypersensitive lines, a positive correlation between the quinine or quinidine transport activity of PfCRT and the parasite's *in vitro* responses to these drugs (Fig 5A and S7B Fig). Moreover, we showed that in most cases, the isoforms of $PfCRT^{K1}$ that possessed CQ transport activity also transported quinine and quinidine and *vice versa*. Together, these findings confirm a common role for PfCRT in reducing the accumulation of CQ, quinine, and quinidine within the DV and explain the tendency of CQ-resistant parasites to exhibit decreased susceptibilities to quinine and quinidine. However,

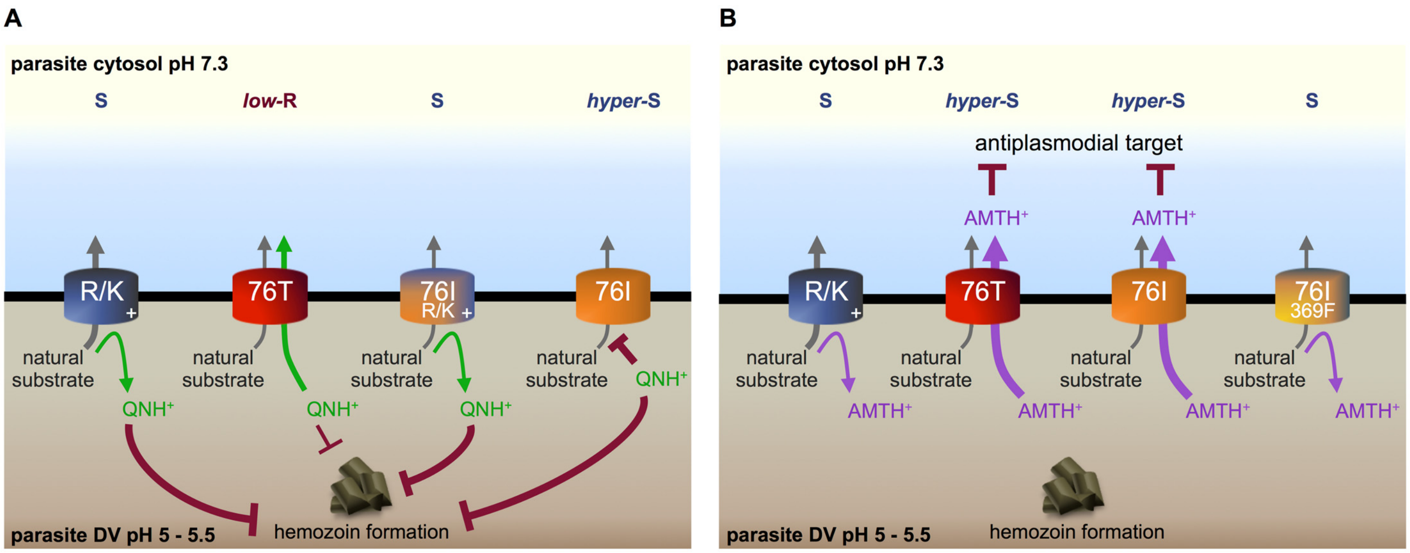

Fig 5. Molecular mechanisms for the drug hypersensitivities induced by PfCRT isoforms in the malaria parasite. (A) The variants of PfCRT^{K1} that contain 72R, 76K, 163R, 352K, or 352R (R/K) do not possess significant quinine (QN) transport activity. The drug would therefore remain in the parasite's DV where it exerts an anti-hemozoin effect that kills the parasite, which is consistent with the QN-sensitive (S) status of the respective lines. PfCRT^{K1} (76T) is able to transport QN out of the DV and thereby imparts low-level resistance (*low*-R) to QN. By contrast, 76I-PfCRT^{K1} has an extremely high affinity for QN coupled with an extremely low maximum rate of transport. This causes QN to clog the binding site of 76I-PfCRT^{K1}, thereby blocking the transport of the natural substrate. Hence, the QN-hypersensitivity (*hyper*-S) observed in 106/1^{76I} parasites results from QN exerting two killing effects—anti-hemozoin and anti-PfCRT^{CQR}. The gain of a positively-charged residue at position 72 or 352 (76I R/K) prevents the interaction of the transporter with QN and returns the parasites to QN-sensitive status. (B) Amantadine (AMT) is a relatively poor inhibitor of both 76I-PfCRT^{K1} and 76I,369F-PfCRT^{K1}, making it unlikely that the AMT-hypersensitivity of CQ-resistant parasites is due to an anti-PfCRT^{CQR} effect. The isoforms of PfCRT from AMT-hypersensitive parasites (PfCRT^{K1} and 76I-PfCRT^{K1}) have the ability to transport this weak-base drug out of the DV (where it accumulates) whereas those from AMT-sensitive parasites either do not possess significant AMT transport activity (e.g., 76K-PfCRT^{K1} and 163R,356V-PfCRT^{K1}; R/K) or transport AMT with low affinity and low capacity (76I,369F-PfCRT^{K1}). The data therefore converge on a scenario in which AMT exerts its main antimalarial activity in the cytosol and AMT-hypersensitivity arises from the redistribution of the drug from the DV into the cytosol via a PfCRT^{CQR} variant (e.g., PfCRT^{K1} or 76I-PfCRT^{K1}).

doi:10.1371/journal.ppat.1005725.g005

our results resolve this phenomenon further by providing a fundamental insight into PfCRT-induced drug phenotypes: whether a given isoform of PfCRT alters the parasite's susceptibility to a drug, and to what extent and in which direction, depends on the kinetics of the drug's transport via PfCRT.

A key example of this principle is the quinine-hypersensitivity conferred by 76I-PfCRT^{K1}. Our work reveals that the introduction of 76I into PfCRT^{K1} has the remarkable effect of transforming the protein into an exceedingly high-affinity, low-capacity transporter of quinine. These highly abnormal kinetic properties will cause the drug to clog PfCRT's substrate-binding cavity, which should block the transport of the natural substrate and thereby prevent the protein from fulfilling its essential physiological role (Fig 5A). Thus, we propose that hypersensitivity to quinine results from the drug exerting at least two killing effects in 106/1^{76I} parasites—anti-hemozoin and anti-PfCRT^{CQR}. This hypothesis provides mechanistic explanations for two previously abstruse observations: (1) despite dramatic differences in their quinine responses, 106/1^{76I} and 106/1 parasites accumulate similar levels of quinine [11] and (2) quinine and CQ produce a synergistic interaction in 106/1^{76I} parasites, whereas a slightly antagonistic interaction occurs in the 106/1^{76T} line [12]. In the case of the first observation, the lack of a difference in quinine accumulation concurs with the exceedingly low capacity of 76I-PfCRT^{K1} for transporting quinine. In regard to the second phenomenon, the synergistic interaction in 106/1^{76I} is readily reconcilable with the ability of quinine to adhere to the binding cavity of 76I-PfCRT^{K1}, as this should both inhibit the normal function of the protein and block the efflux of CQ from the DV. The slightly antagonistic effect observed in the $106/1^{76T}$ parasites is likely to result from the two drugs competing to bind to heme (CQ is the more potent inhibitor of hemozoin formation [25, 27]) and/or other differences in their activities (e.g., CQ also appears to inhibit the glutathione-dependent degradation of heme, whereas quinine is thought to lack this activity [50]).

Cooper and colleagues reported a third perplexing characteristic of the $106/1^{76I}$ line that may likewise arise from quinine's ability to block the normal function of 76I-$PfCRT^{K1}$. The presence of verapamil typically re-sensitizes CQ-resistant parasites to CQ (and to quinine and quinidine) and this resistance-reversing effect was evident for all three drugs in the $106/1^{76T}$ and $106/1^{76N}$ lines [11, 12]. It was also apparent in the $106/1^{76I}$ parasites, but only in the CQ and quinidine treatments. In the quinine treatment, verapamil exerted the opposite effect; i.e., it *decreased* the sensitivity of the $106/1^{76I}$ line to quinine and thus partially suppressed the parasite's hypersensitivity to this drug [11, 12]. One possible explanation for this highly unusual observation is a scenario in which verapamil competes with quinine for binding to 76I-$PfCRT^{K1}$, and that the natural substrate is better able to access the translocation pore when verapamil is bound relative to when quinine is bound. Given that the substrate-binding site of $PfCRT^{Dd2}$ has been shown to behave as a large polyspecific cavity that can bind at least two molecules simultaneously [29], it is conceivable that verapamil and quinine interact with the binding cavity differently and that verapamil presents somewhat less of an obstacle to the transport of the natural substrate via 76I-$PfCRT^{K1}$ than does quinine. Such a scenario would provide a mechanistic explanation for the verapamil-induced reduction in quinine's activity against the $106/1^{76I}$ line.

We recently reported that CQ-resistant parasites are hypersensitive to dimers of quinine, and that this appears to be due to these molecules inhibiting both heme detoxification and $PfCRT^{CQR}$ function (the quinine dimers are potent inhibitors of $PfCRT^{Dd2}$ but are not translocated by the transporter) [46]. Hence, the anti-$PfCRT^{CQR}$ activity of quinine in the $106/1^{76I}$ parasites is not simply an intriguing but extraneous biological oddity; it signifies that one of the parasite's key modulators of drug resistance is itself a druggable antimalarial target.

Our findings suggest that less dramatic changes in the kinetics of transport via PfCRT can also significantly affect the parasite's response to a drug. 76N-$PfCRT^{K1}$ decreases the parasite's susceptibility to CQ and quinine while being without effect on its response to quinidine [11, 12, 14]. A simple interpretation of these observations would be that 76N-$PfCRT^{K1}$ transports CQ and quinine but fails to recognize quinidine. However, we found that 76N-$PfCRT^{K1}$ maintains the ability to transport quinidine, but that its affinity for the drug is slightly reduced, and that its maximum rate of quinidine transport is significantly reduced, relative to the kinetics of quinidine transport via $PfCRT^{K1}$. The low-capacity, low-affinity nature of quinidine transport via 76N-$PfCRT^{K1}$ will limit the protein's ability to reduce the accumulation of the drug within the DV and hence could explain why 76N-$PfCRT^{K1}$ has little net effect on the parasite's susceptibility to quinidine (S7B Fig).

The hypersensitivity of CQ-resistant parasites to amantadine was first reported several decades ago [13], but the molecular basis for this phenomenon has remained unknown. We demonstrate that amantadine hypersensitivity cannot be explained by an anti-$PfCRT^{CQR}$ effect and is instead attributable to a second mechanism. Our work shows that amantadine sequesters within the acidic environment of the DV and that the hypersensitivity of CQ-resistant parasites to amantadine results from the ability of $PfCRT^{CQR}$ isoforms to efflux the drug from the DV into the parasite cytosol (Fig 5B). These findings indicate that amantadine acts on a target outside of the DV and that it exerts its antiplasmodial activity to greater effect when proteins such as $PfCRT^{Dd2}$, $PfCRT^{7G8}$, $PfCRT^{K1}$, and 76I-$PfCRT^{K1}$ leak the accumulated drug back into the cytosol. The antiviral target of amantadine is a proton channel [51] and it is possible that the drug likewise targets an essential cation channel or transporter in the parasite.

All of the mutations that introduced a positively-charged residue into $PfCRT^{K1}$ abolished its ability to transport CQ, quinine, quinidine, and amantadine. Hence, in addition to confirming the importance of electrostatic repulsion in preventing interactions between PfCRT and protonated drugs, our results suggest that the transporter's ability to transport protonated quinolines out of the DV (and thereby confer quinoline resistance) is fundamentally connected to its ability to transport protonated amantadine out of the DV (and thereby induce amantadine hypersensitivity). Furthermore, the detection in field isolates of T76K, C72R, or S163R in otherwise $PfCRT^{CQR}$ isoforms [5] indicates that these types of changes could be occurring in the parasite population in response to selection forces exerted by other drugs and/or because, in the absence of CQ, these parasites are fitter than their CQ-resistant counterparts (most $PfCRT^{CQR}$ isoforms impart a fitness cost [52–55]). Such a phenomenon appears to have taken place in French Guiana; Pelleau and colleagues [56] recently showed that another mutation that introduces a positive charge into $PfCRT^{CQR}$ (C350R) emerged in a CQ-resistant population following the withdrawal of CQ and is attributed with reinstating these parasites to CQ-sensitive status.

Our findings also provide a foundation for understanding and exploiting clinically-relevant cases of reciprocal collateral sensitivity. Most of the current treatments for uncomplicated malaria are combination therapies that pair an artemisinin derivative (all of which are metabolised into dihydroartemisinin) with a quinoline-related partner drug—of which the most widely used is lumefantrine [57]. Cases of severe malaria, as well as *Plasmodium*-infected pregnant women, are typically treated with combinations that include an antibiotic, such as clindamycin. It is, therefore, worth noting that several *in vitro* studies have observed isoforms of $PfCRT^{CQR}$ to induce hypersensitivity to lumefantrine (with 1.5–3.2-fold decreases in the IC_{50} [16, 17, 56, 58–61]), artemisinin and/or dihydroartemisinin (with 1.9–3.7-fold decreases in the IC_{50} [6, 11, 17, 58, 59, 62]) as well as to a number of antibiotics [10, 63–67]—including clindamycin [10, 63, 65, 68]. Moreover, multiple clinical trials undertaken in malarious regions throughout the world have associated the wild-type protein (i.e., $PfCRT^{3D7}$) with significant reductions in the parasite's susceptibility to artemether-lumefantrine [16, 69–71], such that (1) the administration of artemether-lumefantrine was found to cause significant selection of CQ-sensitive parasites carrying $PfCRT^{3D7}$ and (2) the presence of parasites carrying $PfCRT^{3D7}$ prior to artemether-lumefantrine treatment was associated with an increased risk of recrudescence. It is possible that the hypersensitivity of CQ-resistant parasites to lumefantrine, the artemisinins, and/or to the antibiotics results from one of the mechanisms we describe in this study. For instance, the antibiotics are either known or expected to act on targets outside of the DV [63, 72, 73], but due to their weak-base nature, these drugs will sequester within the acidic environment of this organelle. Hence, it is plausible that the antibiotics gain greater access to their antimalarial target by being transported into the cytosol via $PfCRT^{CQR}$. For these antibiotics as well as for lumefantrine and the artemisinins, and for the many other pharmacons that display enhanced activity against CQ-resistant parasites, the set of assays outlined in our study offer the means to determine which of the two mechanisms are involved, or whether an altogether different mechanism is responsible. Such insights have the potential to contribute to the formulation of rational approaches for maintaining and extending the useful lifespan of many antimalarials by exploiting the opposing selection forces they exert upon PfCRT.

Materials and Methods

Generation of PfCRT coding sequences and synthesis of cRNA

The coding sequences of the different isoforms of PfCRT were generated via site-directed mutagenesis using the primer pairs listed in S1 Table and an approach described previously

[42]. The mutations were introduced into a codon-harmonized version of the PfCRT sequence that had been inserted into the pGEM-He-Juel oocyte expression vector [74]. This sequence encodes a version of PfCRT that is free of endosomal-lysosomal trafficking motifs and which is therefore expressed at the plasma membrane of *Xenopus laevis* oocytes [30, 42]. All of the resulting coding sequences were verified by sequencing (undertaken by the ACRF Biomolecular Resource Facility, ANU). The plasmids were linearized with SalI (ThermoFisher Scientific) and 5'-capped complementary RNA (cRNA) was synthesized using the mMessage mMachine T7 transcription kit (Ambion), and then purified with the MEGAclear kit (Ambion).

Harvest, preparation, and microinjection of *X*. *laevis* oocytes

Ethical approval of the work performed with the *X*. *laevis* frogs was obtained from the Australian National University Animal Experimentation Ethics Committee (Animal Ethics Protocol Number A2013/13) in accordance with the Australian Code of Practice for the Care and Use of Animals for Scientific Purposes. Oocytes were harvested and prepared as described in full elsewhere [9]. Briefly, sections of ovary were harvested from adult female frogs (purchased from NASCO) via a minor surgical procedure and single, de-folliculated oocytes were prepared using collagenase D (Roche). Stage V-VI oocytes were microinjected with cRNA (20 ng per oocyte) encoding PfCRT or PfNT1 and were stored at 16–18°C in OR^{2+} buffer (82.5 mM NaCl, 2.5 mM KCl, 1 mM $MgCl_2$, 1 mM Na_2HPO_4, 5 mM HEPES, 1 mM $CaCl_2$, and 50 μg/mL gentamycin; pH 7.8).

Oocyte membrane preparation and western blot analysis

The preparation of oocyte membranes and the semi-quantification of PfCRT protein was carried out using a protocol described in detail elsewhere [42]. Protein samples prepared from oocyte membranes were separated on a 4–12% Bis-Tris SDS-polyacrylamide gel (Life Technologies) and transferred to a Protran 0.45 μM nitrocellulose membrane (Amersham, GE Healthcare Life Sciences). The membranes were probed with rabbit anti-PfCRT antibody (concentration of 1:4,000; Genscript) followed by horseradish peroxidase-conjugated goat anti-rabbit antibody (1:8,000; Life Technologies, cat. no. 656120). Validation of the specificity of the anti-PfCRT antibody has been published in detail elsewhere [42]. The PfCRT band for each variant was detected by chemiluminescence (Pierce), quantified using the Image J software [75], and expressed as a percentage of the intensity measured for the $PfCRT^{K1}$ band. Total protein staining was used to evaluate sample loading and efficiency of transfer as outlined previously [42]. Between five and seven independent experiments were performed (on oocytes from different frogs), and in each experiment measurements were averaged from two independent replicates.

Immunofluorescence of oocytes expressing PfCRT

Immunofluorescence analyses were performed on oocytes three days post-injection using a method adapted from Weise et al. [76]. Unless specified otherwise, both the incubation and wash steps were conducted at room temperature with gentle shaking or rotation. The volume of the incubation solution was 500 μL and the washes were performed with 1 mL of the specified solution. Six oocytes from each treatment type were fixed for 30 min in a solution of phosphate-buffered saline (PBS) and 4% v/v paraformaldehyde and then washed (10 min) three times in PBS. The oocytes were permeabilized with 100% methanol for 20 min (-20°C, without shaking) and washed (10 min) three times in PBS. A blocking solution (4% w/v bovine serum albumin (BSA), 2% v/v normal goat serum (Life Technologies), and 0.1% v/v Triton X-100 in PBS) was applied for 2 h, after which the oocytes were incubated overnight at 4°C in a second blocking solution (4% w/v BSA and 2% v/v normal goat serum in PBS). The samples were then incubated for a further 4 h at room temperature before the blocking solution was replaced with a solution containing the rabbit anti-PfCRT antibody (1:100 in 1.5% w/v BSA and 0.01% v/v Triton X-100 in PBS) and the samples were incubated for 4 h at room temperature and then overnight at 4°C. Three 10-min washes were performed in PBS supplemented with 1.5% w/v BSA and all of the remaining steps were undertaken in the dark (and at room temperature). The Alexa Fluor 488 donkey anti-rabbit antibody (1:500; Molecular Probes, cat. no. A-21206) was incubated with the samples for 4 h in PBS supplemented with 4% w/v BSA and 2% v/v normal goat serum, after which three 10-min washes were performed in PBS.

The oocytes were post-fixed with paraformaldehyde (3.7% v/v in PBS) for 30 min, washed twice (15 min) in 2 mL of PBS, and then dehydrated with a series of incubations in solutions of increasing ethanol content. The solutions (in order of administration) were: 30% v/v ethanol in PBS, 50% v/v ethanol in PBS, 70% v/v ethanol in ultrapure water, 90% v/v ethanol in ultrapure water, and 100% ethanol. In each case, the samples were briefly washed in the ethanol-containing solution before a 15-min incubation was performed. A further two incubations in 100% ethanol were conducted before the oocytes were embedded in an acrylic resin using the Technovit 7100 plastic embedding system (Kulzer). Briefly, the samples were incubated with 500 μL embedding solution (50% v/v Technovit 7100 in 100% ethanol) for 2 h, after which the oocytes were incubated overnight in 500 μL of a second embedding solution (1% w/v Technovit 7100 'hardener 1' in Technovit 7100). A further two incubations (≥2 h each) were performed in the second embedding solution before all of the solution was removed and 800 μL of a third embedding solution (6.66% v/v Technovit 7100 'hardener 2' and 1% w/v Technovit 7100 'hardener 1' in Technovit 7100) was added. After the samples had set (≥4 d), a microtome was used to obtain ~4 μm slices, which were dried on microscope slides. Coverslips with a drop of ProLong Gold Antifade Mountant (Life Technologies) were placed over the slices and sealed with nail polish.

Images of the slices were obtained with a Leica Sp5 inverted confocal laser microscope (Leica Microsystems) using the 63x objective. Excitation was achieved with a 488 nm argon laser and the emissions were captured using a 500–550 nm filter. Images were acquired using the Leica Application Suite Advanced Fluorescence software (Leica Microsystems). At least two independent experiments were performed (on oocytes from different frogs) for each oocyte type, within which slices were examined from a minimum of three oocytes. All of the slices taken from oocytes expressing a PfCRT variant displayed a fluorescent band above the pigment layer (i.e., consistent with the localization of PfCRT to the plasma membrane) that was not present in noninjected oocytes.

Drug transport assays

The radiolabeled drugs were purchased from American Radiolabeled Chemicals ([^{3}H]CQ, [^{3}H]quinine, and [^{3}H]quinidine) or Moravek ([^{3}H]amantadine). The uptake into oocytes of [^{3}H]CQ (0.25 μM; 20 Ci/mmol), [^{3}H]quinine (0.25 μM; 20 Ci/mmol), [^{3}H]quinidine (0.25 μM; 20 Ci/mmol), or [^{3}H]amantadine (0.146 μM; 137 mCi/mmol) was measured 3–6 days post-injection. Unless specified otherwise, the drug influx assays were conducted over 1.5–2 h at 27.5°C and in the presence of a low concentration of the unlabeled drug (CQ, 15 μM; quinine and quinidine, 1 μM; amantadine, 50 μM). The reaction buffer was either ND96 pH 5.0 ([^{3}H]quinine, [^{3}H]quinidine, and [^{3}H]amantadine transport assays) or ND96 pH 6.0 ([^{3}H]CQ transport assays) and contained 96 mM NaCl, 2 mM KCl, 1 mM $MgCl_2$, and 1.8 mM $CaCl_2$ supplemented with either 20 mM homo-PIPES (pH 5.0 buffer) or 10 mM MES and 10 mM Tris-base (pH 6.0 buffer). For each treatment, 10 oocytes were transferred to a 5 mL polystyrene round bottom tube (Falcon) and washed twice with 3.5 mL of ND96 buffer, with the residual buffer removed by pipette. Influx commenced with the addition of 100 μL of ND96 buffer supplemented with the radiolabeled and unlabeled drug and, where specified, an unlabeled inhibitor (e.g., verapamil, saquinavir, or CQ). The assay was terminated by removing the reaction buffer with a pipette and washing the oocytes twice with 3.5 mL of ice-cold ND96 buffer. Each oocyte was transferred to a separate well of a white 96-well plate (NUNC or PerkinElmer), incubated overnight at room temperature in 30 μL of 10% SDS, and mixed on an orbital shaker the following day for approximately 5 min. The lysed oocyte was then combined with 150 μL of MicroScint-40 microscintillant (PerkinElmer), the plate covered with a TopSeal-A (PerkinElmer), and the radioactivity measured with a PerkinElmer MicroBeta^2 microplate liquid scintillation analyzer.

Note that noninjected oocytes and oocytes expressing PfCRT^{3D7} take up [^{3}H]CQ to similar (low) levels via simple diffusion of the neutral species of the drug; this represents the 'background' level of [^{3}H]CQ accumulation in oocytes (refer to Martin et al. [30] for full data and discussion). There is also no detectable difference in the accumulation of [^{3}H]quinine between noninjected and PfCRT^{3D7}-expressing oocytes, nor does the accumulation of [^{3}H]quinidine differ between these two oocyte types, and this background level of uptake has likewise been attributed to simple diffusion [29, 30].

The kinetic parameters for CQ, quinine, and quinidine transport via different isoforms of PfCRT (Table 1 and S3 Fig) were determined in SigmaPlot Windows Version 11.0 (Systat Software Inc.) by a least-squares fit of the Michaelis-Menten equation (v = V_{max} substrate]/(K_m + [substrate]) to the data.

The IC_{50} values presented in Fig 3A were determined in SigmaPlot by a least-squares fit of the equation $y = y_{min} + [(y_{max}—y_{min})/(1 + ([\text{inhibitor}]/IC_{50})c]$ to the data, where y is PfCRT-mediated CQ transport, y_{min} and y_{max} are the minimum and maximum values of y, and c is a fitted constant. PfCRT-mediated CQ transport was calculated by subtracting the uptake measured in the control oocytes (oocytes expressing 76K PfCRT^{K1}) from that in oocytes expressing 76I-PfCRT^{K1} or 76I,369F-PfCRT^{K1}.

A subset of experiments measured the ability of unlabeled amantadine to *trans*-stimulate the uptake of [^{3}H]CQ into the oocyte. Immediately prior to the commencement of the experiment, the oocytes (days 3–4 post-injection of the cRNA) were microinjected with either amantadine (estimated intracellular concentrations of 1, 2.5, 5, 10, 15, or 20 mM) or a control treatment (buffer, spermine, or histidine; the estimated intracellular concentrations of spermine and histidine were 5 and 10 mM). The volume injected was 50 nL and the intracellular concentrations were calculated using previous estimates of the volume of stage V-VI oocytes (~400 nL [77]). The resealed oocytes were then incubated at 16–18°C in OR^{2+} buffer for approximately 5 min and the influx of [^{3}H]CQ was measured as described above. For each amantadine concentration, the rate of CQ influx above that measured in the relevant buffer-injected control was calculated and a least-squares fit of the Hill equation ($y = V_{max}[\text{amantadine}]_i^n/(K_m^n + [\text{amantadine}]_i^n)$) to the data was performed in SigmaPlot, where y is the reaction velocity and n is the Hill coefficient. This analysis yielded Hill coefficients of 1.63 ± 0.12, 1.49 ± 0.07, and 1.46 ± 0.05 for PfCRT^{K1}, 76I-PfCRT^{K1} and 76I,369F-PfCRT^{K1}, respectively. These values indicated that CQ and amantadine either bind independently of one another, or are slightly cooperative (i.e., the binding of one drug enhances the affinity of the transporter for the second drug). The Michaelis-Menten equation was then fitted to the data to derive the kinetic parameters for the *trans*-stimulation of [^{3}H]CQ transport by amantadine.

In most cases, at least five independent experiments were performed (on different days and using oocytes from different frogs), and within each experiment measurements were made from 10 oocytes per treatment.

Culture of *P*. *falciparum*-infected erythrocytes

The use of human blood in this study was approved by the Australian National University's Human Research Ethics Committee. The CQ-sensitive strain '3D7' (isolated from the Netherlands but probably of African origin [78]), the CQ-resistant strain 'Dd2' (isolated from Southeast Asia), and three *pfcrt* transfectant lines [2] ($C2^{GC03}$, $C4^{Dd2}$, and $C6^{7G8}$) were cultured and synchronized as described previously [79, 80]. In the $C4^{Dd2}$ and $C6^{7G8}$ lines, the wild-type *pfcrt* allele of the CQ-sensitive 'GC03' strain has been replaced with the *pfcrt* allele from Dd2 or from the CQ-resistant '7G8' strain (isolated from Brazil), respectively. $C2^{GC03}$ is a CQ-sensitive recombinant control that retains the wild-type *pfcrt* allele (i.e., $PfCRT^{3D7}$). $C6^{7G8}$ contains an additional mutation (I351M) in PfCRT that is not present in 7G8 parasites [36]. The parasite lines were maintained in the presence of the selection agents blasticidin (5 μM; Sigma-Aldrich) and WR99210 (5 nM; Jacobus Pharmaceuticals). These selection agents were not present during the experiments.

P. *falciparum* H^+ efflux assay

Saponin-isolated trophozoite-stage parasites containing the membrane-impermeant pH-sensitive fluorescent indicator fluorescein-dextran (10,000 MW; Life Technologies) in their DVs were prepared as outlined elsewhere [36]. The isolated parasites were washed and suspended in a saline solution (125 mM NaCl, 5 mM KCl, 1 mM $MgCl_2$, 20 mM glucose, 25 mM HEPES; pH 7.1) at a density of $1–3 \times 10^7$ cells/mL. The fluorometry experiments were performed as described previously [35]. The pH of the DV was monitored at 37°C using a PerkinElmer Life Sciences LS50B fluorometer with a dual excitation Fast Filter accessory (excitation 490 and 450 nm; emission 520 nm). The experiments entailed monitoring the alkalinization of the DV upon addition of the V-type H^+-ATPase inhibitor concanamycin A (100 nM; Sigma-Aldrich), in the presence or absence of the drugs of interest. Half-times for DV alkalinization (t1/2) were calculated as outlined elsewhere [34]. In all cases, five independent experiments were performed on different days.

P. *falciparum* drug susceptibility

Parasite proliferation was measured in 96-well plates using a fluorescent DNA-intercalating dye [81] and a protocol described in detail previously [82]. Briefly, cell suspensions containing erythrocytes infected with ring-stage parasites (hematocrit and parasitemia of approximately 2% and 1%, respectively) were incubated at 37°C for 72 h. The samples were frozen, thawed, and then processed by the addition of 100 μL (per well) of SYBR Safe DNA Gel Stain (Molecular Probes; 0.2 μL/mL) in a lysis buffer (20 mM Tris, 5 mM EDTA, 0.008% w/v saponin, and 0.08% v/v Triton X-100; pH 7.5). The fluorescence emanating from each well was measured immediately using a Tecan Infinite M1000 PRO microplate reader (excitation 490 nm; emission 520 nm) and the average fluorescence from wells containing the highest concentration of the drug was subtracted from the resulting values. The level of parasite proliferation in the presence of each drug concentration was expressed as a percentage of the proliferation measured in the absence of the drug for which the IC_{50} was being determined. The IC_{50}s were determined in SigmaPlot by a least-squares fit of the equation $y = a/\ [1\ ([drug]/IC_{50})c]$ to the data, where y is the percent parasite proliferation, a is the maximum change in the percent parasite proliferation, and c is a fitted constant. In all cases, five independent experiments were performed (on different days), and within each experiment measurements were averaged from three replicates.

Statistics

All errors cited in the text and shown in the figures represent the SEM. Statistical comparisons were made using one-way ANOVAs in conjunction with Tukey's multiple comparisons test.

Supporting Information

S1 Fig. Predicted topology of PfCRT showing the mutations present in the PfCRT^{K1} variants characterized in this study. PfCRT is predicted to contain 10 α-helical transmembrane domains (TMDs) and to be orientated in the digestive vacuole (DV) membrane with the N- and C-termini extending into the parasite cytosol [83]. The positions of the mutated residues in PfCRT^{K1} are indicated with black circles. The key CQ resistance-associated mutation (K76T) is represented as a red square. The purple circles show the locations of the additional residues that are mutated in the variants of PfCRT^{K1}. The box attached to each polymorphic residue lists the (non-wild-type) amino acid(s) that occur at that position. The predicted roles of the TMDs are as follows: 4 and 9 (outlined in dark green) are implicated in the binding and translocation of substrates, TMDs 3 and 8 (boxed in light green) are thought to assist in the binding and translocation of the substrate and may also influence the substrate-specificity of the transporter, TMDs 1, 2, 6, and 7 (boxed in black) may be involved in recognizing and discriminating between substrates, and TMDs 5 and 10 (outlined in mid-green) are thought to play a role in the formation of homo-dimers [83].
(TIFF)

S2 Fig. Plots of the quinoline transport activities of PfCRT versus the parasite *in vitro* drug responses. (A-C) The CQ, quinine, or quinidine transport activity of a given PfCRT^{K1} isoform (calculated from the data presented in Fig 2) was plotted against the *in vitro* resistance index for the relevant drug and parasite line (listed in Table 1). Where not shown, error bars fall within the symbols. There was a positive correlation between the *in vitro* response of a parasite line to CQ and the CQ transport properties of the corresponding isoform of PfCRT^{K1} (panel A: $R^2 = 0.856$). This is consistent with our previous observation of a positive correlation ($R^2 = 0.858$; [42]) in an analysis performed with seven field isoforms of PfCRT, but contrasts with the work of Roepe and colleagues, who have not detected a relationship between PfCRT^{CQR}-mediated CQ transport and the parasite's response to CQ [84, 85]. In panel B, the quinine transport activities of many of the PfCRT^{K1} isoforms correlated positively with the *in vitro* responses of the parasites to this drug. However, two key exceptions included the data for the highly QN-hypersensitive lines 106/1^{76I} and 106/1^{76I,369F}. Likewise, in panel C, a positive correlation between the capacity of a given PfCRT^{K1} isoform to transport quinidine and the relevant parasite's *in vitro* quinidine resistance index held for all of the parasites bar the QD-sensitive line 106/1^{76N}. Refer to the main text for a discussion of these outlying points. Note also that other genetic elements, such as the amplification or mutation of the parasite's multidrug resistance protein 1 (PfMDR1) and the altered expression of other genes, can contribute to the quinoline resistance phenotype [7, 86–90]. Hence, the CQ resistance index obtained for the 106/1^{76I} line, which is higher than what might be expected from the CQ transport activity of 76I-PfCRT^{K1}, may be due to changes in the expression of one or more genes, including *pfmdr1* [14, 89]. High-level CQ resistance has been associated with reductions in the *pfmdr1* copy number and a corresponding decrease in the expression of *pfmdr1* [91, 92]. In this regard it is worth noting that the 106/1^{76I} line contains a single copy of *pfmdr1*, whereas the 106/1, 106/1^{76T}, and 106/1^{76N} lines possess two copies, and this difference has been confirmed to result in a lower level of *pfmdr1* expression in the 106/1^{76I} parasites [14, 89]. Hence, it is likely that the relatively high level of CQ resistance displayed by 106/1^{76I} is the product of the effects of the

CQ transport activity of 76I-PfCRT^{K1}, the reduced expression of PfMDR1, and perhaps changes that have occurred elsewhere in the parasite's transcriptome. Thus, while this study and our previous work [42] indicate that the quinoline transport activities of a number of PfCRT variants correlate positively with the *in vitro* responses of the respective parasites to these drugs, changes elsewhere in the genome and transcriptome can modulate the level of quinoline resistance conferred by PfCRT^{CQR}.
(TIF)

S3 Fig. Isoforms of PfCRT^{K1} exhibit different CQ, quinine, and quinidine transport kinetics when expressed in oocytes. (A) The uptake of [^{3}H]CQ (0.25 μM) was measured at pH 6.0 and over an extracellular concentration range of 10 to 1250 μM unlabeled CQ. (B) The uptake of [^{3}H]quinine (0.25 μM) was measured at pH 5.0 and the extracellular concentration of unlabeled quinine ranged between 1 and 300 μM (PfCRT^{K1} and 76N-PfCRT^{K1}) or 0.25 and 12 μM (76I-PfCRT^{K1}). The inset shows a magnified plot of the 76I-PfCRT^{K1} data. (C) The uptake of [^{3}H]quinidine (0.25 μM) was measured at pH 5.0 and the extracellular concentration of unlabeled quinidine ranged between 1 and 500 μM (PfCRT^{K1} and 76I-PfCRT^{K1}) or 1 and 750 μM (76N-PfCRT^{K1}). In all cases, the rate of PfCRT-mediated drug uptake was calculated by subtracting the rate measured in oocytes expressing 76K-PfCRT^{K1} from that measured in oocytes expressing PfCRT^{K1}, 76N-PfCRT^{K1}, 76I-PfCRT^{K1}, or 76I,369F-PfCRT^{K1} at each drug concentration. The Michaelis-Menten equation was fitted to the resulting data using nonlinear regression. The rates of drug uptake are the mean ± SEM of multiple independent experiments (performed using oocytes from different frogs), within which measurements were made from 10 oocytes per treatment. Where not shown, error bars fall within the symbols. The exact *n* values, as well as the kinetic parameters derived from these data, are presented in Table 2.
(TIF)

S4 Fig. Quinine and quinidine transport activities of the 76I and 76N isoforms of PfCRT^{Dd2} and PfCRT^{K1}. Noninjected oocytes accumulate low levels of quinine and quinidine via simple diffusion of the neutral species of the drug [29]. This represents the background level of drug accumulation. The uptake of (A) [^{3}H]quinine and (B) [^{3}H]quinidine was measured at pH 5.0 and in the presence of 1 μM of the respective unlabeled drug. The concentration of the [^{3}H]drug was 0.25 μM. The rates of uptake (pmol per oocyte/h) in noninjected oocytes and oocytes expressing PfCRT^{Dd2} were 0.10 ± 0.01 and 0.44 ± 0.04, respectively, for quinine and 0.05 ± 0.01 and 0.30 ± 0.07, respectively, for quinidine. In both panels, drug uptake is expressed relative to that measured in oocytes expressing PfCRT^{Dd2}. The rates of quinine and quinidine uptake mediated by PfCRT^{K1} were 1.2–1.3 times that measured for PfCRT^{Dd2}, whereas the 76N-PfCRT^{K1} protein possessed 3.1 times the quinine transport activity, and 3.2 times the quinidine transport activity, of 76N-PfCRT^{Dd2}. Moreover, the rate of quinidine transport mediated by 76I-PfCRT^{K1} was 1.5 times that measured for 76I-PfCRT^{Dd2}. The single exception to this trend was the rate of quinine transport via 76I-PfCRT^{K1}, which was 0.55 times that measured for its PfCRT^{Dd2} counterpart. The data are the mean + SEM of at least five independent experiments (performed using oocytes from different frogs), within which measurements were made from 10 oocytes per treatment. The asterisks denote a significant difference in drug uptake between the noninjected treatment and that measured in oocytes expressing a variant of PfCRT: $^{*}P < 0.05$; $^{**}P < 0.01$; $^{***}P < 0.001$ (one-way ANOVA).
(TIF)

S5 Fig. Spermine and histidine do not inhibit the accumulation of [^{3}H]CQ in oocytes expressing PfCRT. The uptake of [^{3}H]CQ (0.25 μM) was measured in the absence (solvent

control) or presence of the test compounds (extracellular concentrations of 1 and 2 mM). The assays were conducted at pH 5.5 and in the presence of 15 μM unlabeled CQ. The rates of CQ uptake (pmol per oocyte/h) in noninjected oocytes and $PfCRT^{Dd2}$-expressing oocytes were 1.41 ± 0.02 and 24 ± 1.3, respectively. The data are the mean + SEM of four independent experiments performed using oocytes from different frogs), within which measurements were made from 10 oocytes per treatment. 'ns' denotes no significant difference from the $PfCRT^{Dd2}$ control ($P > 0.05$; one-way ANOVA).
(TIF)

S6 Fig. Amantadine *trans*-stimulates the uptake of [^{3}H]CQ into oocytes expressing PfCRT in a concentration-dependent manner. Control oocytes (noninjected oocytes and oocytes expressing PfNT1) and oocytes expressing a variant of PfCRT ($PfCRT^{3D7}$, 76K-$PfCRT^{K1}$, $PfCRT^{K1}$, 76I-$PfCRT^{K1}$, or 76I,369F-$PfCRT^{K1}$) were microinjected with buffer containing amantadine to achieve an estimated intracellular concentration ($[amantadine]_i$) of 1 to 20 mM. A control was also performed in which the oocytes were microinjected with buffer alone. The rates of CQ uptake are the mean ± SEM of five independent experiments (performed using oocytes from different frogs), within which measurements were made from 10 oocytes per treatment. Where not shown, error bars fall within the symbols. The data presented in Fig 3E and 3F were calculated by subtracting the rate of CQ uptake measured in the buffer-injected control from that measured in each of the corresponding amantadine treatments (and within the same oocyte type). The noninjected data overlays the data obtained with oocytes expressing PfNT1, $PfCRT^{3D7}$, or 76K-$PfCRT^{K1}$.
(TIF)

S7 Fig. Mechanisms for the CQ and quinidine susceptibilities conferred by PfCRT isoforms in the malaria parasite. (A) The variants of $PfCRT^{K1}$ that contain 72R, 76K, 163R, 352K, or 352R (R/K) do not possess significant CQ transport activity. The drug would therefore remain in the DV where it exerts an anti-hemozoin effect that kills the parasite, which is consistent with the CQ-sensitive (S) status of the respective lines. By contrast, $PfCRT^{K1}$ (76T) and 76I-$PfCRT^{K1}$ transport CQ out of the parasite's DV, thereby conferring CQ resistance (R). The addition of 369F to 76I-$PfCRT^{K1}$ significantly reduces its affinity and capacity for CQ transport. Hence, 76I,369F-$PfCRT^{K1}$ imparts a relatively low level of resistance (*low*-R) to CQ. (B) The R/K variants of $PfCRT^{K1}$ do not possess significant quinidine (QD) transport activity whereas $PfCRT^{K1}$, 76N-$PfCRT^{K1}$ and 76I-$PfCRT^{K1}$ each have the ability to transport QD out of the DV, albeit to varying degrees. These differences in QD transport activity explain, at least in part, the susceptibilities of the corresponding 106/1 parasite strains to QD. 76N-$PfCRT^{K1}$ has a slightly lower affinity for QD then does $PfCRT^{K1}$, and also has a much lower maximum rate of QD transport. The low capacity and low affinity of QD transport via 76N-$PfCRT^{K1}$ explains why this protein has little net effect on the parasite's sensitivity to QD. By contrast, the relatively high capacity of $PfCRT^{K1}$ for QD transport is consistent with the decreased susceptibility of $106/1^{76T}$ parasites to QD (*low*-R). 76I-$PfCRT^{K1}$ has a low maximum rate of QD transport, but this characteristic is counterbalanced by a 3-fold increase in its affinity for QD, and the net capacity of the protein for QD transport appears to be sufficient to reduce the parasite's susceptibility to QD (at least under the conditions of the *in vitro* parasite proliferation assays).
(TIF)

S1 Table. Primer sequences used to introduce mutations into the PfCRT coding sequence via site-directed mutagenesis.
(DOCX)

Acknowledgments

We thank Robert Summers for helpful discussions, Rachel Slatyer and Tessa Attenborough for technical assistance, Prof David Fidock for providing the transfectant *P. falciparum* lines, and the Canberra Branch of the Australian Red Cross Blood Service for the provision of blood.

Author Contributions

Conceived and designed the experiments: REM SNR MNN SHS. Performed the experiments: SNR MNN SHS ESB MWW AML. Analyzed the data: REM SNR MNN SHS MWW AML. Wrote the paper: REM SNR SHS MNN.

References

1. Fidock DA, Nomura T, Talley AK, Cooper RA, Dzekunov SM, Ferdig MT, et al. Mutations in the *P. falciparum* digestive vacuole transmembrane protein PfCRT and evidence for their role in chloroquine resistance. Mol Cell. 2000; 6(4):861–71. PMID: 11090624
2. Sidhu AB, Verdier-Pinard D, Fidock DA. Chloroquine resistance in *Plasmodium falciparum* malaria parasites conferred by *pfcrt* mutations. Science. 2002; 298(5591):210–3. PMID: 12364805
3. Ecker A, Lehane AM, Clain J, Fidock DA. PfCRT and its role in antimalarial drug resistance. Trends Parasitol. 2012; 28(11):504–14. doi: 10.1016/j.pt.2012.08.002 PMID: 23020971
4. Miotto O, Amato R, Ashley EA, MacInnis B, Almagro-Garcia J, Amaratunga C, et al. Genetic architecture of artemisinin-resistant *Plasmodium falciparum*. Nat Genet. 2015; 47(3):226–34. doi: 10.1038/ng.3189 PMID: 25599401
5. Summers RL, Nash MN, Martin RE. Know your enemy: understanding the role of PfCRT in drug resistance could lead to new antimalarial tactics. Cell Mol Life Sci. 2012; 69(12):1967–95. doi: 10.1007/s00018-011-0906-0 PMID: 22286067
6. Chugh M, Scheurer C, Sax S, Bilsland E, van Schalkwyk DA, Wicht KJ, et al. Identification and deconvolution of cross-resistance signals from antimalarial compounds using multidrug-resistant *Plasmodium falciparum* strains. Antimicrob Agents Chemother. 2015; 59(2):1110–8. doi: 10.1128/AAC.03265-14 PMID: 25487796
7. Sa JM, Twu O, Hayton K, Reyes S, Fay MP, Ringwald P, et al. Geographic patterns of *Plasmodium falciparum* drug resistance distinguished by differential responses to amodiaquine and chloroquine. Proc Natl Acad Sci U S A. 2009; 106(45):18883–9. doi: 10.1073/pnas.0911317106 PMID: 19884511
8. Sanchez CP, Mayer S, Nurhasanah A, Stein WD, Lanzer M. Genetic linkage analyses redefine the roles of PfCRT and PfMDR1 in drug accumulation and susceptibility in *Plasmodium falciparum*. Mol Microbiol. 2011; 82(4):865–78. doi: 10.1111/j.1365-2958.2011.07855.x PMID: 21999470
9. van Schalkwyk DA, Nash MN, Shafik SH, Summers RL, Lehane AM, Smith PJ, et al. Verapamil-Sensitive Transport of Quinacrine and Methylene Blue via the *Plasmodium falciparum* Chloroquine Resistance Transporter Reduces the Parasite's Susceptibility to these Tricyclic Drugs. J Infect Dis. 2016; 213(5):800–10. doi: 10.1093/infdis/jiv509 PMID: 26503982
10. Yuan J, Cheng KC, Johnson RL, Huang R, Pattaradilokrat S, Liu A, et al. Chemical genomic profiling for antimalarial therapies, response signatures, and molecular targets. Science. 2011; 333(6043):724–9. doi: 10.1126/science.1205216 PMID: 21817045
11. Cooper RA, Ferdig MT, Su XZ, Ursos LM, Mu J, Nomura T, et al. Alternative mutations at position 76 of the vacuolar transmembrane protein PfCRT are associated with chloroquine resistance and unique stereospecific quinine and quinidine responses in *Plasmodium falciparum*. Mol Pharmacol. 2002; 61(1):35–42. PMID: 11752204
12. Cooper RA, Lane KD, Deng B, Mu J, Patel JJ, Wellems TE, et al. Mutations in transmembrane domains 1, 4 and 9 of the *Plasmodium falciparum* chloroquine resistance transporter alter susceptibility to chloroquine, quinine and quinidine. Mol Microbiol. 2007; 63(1):270–82. PMID: 17163969
13. Evans SG, Havlik I. *Plasmodium falciparum*: effects of amantadine, an antiviral, on chloroquine-resistant and -sensitive parasites *in vitro* and its influence on chloroquine activity. Biochem Pharmacol. 1993; 45(5):1168–70. PMID: 8461046
14. Griffin CE, Hoke JM, Samarakoon U, Duan J, Mu J, Ferdig MT, et al. Mutation in the *Plasmodium falciparum* CRT protein determines the stereospecific activity of antimalarial cinchona alkaloids. Antimicrob Agents Chemother. 2012; 56(10):5356–64. doi: 10.1128/AAC.05667-11 PMID: 22869567

15. Johnson DJ, Fidock DA, Mungthin M, Lakshmanan V, Sidhu AB, Bray PG, et al. Evidence for a central role for PfCRT in conferring *Plasmodium falciparum* resistance to diverse antimalarial agents. Mol Cell. 2004; 15(6):867–77. PMID: 15383277

16. Sisowath C, Petersen I, Veiga MI, Martensson A, Premji Z, Bjorkman A, et al. *In vivo* selection of *Plasmodium falciparum* parasites carrying the chloroquine-susceptible *pfcrt* K76 allele after treatment with artemether-lumefantrine in Africa. J Infect Dis. 2009; 199(5):750–7. doi: 10.1086/596738 PMID: 19210165

17. Eastman RT, Khine P, Huang R, Thomas CJ, Su XZ. PfCRT and PfMDR1 modulate interactions of artemisinin derivatives and ion channel blockers. Sci Rep. 2016; 6:25379. doi: 10.1038/srep25379 PMID: 27147113

18. Lukens AK, Ross LS, Heidebrecht R, Javier Gamo F, Lafuente-Monasterio MJ, Booker ML, et al. Harnessing evolutionary fitness in *Plasmodium falciparum* for drug discovery and suppressing resistance. Proc Natl Acad Sci U S A. 2014; 111(2):799–804. doi: 10.1073/pnas.1320886110 PMID: 24381157

19. Imamovic L, Sommer MO. Use of collateral sensitivity networks to design drug cycling protocols that avoid resistance development. Sci Transl Med. 2013; 5(204):204ra132.

20. Pal C, Papp B, Lazar V. Collateral sensitivity of antibiotic-resistant microbes. Trends Microbiol. 2015; 23(7):401–7. doi: 10.1016/j.tim.2015.02.009 PMID: 25818802

21. Szybalski W, Bryson V. Genetic studies on microbial cross resistance to toxic agents. I. Cross resistance of *Escherichia coli* to fifteen antibiotics. J Bacteriol. 1952; 64(4):489–99. PMID: 12999676

22. Pluchino KM, Hall MD, Goldsborough AS, Callaghan R, Gottesman MM. Collateral sensitivity as a strategy against cancer multidrug resistance. Drug Resist Updat. 2012; 15(1–2):98–105. doi: 10.1016/j.drup.2012.03.002 PMID: 22483810

23. Bray PG, Mungthin M, Hastings IM, Biagini GA, Saidu DK, Lakshmanan V, et al. PfCRT and the *trans*-vacuolar proton electrochemical gradient: regulating the access of chloroquine to ferriprotoporphyrin IX. Mol Microbiol. 2006; 62(1):238–51. PMID: 16956382

24. Fitch CD. Ferriprotoporphyrin IX, phospholipids, and the antimalarial actions of quinoline drugs. Life Sci. 2004; 74(16):1957–72. PMID: 14967191

25. Hawley SR, Bray PG, Mungthin M, Atkinson JD, O'Neill PM, Ward SA. Relationship between antimalarial drug activity, accumulation, and inhibition of heme polymerization in *Plasmodium falciparum in vitro*. Antimicrob Agents Chemother. 1998; 42(3):682–6. PMID: 9517951

26. Mungthin M, Bray PG, Ridley RG, Ward SA. Central role of hemoglobin degradation in mechanisms of action of 4-aminoquinolines, quinoline methanols, and phenanthrene methanols. Antimicrob Agents Chemother. 1998; 42(11):2973–7. PMID: 9797235

27. Combrinck JM, Mabotha TE, Ncokazi KK, Ambele MA, Taylor D, Smith PJ, et al. Insights into the role of heme in the mechanism of action of antimalarials. ACS Chem Biol. 2013; 8(1):133–7. doi: 10.1021/cb300454t PMID: 23043646

28. Saliba KJ, Folb PI, Smith PJ. Role for the *Plasmodium falciparum* digestive vacuole in chloroquine resistance. Biochem Pharmacol. 1998; 56(3):313–20. PMID: 9744568

29. Bellanca S, Summers RL, Meyrath M, Dave A, Nash MN, Dittmer M, et al. Multiple drugs compete for transport via the *Plasmodium falciparum* chloroquine resistance transporter at distinct but interdependent sites. J Biol Chem. 2014; 289(52):36336–51. doi: 10.1074/jbc.M114.614206 PMID: 25378409

30. Martin RE, Marchetti RV, Cowan AI, Howitt SM, Bröer S, Kirk K. Chloroquine transport *via* the malaria parasite's chloroquine resistance transporter. Science. 2009; 325(5948):1680–2. doi: 10.1126/science.1175667 PMID: 19779197

31. Summers RL, Martin RE. Functional characteristics of the malaria parasite's "chloroquine resistance transporter": implications for chemotherapy. Virulence. 2010; 1(4):304–8. doi: 10.4161/viru.1.4.12012 PMID: 21178460

32. Sanchez CP, McLean JE, Rohrbach P, Fidock DA, Stein WD, Lanzer M. Evidence for a *pfcrt*-associated chloroquine efflux system in the human malarial parasite *Plasmodium falciparum*. Biochemistry. 2005; 44(29):9862–70. PMID: 16026158

33. Sanchez CP, McLean JE, Stein W, Lanzer M. Evidence for a substrate specific and inhibitable drug efflux system in chloroquine resistant *Plasmodium falciparum* strains. Biochemistry. 2004; 43(51):16365–73. PMID: 15610031

34. Lehane AM, Hayward R, Saliba KJ, Kirk K. A verapamil-sensitive chloroquine-associated H^+ leak from the digestive vacuole in chloroquine-resistant malaria parasites. J Cell Sci. 2008; 121:1624–32. doi: 10.1242/jcs.016758 PMID: 18445688

35. Lehane AM, Kirk K. Chloroquine resistance-conferring mutations in *pfcrt* give rise to a chloroquine-associated H^+ leak from the malaria parasite's digestive vacuole. Antimicrob Agents Chemother. 2008; 52(12):4374–80. doi: 10.1128/AAC.00666-08 PMID: 18852275

36. Lehane AM, Kirk K. Efflux of a range of antimalarial drugs and 'chloroquine resistance reversers' from the digestive vacuole in malaria parasites with mutant PfCRT. Mol Microbiol. 2010; 77(4):1039–51. doi: 10.1111/j.1365-2958.2010.07272.x PMID: 20598081

37. Naude B, Brzostowski JA, Kimmel AR, Wellems TE. *Dictyostelium discoideum* expresses a malaria chloroquine resistance mechanism upon transfection with mutant, but not wild-type, *Plasmodium falciparum* transporter PfCRT. J Biol Chem. 2005; 280(27):25596–603. PMID: 15883156

38. Papakrivos J, Sa JM, Wellems TE. Functional characterization of the *Plasmodium falciparum* chloroquine-resistance transporter (PfCRT) in transformed *Dictyostelium discoideum* vesicles. PLoS One. 2012; 7(6):e39569. doi: 10.1371/journal.pone.0039569 PMID: 22724026

39. Waller KL, Muhle RA, Ursos LM, Horrocks P, Verdier-Pinard D, Sidhu AB, et al. Chloroquine resistance modulated *in vitro* by expression levels of the *Plasmodium falciparum* chloroquine resistance transporter. J Biol Chem. 2003; 278(35):33593–601. PMID: 12813054

40. Ecker A, Lewis RE, Ekland EH, Jayabalasingham B, Fidock DA. Tricks in *Plasmodium's* molecular repertoire—escaping 3'UTR excision-based conditional silencing of the chloroquine resistance transporter gene. Int J Parasitol. 2012; 42(11):969–74. doi: 10.1016/j.ijpara.2012.09.003 PMID: 23023047

41. Kornhuber J, Henkel AW, Groemer TW, Stadtler S, Welzel O, Tripal P, et al. Lipophilic cationic drugs increase the permeability of lysosomal membranes in a cell culture system. J Cell Physiol. 2010; 224 (1):152–64. doi: 10.1002/jcp.22112 PMID: 20301195

42. Summers RL, Dave A, Dolstra TJ, Bellanca S, Marchetti RV, Nash MN, et al. Diverse mutational pathways converge on saturable chloroquine transport via the malaria parasite's chloroquine resistance transporter. Proc Natl Acad Sci U S A. 2014; 111(17):E1759–67. doi: 10.1073/pnas.1322965111 PMID: 24728833

43. Hayward R, Saliba KJ, Kirk K. The pH of the digestive vacuole of *Plasmodium falciparum* is not associated with chloroquine resistance. J Cell Sci. 2006; 119:1016–25. PMID: 16492710

44. Klonis N, Tan O, Jackson K, Goldberg D, Klemba M, Tilley L. Evaluation of pH during cytostomal endocytosis and vacuolar catabolism of haemoglobin in *Plasmodium falciparum*. Biochem J. 2007; 407 (3):343–54. PMID: 17696875

45. Saliba KJ, Kirk K. pH regulation in the intracellular malaria parasite, *Plasmodium falciparum*. H^+ extrusion via a V-type H^+-ATPase. J Biol Chem. 1999; 274(47):33213–9. PMID: 10559194

46. Hrycyna CA, Summers RL, Lehane AM, Pires MM, Namanja H, Bohn K, et al. Quinine dimers are potent inhibitors of the *Plasmodium falciparum* chloroquine resistance transporter and are active against quinoline-resistant *P. falciparum*. ACS Chem Biol. 2014; 9(3):722–30. doi: 10.1021/cb4008953 PMID: 24369685

47. Martin RE, Butterworth AS, Gardiner DL, Kirk K, McCarthy JS, Skinner-Adams TS. Saquinavir inhibits the malaria parasite's chloroquine resistance transporter. Antimicrob Agents Chemother. 2012; 56 (5):2283–9. doi: 10.1128/AAC.00166-12 PMID: 22354298

48. Carter NS, Ben Mamoun C, Liu W, Silva EO, Landfear SM, Goldberg DE, et al. Isolation and functional characterization of the PfNT1 nucleoside transporter gene from *Plasmodium falciparum*. J Biol Chem. 2000; 275(14):10683–91. PMID: 10744765

49. Deane KJ, Summers RL, Lehane AM, Martin RE, Barrow RA. Chlorpheniramine Analogues Reverse Chloroquine Resistance in *Plasmodium falciparum* by Inhibiting PfCRT. ACS Med Chem Lett. 2014; 5 (5):576–81. doi: 10.1021/ml5000228 PMID: 24900883

50. Famin O, Krugliak M, Ginsburg H. Kinetics of inhibition of glutathione-mediated degradation of ferriprotoporphyrin IX by antimalarial drugs. Biochem Pharmacol. 1999; 58(1):59–68. PMID: 10403519

51. Jing X, Ma C, Ohigashi Y, Oliveira FA, Jardetzky TS, Pinto LH, et al. Functional studies indicate amantadine binds to the pore of the influenza A virus M2 proton-selective ion channel. Proc Natl Acad Sci U S A. 2008; 105(31):10967–72. doi: 10.1073/pnas.0804958105 PMID: 18669647

52. Kublin JG, Cortese JF, Njunju EM, Mukadam RA, Wirima JJ, Kazembe PN, et al. Reemergence of chloroquine-sensitive *Plasmodium falciparum* malaria after cessation of chloroquine use in Malawi. J Infect Dis. 2003; 187(12):1870–5. PMID: 12792863

53. Wang X, Mu J, Li G, Chen P, Guo X, Fu L, et al. Decreased prevalence of the *Plasmodium falciparum* chloroquine resistance transporter 76T marker associated with cessation of chloroquine use against *P. falciparum* malaria in Hainan, People's Republic of China. Am J Trop Med Hyg. 2005; 72(4):410–4. PMID: 15827277

54. Ord R, Alexander N, Dunyo S, Hallett R, Jawara M, Targett G, et al. Seasonal carriage of *pfcrt* and *pfmdr1* alleles in Gambian *Plasmodium falciparum* imply reduced fitness of chloroquine-resistant parasites. J Infect Dis. 2007; 196(11):1613–9. PMID: 18008244

55. Lewis IA, Wacker M, Olszewski KL, Cobbold SA, Baska KS, Tan A, et al. Metabolic QTL analysis links chloroquine resistance in *Plasmodium falciparum* to impaired hemoglobin catabolism. PLoS Genet. 2014; 10(1):e1004085. doi: 10.1371/journal.pgen.1004085 PMID: 24391526

56. Pelleau S, Moss EL, Dhingra SK, Volney B, Casteras J, Gabryszewski SJ, et al. Adaptive evolution of malaria parasites in French Guiana: Reversal of chloroquine resistance by acquisition of a mutation in *pfcrt*. Proc Natl Acad Sci U S A. 2015; 112(37):11672–7. doi: 10.1073/pnas.1507142112 PMID: 26261345

57. World Health Organization. Global Malaria Programme. World malaria report 2013. Geneva: World Health Organization; 2013. 8p.

58. Mwai L, Kiara SM, Abdirahman A, Pole L, Rippert A, Diriye A, et al. *In vitro* activities of piperaquine, lumefantrine, and dihydroartemisinin in Kenyan *Plasmodium falciparum* isolates and polymorphisms in *pfcrt* and *pfmdr1*. Antimicrob Agents Chemother. 2009; 53(12):5069–73. doi: 10.1128/AAC.00638-09 PMID: 19770282

59. Petersen I, Gabryszewski SJ, Johnston GL, Dhingra SK, Ecker A, Lewis RE, et al. Balancing drug resistance and growth rates via compensatory mutations in the *Plasmodium falciparum* chloroquine resistance transporter. Mol Microbiol. 2015; 97(2):381–95. doi: 10.1111/mmi.13035 PMID: 25898991

60. Valderramos SG, Valderramos JC, Musset L, Purcell LA, Mercereau-Puijalon O, Legrand E, et al. Identification of a mutant PfCRT-mediated chloroquine tolerance phenotype in *Plasmodium falciparum*. PLoS Pathog. 2010; 6(5):e1000887. doi: 10.1371/journal.ppat.1000887 PMID: 20485514

61. Van Tyne D, Park DJ, Schaffner SF, Neafsey DE, Angelino E, Cortese JF, et al. Identification and functional validation of the novel antimalarial resistance locus PF10_0355 in *Plasmodium falciparum*. PLoS Genet. 2011; 7(4):e1001383. doi: 10.1371/journal.pgen.1001383 PMID: 21533027

62. Mu J, Myers RA, Jiang H, Liu S, Ricklefs S, Waisberg M, et al. *Plasmodium falciparum* genome-wide scans for positive selection, recombination hot spots and resistance to antimalarial drugs. Nat Genet. 2010; 42(3):268–71. doi: 10.1038/ng.528 PMID: 20101240

63. Dahl EL, Rosenthal PJ. Multiple antibiotics exert delayed effects against the *Plasmodium falciparum* apicoplast. Antimicrob Agents Chemother. 2007; 51(10):3485–90. PMID: 17698630

64. Delves M, Plouffe D, Scheurer C, Meister S, Wittlin S, Winzeler EA, et al. The activities of current antimalarial drugs on the life cycle stages of *Plasmodium*: a comparative study with human and rodent parasites. PLoS Med. 2012; 9(2):e1001169. doi: 10.1371/journal.pmed.1001169 PMID: 22363211

65. Held J, Zanger P, Issifou S, Kremsner PG, Mordmuller B. *In vitro* activity of tigecycline in *Plasmodium falciparum* culture-adapted strains and clinical isolates from Gabon. Int J Antimicrob Agents. 2010; 35 (6):587–9. doi: 10.1016/j.ijantimicag.2010.02.003 PMID: 20227854

66. Pradines B, Rogier C, Fusai T, Mosnier J, Daries W, Barret E, et al. *In vitro* activities of antibiotics against *Plasmodium falciparum* are inhibited by iron. Antimicrob Agents Chemother. 2001; 45(6):1746–50. PMID: 11353621

67. Sahu R, Walker LA, Tekwani BL. *In vitro* and *in vivo* anti-malarial activity of tigecycline, a glycylcycline antibiotic, in combination with chloroquine. Malar J. 2014; 13:414. doi: 10.1186/1475-2875-13-414 PMID: 25336038

68. Pulcini S, Staines HM, Lee AH, Shafik SH, Bouyer G, Moore CM, et al. Mutations in the *Plasmodium falciparum* chloroquine resistance transporter, PfCRT, enlarge the parasite's food vacuole and alter drug sensitivities. Sci Rep. 2015; 5:14552. doi: 10.1038/srep14552 PMID: 26420308

69. Venkatesan M, Gadalla NB, Stepniewska K, Dahal P, Nsanzabana C, Moriera C, et al. Polymorphisms in *Plasmodium falciparum* chloroquine resistance transporter and multidrug resistance 1 genes: parasite risk factors that affect treatment outcomes for *P*. *falciparum* malaria after artemether-lumefantrine and artesunate-amodiaquine. Am J Trop Med Hyg. 2014; 91(4):833–43. doi: 10.4269/ajtmh.14-0031 PMID: 25048375

70. Conrad MD, LeClair N, Arinaitwe E, Wanzira H, Kakuru A, Bigira V, et al. Comparative impacts over 5 years of artemisinin-based combination therapies on *Plasmodium falciparum* polymorphisms that modulate drug sensitivity in Ugandan children. J Infect Dis. 2014; 210(3):344–53. doi: 10.1093/infdis/jiu141 PMID: 24610872

71. Somé AF, Sere YY, Dokomajilar C, Zongo I, Rouamba N, Greenhouse B, et al. Selection of known *Plasmodium falciparum* resistance-mediating polymorphisms by artemether-lumefantrine and amodiaquine-sulfadoxine-pyrimethamine but not dihydroartemisinin-piperaquine in Burkina Faso. Antimicrob Agents Chemother. 2010; 54(5):1949–54. doi: 10.1128/AAC.01413-09 PMID: 20231394

72. Ramya TN, Mishra S, Karmodiya K, Surolia N, Surolia A. Inhibitors of nonhousekeeping functions of the apicoplast defy delayed death in *Plasmodium falciparum*. Antimicrob Agents Chemother. 2007; 51 (1):307–16. PMID: 17060533

73. Sidhu AB, Sun Q, Nkrumah LJ, Dunne MW, Sacchettini JC, Fidock DA. *In vitro* efficacy, resistance selection, and structural modeling studies implicate the malarial parasite apicoplast as the target of azithromycin. J Biol Chem. 2007; 282(4):2494–504. PMID: 17110371

74. Bröer S, Rahman B, Pellegri G, Pellerin L, Martin JL, Verleysdonk S, et al. Comparison of lactate transport in astroglial cells and monocarboxylate transporter 1 (MCT 1) expressing *Xenopus laevis* oocytes. Expression of two different monocarboxylate transporters in astroglial cells and neurons. J Biol Chem. 1997; 272(48):30096–102. PMID: 9374487

75. Schneider CA, Rasband WS, Eliceiri KW. NIH Image to ImageJ: 25 years of image analysis. Nat Methods. 2012; 9(7):671–5. PMID: 22930834

76. Weise A, Becker HM, Deitmer JW. Enzymatic suppression of the membrane conductance associated with the glutamine transporter SNAT3 expressed in *Xenopus* oocytes by carbonic anhydrase II. J Gen Physiol. 2007; 130(2):203–15. PMID: 17664347

77. Taylor MA, Smith LD. Accumulation of free amino acids in growing *Xenopus laevis* oocytes. Dev Biol. 1987; 124(1):287–90. PMID: 2889640

78. Mu J, Awadalla P, Duan J, McGee KM, Joy DA, McVean GA, et al. Recombination hotspots and population structure in *Plasmodium falciparum*. PLoS Biol. 2005; 3(10):e335. PMID: 16144426

79. Allen RJ, Kirk K. *Plasmodium falciparum* culture: the benefits of shaking. Mol Biochem Parasitol. 2010; 169(1):63–5. doi: 10.1016/j.molbiopara.2009.09.005 PMID: 19766147

80. Lambros C, Vanderberg JP. Synchronization of *Plasmodium falciparum* erythrocytic stages in culture. J Parasitol. 1979; 65(3):418–20. PMID: 383936

81. Smilkstein M, Sriwilaijaroen N, Kelly JX, Wilairat P, Riscoe M. Simple and inexpensive fluorescence-based technique for high-throughput antimalarial drug screening. Antimicrob Agents Chemother. 2004; 48(5):1803–6. PMID: 15105138

82. Spry C, Macuamule C, Lin Z, Virga KG, Lee RE, Strauss E, et al. Pantothenamides are potent, on-target inhibitors of *Plasmodium falciparum* growth when serum pantetheinase is inactivated. PLoS One. 2013; 8(2):e54974. doi: 10.1371/journal.pone.0054974 PMID: 23405100

83. Martin RE, Kirk K. The malaria parasite's chloroquine resistance transporter is a member of the drug/metabolite transporter superfamily. Mol Biol Evol. 2004; 21(10):1938–49. PMID: 15240840

84. Baro NK, Callaghan PS, Roepe PD. Function of resistance conferring *Plasmodium falciparum* chloroquine resistance transporter isoforms. Biochemistry. 2013; 52(24):4242–9. doi: 10.1021/bi400557x PMID: 23688277

85. Callaghan PS, Hassett MR, Roepe PD. Functional Comparison of 45 Naturally Occurring Isoforms of the *Plasmodium falciparum* Chloroquine Resistance Transporter (PfCRT). Biochemistry. 2015; 54 (32):5083–94. doi: 10.1021/acs.biochem.5b00412 PMID: 26208441

86. Sidhu AB, Valderramos SG, Fidock DA. *pfmdr1* mutations contribute to quinine resistance and enhance mefloquine and artemisinin sensitivity in *Plasmodium falciparum*. Mol Microbiol. 2005; 57 (4):913–26. PMID: 16091034

87. Reed MB, Saliba KJ, Caruana SR, Kirk K, Cowman AF. Pgh1 modulates sensitivity and resistance to multiple antimalarials in *Plasmodium falciparum*. Nature. 2000; 403:906–9. PMID: 10706290

88. Adjalley SH, Scanfeld D, Kozlowski E, Llinas M, Fidock DA. Genome-wide transcriptome profiling reveals functional networks involving the *Plasmodium falciparum* drug resistance transporters PfCRT and PfMDR1. BMC genomics. 2015; 16:1090. doi: 10.1186/s12864-015-2320-8 PMID: 26689807

89. Jiang H, Patel JJ, Yi M, Mu J, Ding J, Stephens R, et al. Genome-wide compensatory changes accompany drug- selected mutations in the *Plasmodium falciparum crt* gene. PLoS One. 2008; 3(6):e2484. doi: 10.1371/journal.pone.0002484 PMID: 18575593

90. Siwo GH, Tan A, Button-Simons KA, Samarakoon U, Checkley LA, Pinapati RS, et al. Predicting functional and regulatory divergence of a drug resistance transporter gene in the human malaria parasite. BMC genomics. 2015; 16:115. doi: 10.1186/s12864-015-1261-6 PMID: 25765049

91. Barnes DA, Foote SJ, Galatis D, Kemp DJ, Cowman AF. Selection for high-level chloroquine resistance results in deamplification of the *pfmdr1* gene and increased sensitivity to mefloquine in *Plasmodium falciparum*. EMBO J. 1992; 11(8):3067–75. PMID: 1353446

92. Peel SA, Bright P, Yount B, Handy J, Baric RS. A strong association between mefloquine and halofantrine resistance and amplification, overexpression, and mutation in the P-glycoprotein gene homolog (*pfmdr*) of *Plasmodium falciparum in vitro*. Am J Trop Med Hyg. 1994; 51(5):648–58. PMID: 7985758

PLOS BIOLOGY

RESEARCH ARTICLE

Mechanistic basis for multidrug resistance and collateral drug sensitivity conferred to the malaria parasite by polymorphisms in PfMDR1 and PfCRT

Sarah Heckmatt Shafik*☯, Sashika Natasha Richards*☯, Ben Corry, Rowena Elizabeth Martin

Research School of Biology, The Australian National University, Canberra, Australian Capital Territory, Australia

☯ These authors contributed equally to this work.
* sarah.shafik@anu.edu.au (SHS); sashika.richards@anu.edu.au (SNR)

Check for updates

OPEN ACCESS

Citation: Shafik SH, Richards SN, Corry B, Martin RE (2022) Mechanistic basis for multidrug resistance and collateral drug sensitivity conferred to the malaria parasite by polymorphisms in PfMDR1 and PfCRT. PLoS Biol 20(5): e3001616. https://doi.org/10.1371/journal.pbio.3001616

Academic Editor: Andrew Fraser Read, The Pennsylvania State University, UNITED STATES

Received: August 23, 2021

Accepted: March 31, 2022

Published: May 4, 2022

Copyright: © 2022 Shafik et al. This is an open access article distributed under the terms of the Creative Commons Attribution License, which permits unrestricted use, distribution, and reproduction in any medium, provided the original author and source are credited.

Data Availability Statement: All relevant data are within the paper and its Supporting Information files.

Funding: This work was supported by the Australian Research Council (fellowship FT160100226 to R.E.M.), the National Health and Medical Research Council (project grant 1127338 to R.E.M. and fellowship 1053082 to R.E.M.), and the Australian Department of Education (Australian Postgraduate Awards to S.H.S. and S.N.R.). The funders had no role in study design, data collection

Abstract

Polymorphisms in the *Plasmodium falciparum* multidrug resistance protein 1 (*pfmdr1*) gene and the *Plasmodium falciparum* chloroquine resistance transporter (*pfcrt*) gene alter the malaria parasite's susceptibility to most of the current antimalarial drugs. However, the precise mechanisms by which PfMDR1 contributes to multidrug resistance have not yet been fully elucidated, nor is it understood why polymorphisms in *pfmdr1* and *pfcrt* that cause chloroquine resistance simultaneously increase the parasite's susceptibility to lumefantrine and mefloquine—a phenomenon known as collateral drug sensitivity. Here, we present a robust expression system for PfMDR1 in *Xenopus* oocytes that enables direct and high-resolution biochemical characterizations of the protein. We show that wild-type PfMDR1 transports diverse pharmacons, including lumefantrine, mefloquine, dihydroartemisinin, piperaquine, amodiaquine, methylene blue, and chloroquine (but not the antiviral drug amantadine). Field-derived mutant isoforms of PfMDR1 differ from the wild-type protein, and each other, in their capacities to transport these drugs, indicating that PfMDR1-induced changes in the distribution of drugs between the parasite's digestive vacuole (DV) and the cytosol are a key driver of both antimalarial resistance and the variability between multidrug resistance phenotypes. Of note, the PfMDR1 isoforms prevalent in chloroquine-resistant isolates exhibit reduced capacities for chloroquine, lumefantrine, and mefloquine transport. We observe the opposite relationship between chloroquine resistance-conferring mutations in PfCRT and drug transport activity. Using our established assays for characterizing PfCRT in the *Xenopus* oocyte system and in live parasite assays, we demonstrate that these PfCRT isoforms transport all 3 drugs, whereas wild-type PfCRT does not. We present a mechanistic model for collateral drug sensitivity in which mutant isoforms of PfMDR1 and PfCRT cause chloroquine, lumefantrine, and mefloquine to remain in the cytosol instead of sequestering within the DV. This change in drug distribution increases the access of lumefantrine and mefloquine to their primary targets (thought to be located outside of the DV), while simultaneously decreasing chloroquine's access to its target within the DV. The mechanistic insights

and analysis, decision to publish, or preparation of the manuscript.

Competing interests: The authors have declared that no competing interests exist.

Abbreviations: ABC, ATP-binding cassette; BLAST, Basic Local Alignment Search Tool; app Km, apparent Michaelis constant; app Vmax, apparent maximal velocity; DOPE, discrete optimized protein energy; DV, digestive vacuole; HA, hemagglutinin; NBD, nucleotide-binding domain; ne, nonexpressing oocytes; PfCRT, *Plasmodium falciparum* chloroquine resistance transporter; PfMDR1, *Plasmodium falciparum* multidrug resistance protein 1; PfNT1, *Plasmodium falciparum* nucleoside transporter 1; P-gp, P-glycoprotein; VMD, Visual Molecular Dynamics.

presented here provide a basis for developing approaches that extend the useful life span of antimalarials by exploiting the opposing selection forces they exert upon PfCRT and PfMDR1.

Introduction

Elucidating the molecular mechanisms that underpin the malaria parasite's acquisition of multidrug resistance is crucial to the ongoing efforts to control and eliminate malaria. Polymorphisms in 2 genes have been associated with many of the multidrug resistance phenotypes identified in field isolates of the parasite—the *Plasmodium falciparum* multidrug resistance protein 1 (*pfmdr1*) gene and the *Plasmodium falciparum* chloroquine resistance transporter (*pfcrt*) gene. Mutations in PfMDR1 and PfCRT, and/or variations in *pfmdr1* copy number, can alter the parasite's susceptibility to diverse pharmacons, including most of the current antimalarial drugs and a number of the antimalarial candidates in the development pipeline [1]. Moreover, certain field isoforms of PfMDR1 and PfCRT increase the parasite's susceptibility to lumefantrine, mefloquine, and dihydroartemisinin while simultaneously increasing resistance to chloroquine and amodiaquine [2–4]. However, the molecular basis for this pattern of collateral drug sensitivity—whereby resistance to one antimalarial drug causes sensitivity to another—remains unresolved.

PfMDR1 and PfCRT reside in the membrane of the parasite's digestive vacuole (DV), the lysosomal-type compartment (pH 5.0 to 5.5) in which many antimalarials accumulate, act, and/or are activated. Both proteins are therefore ideally positioned to modulate the parasite's susceptibility to many different drugs. In addition to their roles in mediating multidrug resistance, PfMDR1 and PfCRT are essential for parasite survival and are thus themselves potential drug targets [1,5]. Heterologous expression systems have been invaluable in characterizing the natural function of PfCRT as well as its roles in multidrug resistance [6–14]. PfCRT normally mediates the H^+-dependent transport of hemoglobin-derived peptides from the DV into the parasite's cytosol [10], but the mutations associated with drug resistance (which typically include K76T with either N75E or N326D [7,15–17]) alter its substrate range to include many other compounds, such as chloroquine, quinine, quinacrine, and methylene blue as well as the antiviral drug amantadine [6–9,18–22]. This enables the mutant isoforms of PfCRT to transport these drugs from the DV (where they would normally accumulate) back into the parasite's cytosol.

Considerably less is understood about the function(s) of PfMDR1. The *pfmdr1* polymorphisms linked to multidrug resistance and collateral drug sensitivity include N86Y and N1042D. These mutations are associated with reductions in the parasite's susceptibility to chloroquine (N86Y) [23–28] or quinine (N1042D) [29] as well as concomitant increases in the parasite's sensitivity to lumefantrine and mefloquine [3,4,23,24,29–35]. However, it is not clear how these mutations, or any other polymorphisms in *pfmdr1*, alter the parasite's susceptibility to drugs. PfMDR1 is a putative ATP-binding cassette (ABC) transporter (i.e., a pump that expends ATP to move solutes against their electrochemical gradients) and a homolog of the human P-glycoprotein (P-gp), which mediates multidrug resistance in cancer cells. The location of PfMDR1's ATPase domains at the cytosolic face of the membrane indicates that it transports solutes into the DV [36]. Attempts to characterize PfMDR1 in heterologous expression systems have not provided robust results and/or direct measurements of its transport activity [1]. For example, an attempt to express PfMDR1 in *Xenopus* oocytes resulted in a poor transport signal-to-background ratio [37], and other efforts did not make direct measurements of drug transport and thus only made inferences about PfMDR1's function from ATPase activity [38–41] (and one study was subsequently retracted [42]).

We sought to develop a reliable system for the heterologous expression of PfMDR1 that enables detailed examinations of its transport properties and thus a resolution of its roles in multidrug resistance and collateral drug sensitivity. Using *Xenopus* oocytes, we achieved a robust expression system that provides a very high transport signal-to-background ratio and which allows direct and high-resolution measurements of drug transport via PfMDR1. Our findings show that wild-type PfMDR1 transports structurally diverse antimalarial drugs, including lumefantrine, dihydroartemisinin, piperaquine, and methylene blue, as well as known substrates of human P-gp (e.g., vinblastine and rhodamine B [43–45]). We provide extensive validation of our system by showing, for example, (1) time and ATP dependence of PfMDR1-mediated transport; (2) inhibition of PfMDR1 by inhibitors of human P-gp; and (3) an absence of an interaction with amantadine (which also does not interact with human P-gp [46–48]).

In all bar one case, the introduction of field-derived mutations into PfMDR1 reduces the protein's drug transport activity, and we also observe differences in transport capacities between the mutant isoforms as well as between drugs for a given isoform. The single exception is a mutant isoform that exhibits enhanced transport, relative to wild-type PfMDR1, of the antimalarials quinine and quinidine. By generating a homology model of PfMDR1, we highlight the interactions between quinine and the binding cavity of the transporter and propose that this creates an alternative binding site specific for quinine and quinidine.

Sequestration of a drug away from its primary target is a commonly observed resistance mechanism, and our finding of diverse transport capacities across multiple field isoforms of PfMDR1 suggests that the redistribution of drugs between the DV and the cytosol is a key mechanism by which polymorphisms in *pfmdr1* contribute to multidrug resistance phenotypes. We extend these mechanistic insights by delineating the roles of PfMDR1 and PfCRT in the collateral drug sensitivity patterns observed for lumefantrine, mefloquine, and chloroquine in the malaria parasite. We demonstrate that wild-type PfMDR1 has a greater capacity for the transport of these drugs than the mutant PfMDR1 isoforms. We observe the opposite trend for PfCRT: The mutations that confer chloroquine transport activity upon PfCRT also allow the protein to transport lumefantrine and mefloquine, whereas the wild-type protein lacks these activities. Hence, when present together, mutant isoforms of PfMDR1 and PfCRT change the distribution of these 3 drugs, such that they remain in the cytosol rather than accumulating within the DV. This evidently increases the access of lumefantrine and mefloquine to their primary targets (mefloquine is thought to act in the parasite cytosol [49,50] and the target(s) of lumefantrine are currently unknown) and thereby enhances their antimalarial activities. By contrast, the killing effect of chloroquine, which is primarily exerted against the detoxification of heme within the DV [51,52], is greatly diminished. Together, our datasets provide significant new mechanistic insights into how PfMDR1 and PfCRT contribute to multidrug resistance phenotypes.

Results

Expression and functional characterization of human P-gp and PfMDR1 in *Xenopus* oocytes

Since human transporters are relatively straightforward to express in oocytes [53], human P-gp was first expressed in *Xenopus* oocytes to optimize the expression conditions and to develop a transport assay. The optimized methods were then applied to PfMDR1. Direct measurements of transport via human P-gp were undertaken by microinjecting a tritiated version of vinblastine ([^{3}H]vinblastine; a known substrate of human P-gp) into the oocyte and measuring its efflux (Fig 1A). Given that the relationship between the quantity of cRNA microinjected into the oocyte and the level of [^{3}H]vinblastine transport measured was approximately linear between 2.5 and 10 ng (Fig 1B), all subsequent experiments used oocytes microinjected with 10 ng of human P-gp cRNA. Next, we determined that the transport of [^{3}H]vinblastine via human P-gp was approximately linear with time for at least 2 hours (Fig 1C). Hence, all of the subsequent transport measurements were made at 1.5 hours. To confirm that the [^{3}H]vinblastine transport detected in these assays was mediated by human P-gp (and was not due to the nonspecific leakage of [^{3}H]vinblastine from the oocyte), compounds known to interact with the transporter (nicardipine [46,54], PSC833 [55,56], vanadate [57,58], and verapamil [46,59]) were shown to inhibit [^{3}H]vinblastine efflux (Fig 1D and S2 Fig). Furthermore, [^{3}H]vinblastine transport was unaffected by amantadine—a drug that human P-gp does not interact with [46–48] (Fig 1D). Finally, we showed that other known substrates of human P-gp, such as rhodamine B, quinacrine, and methylene blue, are also transported by human P-gp in our oocyte system (S1 Data). The negative controls used in these experiments were nonexpressing oocytes (ne) and those expressing an unrelated transporter, the *Plasmodium falciparum* nucleoside transporter 1 (PfNT1; S1 Fig) [60,61]. The low level leakage of [^{3}H]vinblastine from the negative control oocytes is most likely due to the simple diffusion of the neutral species of the drug (Fig 1C and 1D). Together, these datasets confirmed that we had achieved the functional expression of human P-gp in *Xenopus* oocytes, with the optimization process yielding relatively high rates of transport for vinblastine (304 ± 10 fmol/oocyte/h) and for other known substrates of human P-gp (S1 Data), as well as a high transport signal-to-background ratio (approximately 28-fold).

The optimized method and assays were then applied to wild-type PfMDR1 (PfMDR1^{NYSND}), 5 field mutant isoforms of PfMDR1 (PfMDR1^{NFSDD}, PfMDR1^{YYSND}, PfMDR1^{FYSND}, PfMDR1^{YFSND}, and PfMDR1^{NFCDY}), and a catalytically inactive version of PfMDR1^{NYSND} (Fig 1E, S1 Table, S3 Fig, and S1 File). The latter contains mutations in the protein's nucleotide-binding domains (NBDs) that impede ATP hydrolysis. Immunofluorescence assays confirmed the presence of hemagglutinin (HA)-tagged versions of each isoform at the oocyte plasma membrane (Fig 1F and S4 Fig). Furthermore, PfMDR1 was shown to adopt the same orientation in the oocyte plasma membrane as it does in the membrane of the parasite's DV [36], with its amino terminus and carboxyl terminus located in the cytosol (S4 Fig). Semi-quantitative western blot analyses and densitometric evaluations of total protein confirmed that each of the PfMDR1 isoforms were expressed at comparable levels in the oocyte membrane (Fig 1G, S5 Fig, and S1 Text). Hence, any differences in drug transport activity between these PfMDR1 isoforms can be attributed to differences in their transport properties (and the mutations they carry), rather than to differences in expression levels.

All 6 field isoforms of PfMDR1 transported [^{3}H]vinblastine, albeit to varying degrees (Fig 1H). The catalytically inactive version of PfMDR1^{NYSND} exhibited a very low level of [^{3}H]vinblastine transport activity, consistent with the mutations in the NBDs hampering ATP hydrolysis. The ability of PfMDR1^{NYSND} to transport [^{3}H]lumefantrine was then tested in the absence or presence of human P-gp inhibitors (Fig 1I). The PfMDR1^{NYSND}-mediated transport of [^{3}H]lumefantrine was inhibited by nicardipine, PSC833, vanadate, and verapamil, but was unaffected by amantadine (Fig 1I and S2 Fig). The relationship between the quantity of PfMDR1^{NYSND} cRNA microinjected into the oocyte and the level of [^{3}H]lumefantrine transport achieved was very similar to that obtained for [^{3}H]vinblastine transport via human P-gp (with 10 ng of PfMDR1^{NYSND} cRNA falling within the linear range) (Fig 1J) and the transport of [^{3}H]lumefantrine via PfMDR1^{NYSND} was also approximately linear with time for at least 2

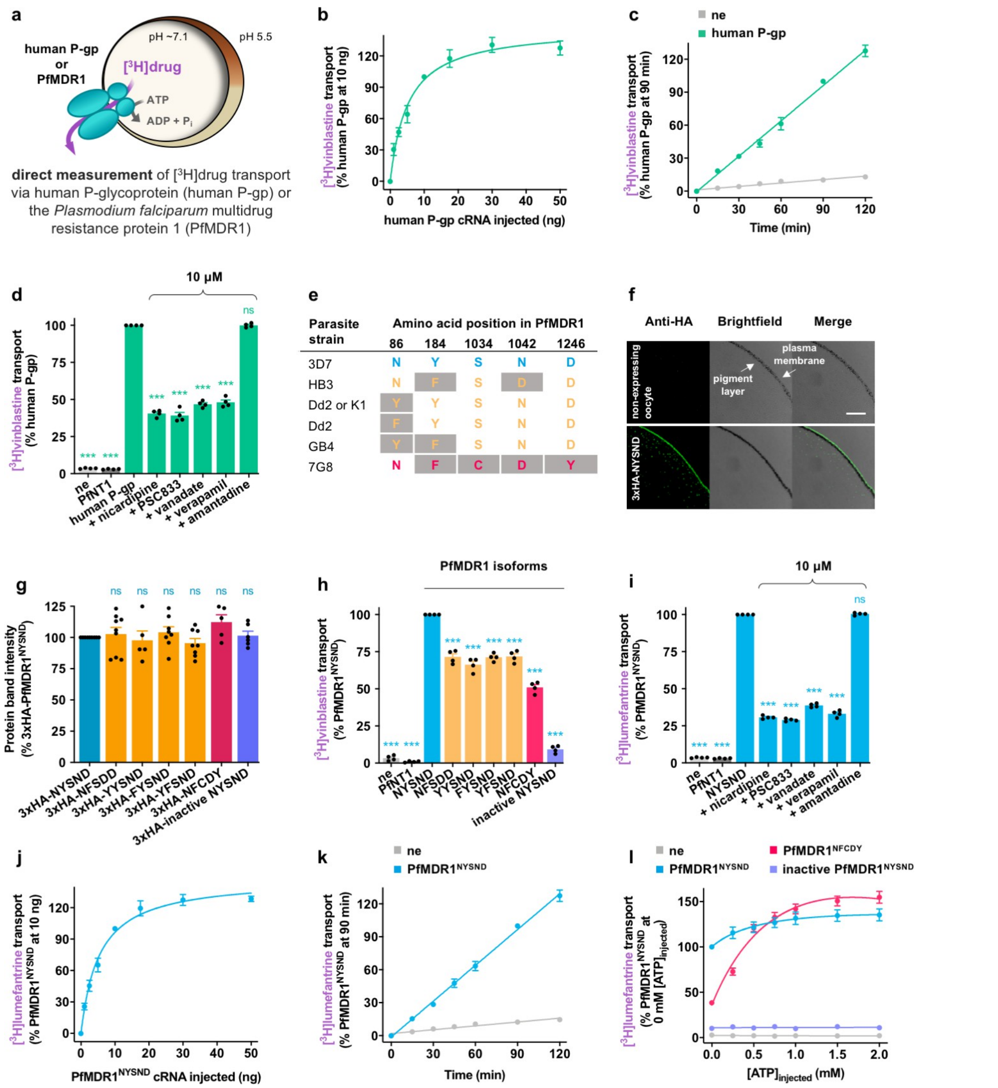

Fig 1. Heterologous expression of functional human P-gp and PfMDR1 in *Xenopus* oocytes. **(a)** Schematic showing the transport of a $[^{3}\text{H}]$drug via human P-gp or PfMDR1 in the *Xenopus* oocyte system. **(b)** The relationship between the quantity of human P-gp cRNA injected into the oocyte and the level of human P-gp–mediated $[^{3}\text{H}]$vinblastine transport measured. **(c)** The transport of $[^{3}\text{H}]$vinblastine via human P-gp was approximately linear with time for at least 2 hours. **(d)** The human P-gp–mediated efflux of $[^{3}\text{H}]$vinblastine from oocytes was reduced by known inhibitors of the transporter (nicardipine, PSC8333, vanadate, and verapamil) and was unaffected by amantadine (a drug that does not interact with human P-gp). **(e)** The field isoforms of PfMDR1 characterized in this study. Residues that differ from the wild-type amino acid sequence are shaded gray. **(f)** Immunofluorescence microscopy images confirmed that PfMDR1 localized to the oocyte plasma membrane. The expression of 3xHA-tagged PfMDR1^{NYSND} resulted in a fluorescent band external to the pigment layer, indicating that the protein was expressed at the oocyte surface. The band was not present in ne. The length of the scale bar is 50 μm. Images showing the presence of the other HA-tagged PfMDR1 isoforms at the oocyte surface are shown in S4 Fig. **(g)** Semiquantification of PfMDR1 protein levels in the membranes of oocytes expressing different 3xHA-PfMDR1 isoforms indicated that the 7 isoforms were expressed at similar levels. **(h)** The transport of $[^{3}\text{H}]$vinblastine via PfMDR1. **(i)** The efflux of $[^{3}\text{H}]$lumefantrine from oocytes expressing PfMDR1^{NYSND} was reduced by nicardipine, PSC8333, vanadate, and verapamil and was unaffected by amantadine. **(j)** The relationship between the quantity of PfMDR1^{NYSND} cRNA microinjected into the oocyte and the level of PfMDR1^{NYSND}-mediated $[^{3}\text{H}]$lumefantrine transport measured. **(k)** The transport of $[^{3}\text{H}]$lumefantrine via PfMDR1^{NYSND} was approximately linear with time for at least 2 hours. **(l)** Microinjection of additional ATP into the oocyte greatly stimulated $[^{3}\text{H}]$lumefantrine transport via PfMDR1^{NFCDY}. The data are the mean of $n = 4$ to 9 independent experiments, each yielding similar results and overlaid as individual data points in panels **d**, **g**, **h**, and **i**, and the error is the SEM. Where not visible, the error bars fall within the symbols. The asterisks denote a significant difference from human P-gp (panel **d**), 3xHA-PfMDR1^{NYSND} (panel **g**), or PfMDR1^{NYSND} (panels **h** and **i**); $^{***}P < 0.001$, ns, not significant (1-way ANOVA). The data underlying this figure is supplied in S3 Data. ne, nonexpressing oocytes; PfMDR1, *Plasmodium falciparum* multidrug resistance protein 1; P-gp, P-glycoprotein.

https://doi.org/10.1371/journal.pbio.3001616.g001

hours (Fig 1K). Furthermore, as was the case for human P-gp, a high rate of vinblastine transport (275 ± 3 fmol/oocyte/h) and a high transport signal-to-background ratio (approximately 29-fold) were obtained for PfMDR1^{NYSND}. The microinjection of ATP into the oocyte greatly stimulated [^{3}H]lumefantrine transport via PfMDR1^{NFCDY} but had a milder effect on PfMDR1^{NYSND} (Fig 1L). This is consistent with previous reports that D1246Y (located in NBD 2 of PfMDR1^{NFCDY}) impedes ATP hydrolysis [39] and that PfMDR1^{NFCDY} has a lower basal ATPase activity than the wild-type protein [39,40].

Field isoforms of PfMDR1 differ significantly in their capacities for antimalarial drug transport

Our achievement of a robust expression system for PfMDR1 enabled direct characterizations of its function and of how this varies between different isoforms of the protein. We found that the 6 field isoforms of PfMDR1 exhibited varying capacities for the transport of a broad range of drugs and related compounds (Figs 2–4, S1 Data, and S2 Text). All of the antimalarial drugs tested—lumefantrine, mefloquine, chloroquine, quinine, quinidine, amodiaquine, piperaquine, dihydroartemisinin, methylene blue, and quinacrine—were shown to be substrates of the PfMDR1 isoforms included for study. The PfMDR1 isoforms also transported vinblastine and rhodamine B (known substrates of human P-gp), but none of the proteins transported amantadine (Fig 2 and S1 Data). The rates of antimalarial drug transport via PfMDR1^{NYSND} (in fmol/oocyte/h) were as follows: lumefantrine (731 ± 22), mefloquine (657 ± 23), amodiaquine (552 ± 11), chloroquine (531 ± 18), piperaquine (491 ± 17), quinidine (439 ± 11), quinine (432 ± 13), quinacrine (356 ± 11), methylene blue (333 ± 10), and dihydroartemisinin (293 ± 10). The low level of drug efflux observed from the negative control oocytes was most likely due to the simple diffusion of the neutral drug species.

In almost all cases, the introduction of mutations into PfMDR1^{NYSND} caused a significant reduction in drug transport activity. The most striking example of this observation was PfMDR1^{NFCDY}, which had the lowest level of transport activity for all of the compounds tested (Figs 2–4 and S1 Data). The rates of antimalarial drug transport via PfMDR1^{NFCDY} (in fmol/oocyte/h) and the corresponding fold change relative to drug transport via PfMDR1^{NYSND} were as follows: lumefantrine (299 ± 23, approximately 0.4-fold), chloroquine (286 ± 11, approximately 0.5-fold), piperaquine (223 ± 9, approximately 0.5-fold), quinidine (191 ± 8, approximately 0.4-fold), quinine (188 ± 10, approximately 0.4-fold), mefloquine (175 ± 7, approximately 0.3-fold), amodiaquine (155 ± 9, approximately 0.3-fold), quinacrine (121 ± 4, approximately 0.3-fold), methylene blue (108 ± 3, approximately 0.3-fold), and dihydroartemisinin (92 ± 3, approximately 0.3-fold).

No 2 drugs produced the same profile of transport activities across the 6 field isoforms of PfMDR1. There were, however, strong similarities between some of the datasets (see S3 Text for an extended analysis). For example, commonalities were evident within the following groups (1) lumefantrine and mefloquine; (2) chloroquine and piperaquine; (3) mefloquine, quinine, quinidine, and dihydroartemisinin; and (4) lumefantrine, methylene blue, and quinacrine (Figs 2 and 4, and S3 Text).

Characterization of lumefantrine, mefloquine, and chloroquine transport via PfMDR1

Having identified that the 6 field isoforms of PfMDR1 exhibit different capacities for the transport of lumefantrine, mefloquine, and chloroquine (Fig 2A–2C), we characterized the interactions of these 3 drugs with the transporter in more detail. A kinetic analysis of the

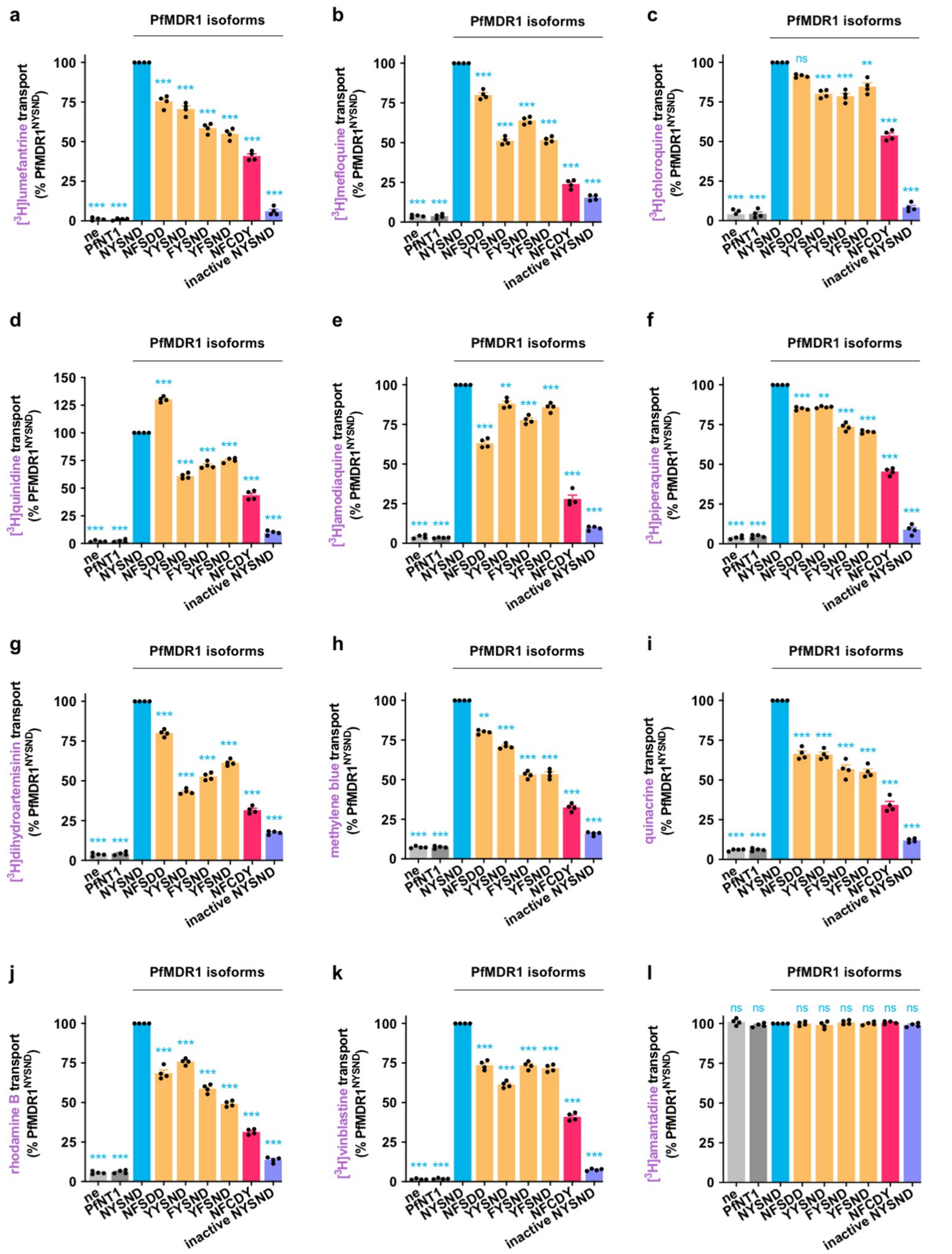

Fig 2. Field isoforms of PfMDR1 differ significantly in their capacities for antimalarial drug transport. (a–i) Field isoforms of PfMDR1 transported the antimalarial drugs [^{3}H]lumefantrine (a), [^{3}H]mefloquine (b), [^{3}H]chloroquine (c), [^{3}H]quinidine (d), [^{3}H]amodiaquine (e), [^{3}H]piperaquine (f), [^{3}H]dihydroartemisinin (g), methylene blue (h), and quinacrine (i). **(j–l)** All of the field isoforms of PfMDR1 also transported the human P-gp substrates rhodamine B (j) and [^{3}H]vinblastine (k), but none transported [^{3}H]amantadine (l). The transport of methylene blue, quinacrine, and rhodamine B was detected using the intrinsic fluorescence of these compounds and a fluorescence-based transport assay (see S2 Text). The data are the mean of $n = 4$ independent experiments (each yielding similar results and overlaid as individual data points), and the error is the SEM. The asterisks denote a significant difference from PfMDR1^{NYSND}; $^{*}P < 0.05$, $^{**}P < 0.01$, $^{***}P < 0.001$, ns, not significant (1-way ANOVA). The data underlying this figure is supplied in S3 Data. ne, nonexpressing oocytes; PfMDR1, *Plasmodium falciparum* multidrug resistance protein 1.

https://doi.org/10.1371/journal.pbio.3001616.g002

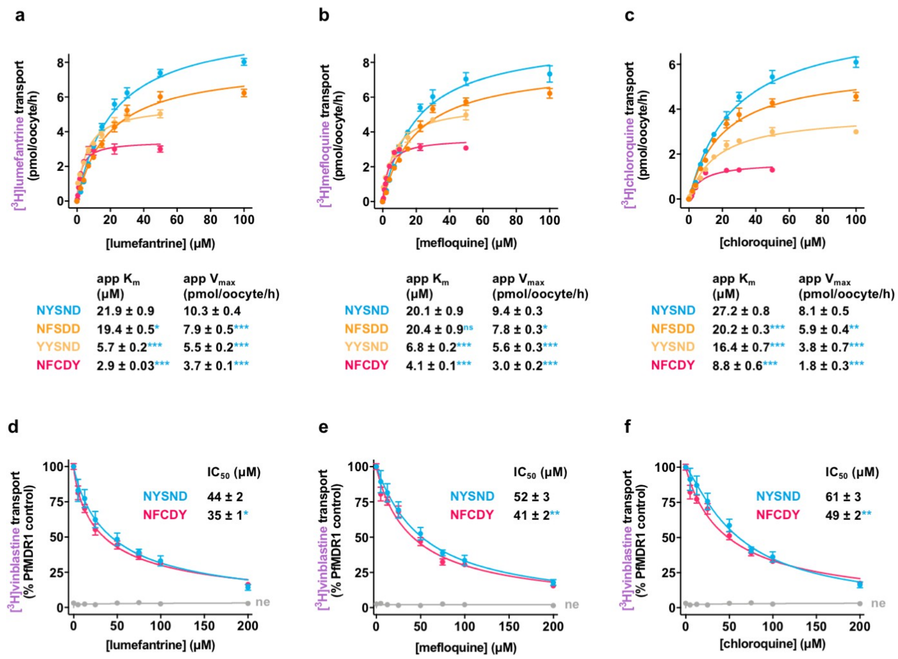

Fig 3. Characterization of lumefantrine, mefloquine, and chloroquine transport via PfMDR1. (a–c) There were significant differences in the apparent kinetic parameters of lumefantrine (a), mefloquine (b), and chloroquine (c) transport between field isoforms of PfMDR1. The concentration dependence of PfMDR1-mediated drug transport was calculated by subtracting the leakage from ne from that of oocytes expressing a PfMDR1 isoform at each drug concentration. **(d–f)** The transport of [^{3}H]vinblastine via PfMDR1 was inhibited by lumefantrine (d), [^{3}H]mefloquine (e), and [^{3}H]chloroquine (f). The data are the mean of $n = 4$ independent experiments (each yielding similar results), and the error is the SEM. The asterisks denote a significant difference from PfMDR1^{NYSND}; $^{*}P < 0.05$, $^{**}P < 0.01$, $^{***}P < 0.001$, ns nonsignificant (1-way ANOVA). The data underlying this figure is supplied in S3 Data. ne, nonexpressing oocytes; PfMDR1, *Plasmodium falciparum* multidrug resistance protein 1.

https://doi.org/10.1371/journal.pbio.3001616.g003

PfMDR1-mediated transport of lumefantrine, mefloquine, and chloroquine revealed that the apparent Michaelis constant (app K_m) and the apparent maximal velocity (app V_{max}) values decreased in the order PfMDR1^{NYSND} ≥ PfMDR1^{NFSDD} > PfMDR1^{YYSND} > PfMDR1^{NFCDY} (Fig 3A–3C). Hence, PfMDR1^{NFCDY} has both the lowest app K_m and the lowest app V_{max} for all 3 antimalarials. PfMDR1^{NFCDY} is the only isoform included in this study that contains D1246Y. This mutation is located upstream of the Q-loop within NBD 2, which is thought to be involved in coordinating Mg^{2+} for ATP hydrolysis and/or in facilitating conformational changes of the NBDs in human P-gp [62–65]. Thus, it is possible that D1246Y disrupts ATP hydrolysis and/or the coupling of ATP hydrolysis to drug transport in PfMDR1, and that this contributes to the lower drug transport activity exhibited by PfMDR1^{NFCDY}.

A subset of experiments measuring the abilities of lumefantrine, mefloquine, and chloroquine to inhibit [^{3}H]vinblastine transport via PfMDR1^{NYSND} and PfMDR1^{NFCDY} was performed to ascertain whether these drugs are potent inhibitors of the transporter. None of the antimalarials were potent inhibitors of transport via either isoform of the protein, with all 3 drugs producing IC_{50}s that are 20- to 11-fold higher than those obtained with nicardipine (Fig 3D–3F and S2 Fig). Moreover, in all cases, the antimalarials were slightly more effective in inhibiting transport via the mutant field isoform. This is not the trend that would be expected if these drugs exerted an antimalarial effect against wild-type PfMDR1 (e.g., by blocking the transport of its (currently unknown) natural substrates) that is alleviated by the introduction of mutations into the transporter.

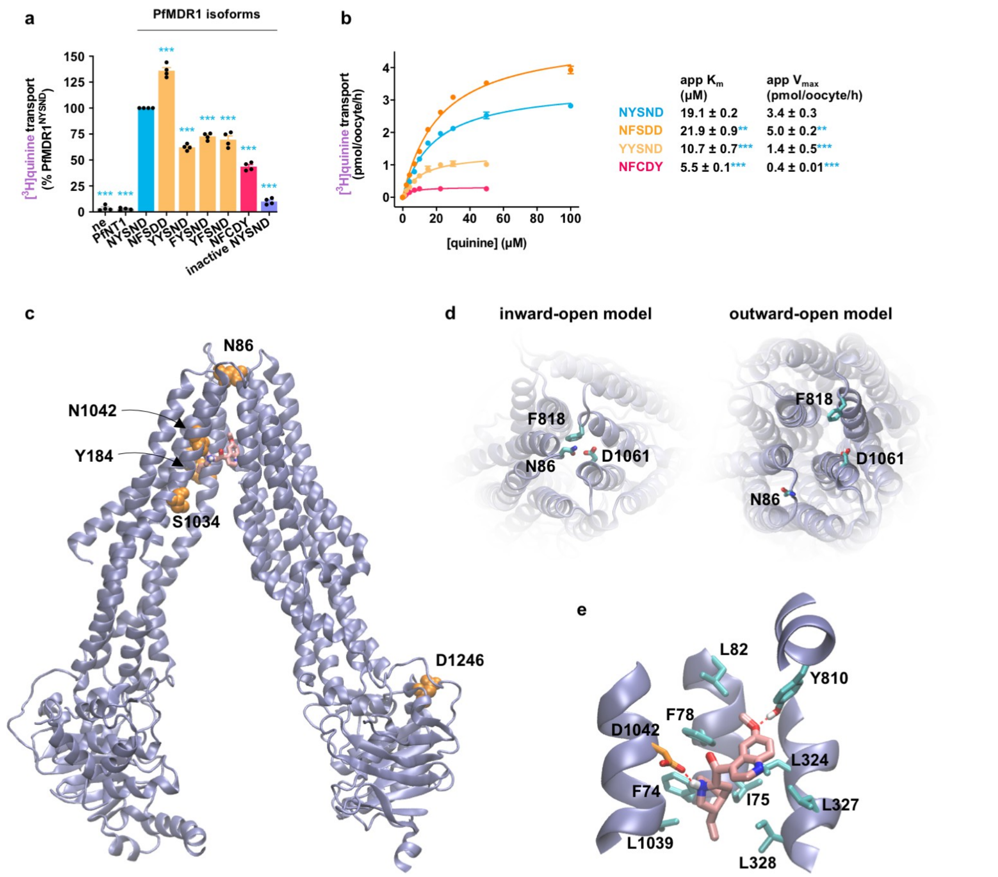

Fig 4. Quinine transport via PfMDR1. **(a)** Field isoforms of PfMDR1 transported [^{3}H]quinine, with PfMDR1^{NFSDD} exhibiting the highest level of quinine transport activity. **(b)** There were significant differences in the apparent kinetic parameters for quinine transport via field isoforms of PfMDR1. The concentration dependence of PfMDR1-mediated quinine transport was calculated by subtracting the leakage from ne from that of oocytes expressing a PfMDR1 isoform at each drug concentration. The data are the mean of $n = 4$ independent experiments (each yielding similar results and overlaid as individual data points in panel **a**), and the error is the SEM. The asterisks denote a significant difference from PfMDR1^{NYSND}; $^{**}P < 0.01$ and $^{***}P < 0.001$ (1-way ANOVA). The data underlying panels **a** and **b** of this figure is supplied in S3 Data. **(c)** Inward-open homology model of PfMDR1 based on the *C. elegans* P-gp crystal structure (PDB 4F4C) showing the location of the mutations found in the 5 field PfMDR1 isoforms characterized in this study (orange). A putative binding pose of quinine in the central cavity is shown (pink). **(d)** A comparison of the inward-open model and outward-open models (based on the crystal structure of human P-gp; PDB 6C0V) as viewed from the side of the protein facing into the DV lumen. The N86Y mutation is part of a cluster of 3 residues forming the extracellular gate of the transporter (the participating residues are shown). These 3 residues are in close proximity in the inward-open state but move apart in the outward-open conformation. **(e)** Putative quinine binding site in PfMDR1^{NFSDD}. Amino acids interacting with quinine are indicated (apart from L71, I1071, and F1072 that are removed to clearly view the binding pose). Atoms are shaded as follows: carbon in quinine, pink; carbon in the 1042D residue, orange; nitrogen, blue; oxygen, red; hydrogen, white. ne, nonexpressing oocytes; PfMDR1, *Plasmodium falciparum* multidrug resistance protein 1; P-gp, P-glycoprotein.

https://doi.org/10.1371/journal.pbio.3001616.g004

Quinine transport via PfMDR1

Although the addition of mutations to PfMDR1^{NYSND} reduced drug transport activity in most cases, there were 2 exceptions to this trend. The introduction of the Y184F and N1042D mutations—yielding PfMDR1^{NFSDD}—increased the protein's capacity for the transport of both quinine and its stereoisomer quinidine (Figs 2D and 4A). A kinetic analysis of quinine transport via PfMDR1 revealed several valuable insights (Fig 4B). First, the range of app K_m values obtained for quinine transport via the different PfMDR1 isoforms (5.5 ± 0.1 μM to 21.9 ± 0.9 μM) was similar to those observed for the transport of lumefantrine, mefloquine, and chloroquine (e.g., the lumefantrine app K_m values ranged from 2.9 ± 0.03 μM to 21.9 ± 0.9 μM). By contrast, the app V_{max} values for quinine transport (0.4 ± 0.01 to 5.0 ± 0.2 pmol/oocyte/h) were lower than those obtained for the other 3 drugs (e.g., the lumefantrine app V_{max} values were 3.7 ± 0.1 to 10.3 ± 0.4 pmol/oocyte/h). In general terms, these observations indicate that quinine occupies the transporter's binding cavity for a much longer period than lumefantrine, mefloquine, or chloroquine. It is possible that in the parasite, this relatively low rate of quinine translocation impedes the transport of the natural substrates of PfMDR1.

The second key observation from the kinetic analysis of quinine transport was the finding that PfMDR1^{NFSDD} has a higher app V_{max} (5.0 ± 0.2 pmol/oocyte/h versus 3.4 ± 0.3 pmol/oocyte/h) as well as a slightly higher app K_m (21.9 ± 0.9 μM versus 19.1 ± 0.2 μM) than the wild-type protein (Fig 4A and 4B). We sought a structural explanation for this unusual result by generating a homology model of PfMDR1 to determine how quinine interacts with the transporter's binding cavity.

Two homology models of PfMDR1 have previously been generated using either the bacterial MsbA protein or mouse P-gp as the template sequences [66,67]. However, the low sequence identity between PfMDR1 and these sequences (26% to 29%) reduces the versatility of these homology models. We identified the recently elucidated structures of *Caenorhabditis elegans* P-gp [68] and human P-gp [69], which have slightly higher sequence identity (33%), as better templates for inward-open and outward-open homology models of PfMDR1 (S1 File), although structural predictions should still be made with caution at this level of sequence identity. The locations of the 5 field mutations are depicted in the inward-open model of PfMDR1 (Fig 4C). Consistent with previous reports, both S1034 and N1042 line the central cavity (where they could interact with substrates), Y184 faces into the membrane, and D1246 is located in NBD 2 of the protein [66,67]. However, contrary to previous models that suggested that N86 forms part of the substrate-binding cavity [66,67], our inward-open model proposes that N86 is located on the side of the protein that faces into the DV lumen, forming part of the gate and obscuring the central cavity of the protein from this compartment (Fig 4D). A comparison with the outward-open model shows that the residues in this gate (N86, F818, and D1061) move far apart to expose the substrate-binding cavity to the DV lumen (Fig 4D). Thus, it is plausible that mutation of N86 could alter these interactions and consequently stabilize the inward-open conformation.

Since the Y184F mutation in PfMDR1^{NFSDD} protrudes into the membrane (rather than into the binding cavity), it is unlikely to be involved in coordinating quinine. Thus, it is more likely that the N1042D mutation is the cause of the enhanced quinine transport activity exhibited by PfMDR1^{NFSDD}. To investigate this hypothesis, we used molecular dynamics simulations of PfMDR1 containing N1042D to examine the likely binding poses of quinine in the binding cavity. Seven simulations were performed, each with a different random starting position and orientation of quinine inside the substrate-binding cavity. In 4 of the 7 simulations, quinine quickly moved to interact with 1042D (within 20 ns; S6 Fig). This interaction with the negatively charged carboxylate oxygen of the aspartate residue occurred through the protonated nitrogen on the cyclic amine ring of quinine. Indeed, quinine adopted a very stable position in a predominantly hydrophobic pocket in which 3 of the 4 polar atoms on the molecule found hydrogen bonding partners on the protein (stabilized by the nitrogen on the cyclic amine ring, as well as the central hydroxyl group on the quinine molecule forming hydrogen bonds with 1042D, in addition to the ether oxygen of quinine forming a hydrogen bond with Y810; Fig 4E). Thus, the stability of the putative quinine binding site (as determined in our simulations) could plausibly represent an alternative binding site for the drug in PfMDR1^{NFSDD} that is not present in the other isoforms. This could alter the rate of quinine transport by influencing the rate of the protein conformational change or, perhaps less likely, ligand unbinding.

Correlations between rates of drug transport via PfMDR1 in *Xenopus* oocytes and in vitro drug resistance indices

We used the PfMDR1-mediated rates of lumefantrine, mefloquine, chloroquine, and quinine transport obtained in the *Xenopus* oocyte system (S1 Data) to determine relationships between the drug transport capacities of the different PfMDR1 field isoforms and the in vitro drug response of parasite strains that express these proteins. In vitro drug resistance indices were calculated using IC_{50} values collated from the literature [16,23,24,26,70–86] (S3 Table) and then plotted against the PfMDR1-mediated transport rate for the relevant drug and parasite strain. We found strong positive correlations for lumefantrine (Pearson correlation coefficient = 0.76; Fig 5A and S3 Text) and mefloquine (Pearson correlation coefficient = 0.75; Fig 5B and S3 Text), and a strong negative correlation for chloroquine (Pearson correlation coefficient = −0.86; Fig 5C and S3 Text). No correlation was found between the rate of quinine transport via PfMDR1 and the in vitro quinine response (Fig 5D and S4 Text).

Transport of lumefantrine and mefloquine via PfCRT in *Xenopus* oocytes and in situ

We sought to elucidate the role of PfCRT in modulating the parasite's response to lumefantrine and mefloquine by measuring its ability to transport these drugs in *Xenopus* oocytes (see S2 Table and S3 Fig for the positions of the mutations in the PfCRT isoforms studied here). Wild-type PfCRT ($PfCRT^{3D7}$) did not transport lumefantrine or mefloquine, whereas 2 chloroquine resistance-conferring isoforms of PfCRT ($PfCRT^{7G8}$ and $PfCRT^{Dd2}$) exhibited significant transport of both drugs (Fig 6A and 6D and S7 Fig). The transport of lumefantrine and mefloquine via $PfCRT^{7G8}$ and $PfCRT^{Dd2}$ was inhibited by compounds known to interact with the transporter, including verapamil [6,18], chlorpheniramine [90], and saquinavir [10,91], but was unaffected by histidine and the dipeptide LH (neither of which interact with PfCRT [10,91]) (Fig 6A and 6D, and S7 Fig). Lumefantrine and mefloquine transport via $PfCRT^{7G8}$ and $PfCRT^{Dd2}$ was saturable, with $PfCRT^{Dd2}$ having a slightly lower affinity and a higher capacity for drug transport relative to $PfCRT^{7G8}$ (Fig 6B and 6E). When compared with chloroquine transport via $PfCRT^{Dd2}$ (K_m = 232 ± 11 μM; V_{max} = 61 ± 6 pmol/oocyte/h [7]), the transport of lumefantrine and mefloquine is a high-affinity, low-capacity process.

Lumefantrine and mefloquine were shown to inhibit the transport of a natural substrate of PfCRT (the hemoglobin-derived hexapeptide VDPVNF [10]) via all 3 isoforms (Fig 6C and 6F). However, all of the resulting IC_{50}s were above 45 μM, which is substantially higher than the IC_{50}s previously obtained for the quinine dimer "Q_2C" (IC_{50}s = 0.01 to 0.6 μM)—a drug that has been established as exerting an antiplasmodial effect via its potent inhibition of PfCRT's natural function [10,92]. The lumefantrine and mefloquine IC_{50}s are also significantly higher than those observed for 2 other inhibitors of PfCRT—verapamil (IC_{50}s = 6.8 to 17.5 μM) and chlorpheniramine (IC_{50}s = 5.0 to 9.8 μM)—but are very similar to the IC_{50}s obtained with chloroquine (e.g., 110 ± 5.9 μM against $PfCRT^{3D7}$ and 53 ± 2.8 μM against $PfCRT^{Dd2}$) [10]. It seems unlikely, therefore, that lumefantrine and mefloquine possess significant anti-PfCRT activity.

We then tested whether $PfCRT^{7G8}$ and $PfCRT^{Dd2}$ transport lumefantrine and mefloquine within their native environment in the DV membrane of live parasites. The transport of lumefantrine and mefloquine via PfCRT was measured in situ using the "H^+-efflux assay" with a set of *P. falciparum* transfectants—the $C2^{GC03}$, $C6^{7G8}$, and $C4^{Dd2}$ lines—that are isogenic except for the *pfcrt* allele. These lines express either $PfCRT^{3D7}$ ($C2^{GC03}$), $PfCRT^{7G8}$ ($C6^{7G8}$), or $PfCRT^{Dd2}$ ($C4^{Dd2}$) [17]. Lumefantrine and mefloquine enter the DV via simple diffusion of the neutral species and also via PfMDR1 (Figs 2 and 3), where they become protonated in the

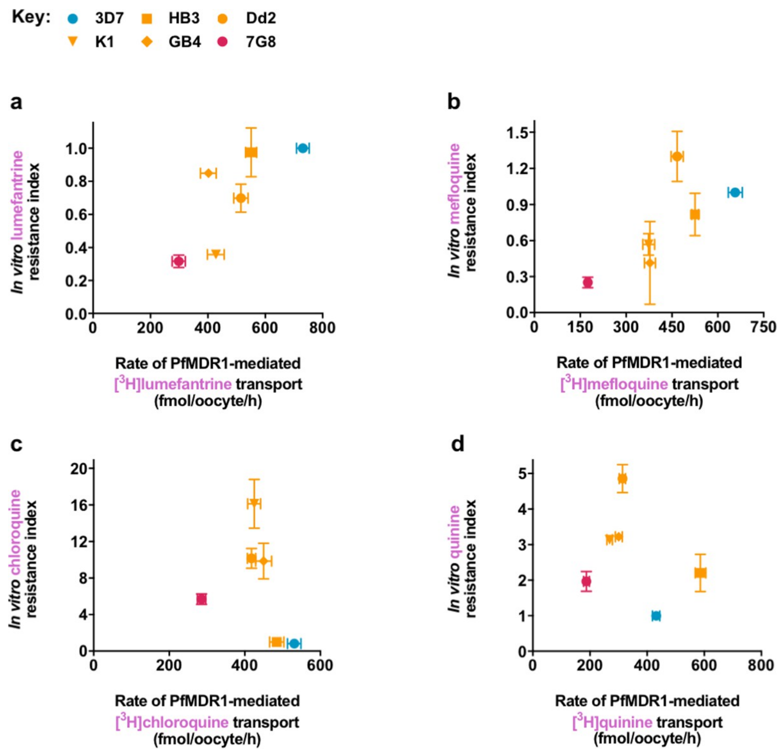

Fig 5. Correlations between rates of drug transport via PfMDR1 in *Xenopus* oocytes and in vitro parasite drug resistance indices. The rates of PfMDR1-mediated transport of lumefantrine, mefloquine, chloroquine, and quinine (Figs 2 and 4, and S1 Data) were plotted against the in vitro resistance index for the relevant drug and parasite strain (S3 Table). Where not shown, error bars fall within the symbols. **(a)** A positive correlation was observed between the rate of lumefantrine transport via PfMDR1 and the in vitro lumefantrine response (Pearson correlation coefficient = 0.76, $r^2 = 0.58$, $P = 0.078$). **(b)** A positive correlation was observed between the rate of mefloquine transport via PfMDR1 and the in vitro mefloquine response (Pearson correlation coefficient = 0.75, $r^2 = 0.56$, $P = 0.008$). The data point for Dd2 is an outlier and its removal significantly improved the correlation (Pearson correlation coefficient = 0.97, $r^2 = 0.94$, $P = 0.006$). Dd2 parasites typically harbor 2 to 4 copies of PfMDR1 and have been reported to express greater levels of PfMDR1 than the other parasite strains included in the analysis [85,87]. Given that *pfmdr1* amplification has been associated with mefloquine resistance [30–32,88,89], it is possible that the overexpression of PfMDR1 in Dd2 parasites imparts a higher level of resistance to this strain (see S3 Text for an extended analysis). **(c)** An inverse correlation was observed between the rate of chloroquine transport via PfMDR1 and the in vitro chloroquine response. The removal of the 7G8 data point (see S3 Text for an extended analysis) resulted in a stronger correlation between the rate of chloroquine transport via PfMDR1 and the parasite's chloroquine response in vitro (Pearson correlation coefficient = −0.86, $r^2 = 0.74$, $P = 0.054$). **(d)** There was no correlation between the rate of quinine transport via PfMDR1 and the in vitro quinine response (see S4 Text for an extended analysis). The data for the in vitro resistance indices are the mean of $n = 2$ to 18 published studies, and the data for the PfMDR1-mediated drug transport rates are the mean of $n = 4$ independent experiments. The error is the SEM except for the in vitro resistance indices that were calculated from 2 studies, in which case the error is the range/2. The data underlying this figure is supplied in S3 Data. PfMDR1, *Plasmodium falciparum* multidrug resistance protein 1.

https://doi.org/10.1371/journal.pbio.3001616.g005

acidic lumen. The H^+-efflux assay uses a fluorescent pH-sensitive probe to provide an indirect method of detecting the efflux of protonated drugs from the DV via PfCRT, which manifests as an increase in the rate of DV alkalinization. The positive controls were chloroquine and saquinavir (a peptide mimic that is a substrate of all 3 PfCRT isoforms [10]). Consistent with previous reports [9,10,20–22], chloroquine increased the rate of DV alkalinization in the $C6^{7G8}$ and $C4^{Dd2}$ lines and was without effect in the $C2^{GC03}$ line, whereas saquinavir increased the rate of DV alkalinization in all 3 parasite lines (Fig 6G). We found that lumefantrine and mefloquine induced a H^+ leak in the $C6^{7G8}$ and $C4^{Dd2}$ lines, but not in the $C2^{GC03}$ line. These observations are consistent with both drugs being substrates of $PfCRT^{7G8}$ and $PfCRT^{Dd2}$, but

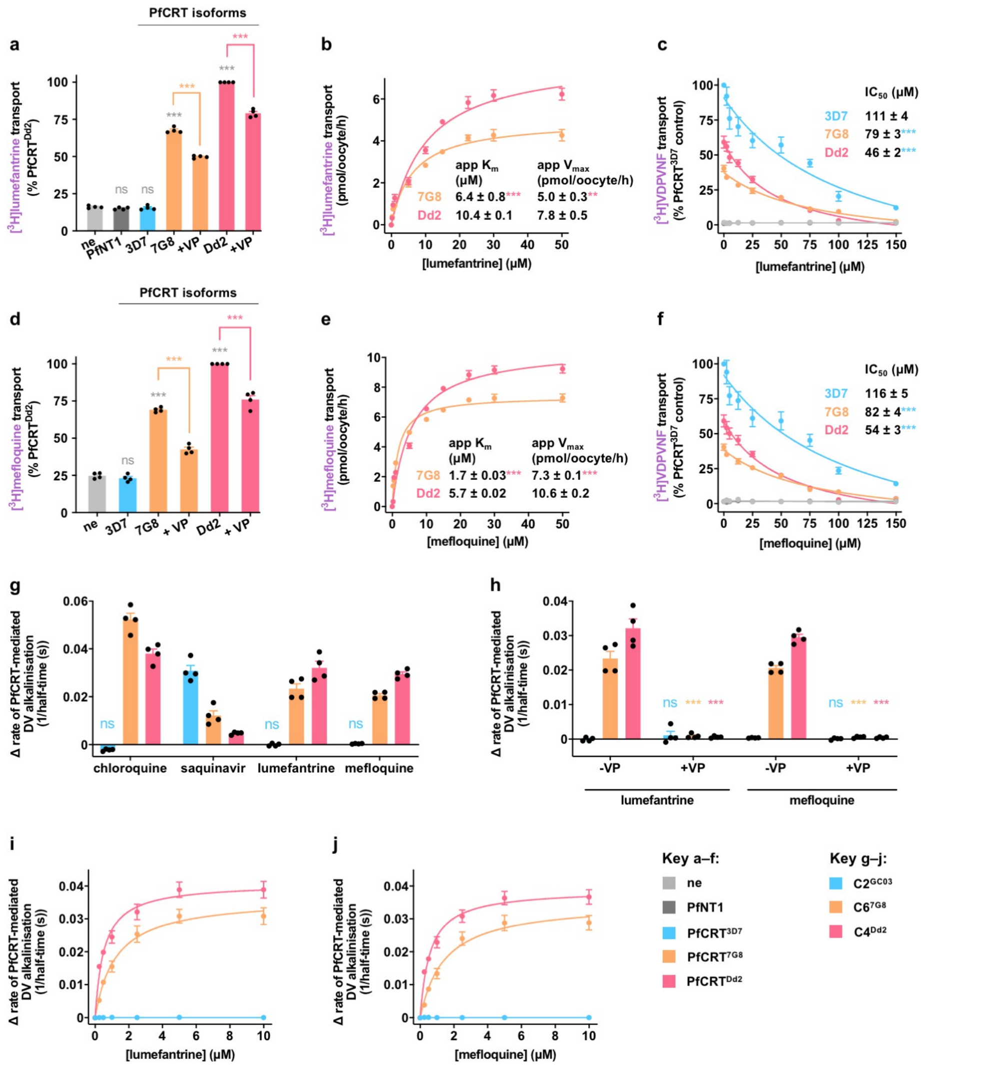

Fig 6. Transport of lumefantrine and mefloquine via PfCRT in *Xenopus* oocytes and in situ. (a, d) The transport of [^{3}H]lumefantrine (a) and [^{3}H]mefloquine (d) via PfCRT^{Dd2} and PfCRT^{7G8} was reduced by verapamil (VP; 100 μM). The asterisks denote a significant difference from the ne (gray asterisks), the PfCRT^{7G8} control (orange asterisks), or the PfCRT^{Dd2} control (red asterisks). **(b, e)** The transport of lumefantrine (b) and mefloquine (e) via PfCRT^{Dd2} and PfCRT^{7G8} was saturable. The asterisks denote a significant difference from PfCRT^{Dd2} (red asterisks). **(c, f)** The effects of unlabeled lumefantrine (c) and unlabeled mefloquine (f) on [^{3}H]VDPVNF transport via PfCRT^{3D7}, PfCRT^{Dd2}, and PfCRT^{7G8}. The asterisks denote a significant difference from PfCRT^{3D7} (blue asterisks). **(g)** Lumefantrine and mefloquine (2.5 μM) increased the rate of DV alkalinization in the chloroquine-resistant C6^{7G8} and C4^{Dd2} parasite lines but not in the chloroquine-sensitive C2^{GC03} line. Unless labeled ns, $P < 0.05$ relative to the absence of a test solute. **(h)** The increase in the rate of DV alkalinization caused by lumefantrine and mefloquine was inhibited by VP (50 μM). The asterisks denote a significant difference from the relevant C2^{GC03} (blue asterisks), C6^{7G8} (orange asterisks), or C4^{Dd2} (red asterisks) treatments in the absence of verapamil. **(i, j)** Lumefantrine (i) and mefloquine (j) increased the rate of DV alkalinization in a concentration-dependent manner. The data are the mean of $n = 4$ independent experiments, each yielding similar results and overlaid as individual data points in panels **a**, **d**, **g**, and **h**, and the error is the SEM. Where not visible, the error bars fall within the symbols. $^{**}P < 0.01$, $^{***}P < 0.001$, ns, not significant (1-way ANOVA). The data underlying this figure is supplied in S3 Data. ne, nonexpressing oocytes; PfCRT, *Plasmodium falciparum* chloroquine resistance transporter.

https://doi.org/10.1371/journal.pbio.3001616.g006

not PfCRT^{3D7} (Fig 6G–6J). Furthermore, verapamil inhibited the lumefantrine- and mefloquine-induced H^+ leaks (Fig 6H), providing further evidence that the drug-induced efflux of H^+ from the DV was mediated by PfCRT^{7G8} and PfCRT^{Dd2}. Both drugs increased the rate of

Table 1. In vitro antiplasmodial activities of chloroquine, lumefantrine, and mefloquine against *P. falciparum pfcrt* transfectant lines.

Parasite line	IC_{50} (nM)[a]					
	Chloroquine		Lumefantrine		Mefloquine	
	Control	+ verapamil	Control	+ verapamil	Control	+ verapamil
$C2^{GC03}$	25 ± 1.1	26 ± 1.7	71 ± 3.5	68 ± 2.5	52 ± 1.7	50 ± 2.7
$C6^{7G8}$	84 ± 3.5[b]	27 ± 1.0[c]	42 ± 1.6[b]	69 ± 1.8[c]	29 ± 1.2[b]	53 ± 2.1[c]
$C4^{Dd2}$	132 ± 4.9[b]	28 ± 1.1[c]	45 ± 1.8[b]	67 ± 1.9[c]	32 ± 1.8[b]	50 ± 1.9[c]

[a]The IC_{50} values are the mean ± SEM of 4 independent experiments (performed on different days), within which measurements were averaged from 3 replicates.

[b]The *P* values determined from a 1-way ANOVA were less than 0.001 for comparisons with the $C2^{GC03}$ line, within a control treatment.

[c]The *P* values determined from a 1-way ANOVA were less than 0.001 for comparisons between the control treatment and the relevant + verapamil treatment within the same line.

The data underlying this figure is supplied in S3 Data.

https://doi.org/10.1371/journal.pbio.3001616.t001

DV alkalinization in a concentration-dependent manner, with $PfCRT^{Dd2}$ again exhibiting a higher capacity for lumefantrine and mefloquine transport than $PfCRT^{7G8}$ (Fig 6I and 6J). Together, these findings support the datasets obtained with the *Xenopus* oocyte system by providing an in situ demonstration that lumefantrine and mefloquine accumulate within the DV and that chloroquine resistance-conferring isoforms of PfCRT transport both of these drugs back out into the parasite's cytosol.

If lumefantrine and mefloquine exert their primary antimalarial activities on targets outside of the DV, the PfCRT-mediated efflux of these drugs from the DV of the $C6^{7G8}$ and $C4^{Dd2}$ lines should heighten parasite sensitivity to lumefantrine and mefloquine, and verapamil should reduce this effect. We tested this hypothesis by measuring the susceptibility of the isogenic parasite lines to lumefantrine, mefloquine, and chloroquine in the presence or absence of verapamil. The resulting IC_{50}s confirmed that the $C6^{7G8}$ and $C4^{Dd2}$ lines are more susceptible to lumefantrine and mefloquine than the $C2^{GC03}$ parasites (Table 1), a finding that is consistent with previous reports [2,17]. Furthermore, verapamil decreased the sensitivity of the $C6^{7G8}$ and $C4^{Dd2}$ lines to lumefantrine and mefloquine, while simultaneously increasing their sensitivity to chloroquine. Together, our in situ datasets show that chloroquine resistance-conferring isoforms of PfCRT can mediate the transport of lumefantrine and mefloquine from the DV into the parasite cytosol and that this "gain of transport function" underlies the heightened sensitivity of chloroquine-resistant parasites to lumefantrine and mefloquine.

Discussion

The roles of PfMDR1 in the phenomenon of antimalarial drug resistance have remained unclear for several decades, despite it being one of the key determinants of multidrug resistance in the parasite. Our development of a robust expression system for PfMDR1 in *Xenopus* oocytes has enabled direct and detailed characterizations of its capacity for drug transport, and of how this varies between different field isoforms of the transporter. Using this system, we have provided new fundamental insights into the function of PfMDR1, such as its ability to transport a wide range of structurally diverse drugs that includes most of the antimalarials currently in use. We found that the mutant isoforms of PfMDR1 differed from the wild-type protein, and each other, in their capacities to transport these drugs. Furthermore, in almost all cases, the introduction of mutations into PfMDR1 decreased its capacity for drug transport. In the parasite, the reduced capacities of the mutant isoforms for drug transport will result in less of the drug entering and accumulating within the DV, and thus a greater proportion of the drug will remain in the cytosol. By contrast, the overexpression of PfMDR1 (which increases the level of PfMDR1 at the DV membrane [93,94]) will heighten the rate of drug transport into the DV, thereby increasing the sequestration of drugs within this organelle. These findings suggest that changes in PfMDR1 contribute to multidrug resistance phenotypes primarily by altering the distribution of drugs between the parasite cytosol and the DV.

We delved into this possibility further by examining the mechanistic basis for the patterns of collateral drug sensitivity induced by polymorphisms in *pfmdr1* and *pfcrt*. We focused upon characterizing the interactions of chloroquine, lumefantrine, and mefloquine with PfMDR1, and of lumefantrine and mefloquine with PfCRT (given that chloroquine transport via PfCRT has already been extensively studied in the *Xenopus* oocyte system and in situ [6,7,9,20,21]). Kinetic analyses confirmed that wild-type PfMDR1 possesses the highest capacity for the transport of lumefantrine, mefloquine, and chloroquine and that all of the mutant isoforms included for study exhibit reduced capacities for the transport of these drugs. In all cases, the $\text{PfMDR1}^{\text{NFCDY}}$ isoform (carried by the chloroquine-resistant strain 7G8) exhibited the lowest capacity for drug transport. We observed a very different relationship between mutations in PfCRT and the protein's capacity for drug transport. Wild-type PfCRT was found to lack the ability to transport lumefantrine or mefloquine in both the *Xenopus* oocyte system and a complementary in situ assay. By contrast, mutant isoforms of PfCRT (carried by the chloroquine-resistant strains 7G8 and Dd2) displayed significant capacities for the transport of these 2 drugs. That said, relative to chloroquine transport via $\text{PfCRT}^{\text{Dd2}}$ [7], the mutant proteins are high-affinity, low-capacity transporters of lumefantrine and mefloquine. In the parasite, the mutant transporters will mediate the efflux of chloroquine, lumefantrine, or mefloquine from the DV back into the parasite's cytosol, thereby decreasing the concentration of these drugs within the DV. By contrast, little or no drug will exit the DV of parasites carrying wild-type PfCRT, which means that chloroquine, lumefantrine, and mefloquine will continue to sequester within this compartment.

Given that PfMDR1 and PfCRT are potential drug targets themselves [1,95], we investigated whether they might be potently blocked by lumefantrine, mefloquine, or chloroquine. However, all 3 antimalarials were relatively poor inhibitors of transport via PfMDR1 and all 3 drugs also lacked potency against PfCRT; chloroquine [10], lumefantrine, and mefloquine were (similarly) weak inhibitors of the transport of a natural substrate via PfCRT. It is therefore unlikely that the natural functions of PfMDR1 and PfCRT are targeted to a significant extent by chloroquine, lumefantrine, or mefloquine.

Having obtained rates for the transport of lumefantrine, mefloquine, and chloroquine via 6 field isoforms of PfMDR1, we sought to identify relationships between capacities for drug transport and the in vitro drug responses of parasites carrying these PfMDR1 isoforms. We observed positive correlations between the rates of lumefantrine and mefloquine transport via PfMDR1 and the corresponding in vitro drug responses (see S3 Text for an extended discussion). For example, PfMDR1 isoforms with relatively high capacities for mefloquine transport tended to be present in the parasites with relatively high mefloquine IC_{50}s (and thus increased resistance to the drug), whereas isoforms with low capacities for mefloquine transport tended to be present in the parasites with low mefloquine IC_{50}s (and thus increased sensitivity to the drug). We observed the opposite relationship for chloroquine, with the chloroquine transport capacities of the PfMDR1 field isoforms correlating negatively with the corresponding in vitro chloroquine responses (see S3 Text for an extended discussion). These analyses identify the rate of drug transport via PfMDR1 as being a key contributor to the collateral drug sensitivity patterns observed for lumefantrine, mefloquine, and chloroquine in field isolates and laboratory-adapted strains. In parasites carrying a mutant PfMDR1 isoform, the decrease in the rate of drug transport into the DV will lessen the accumulation of lumefantrine, mefloquine, and chloroquine within this organelle and cause a concomitant increase in the cytosolic

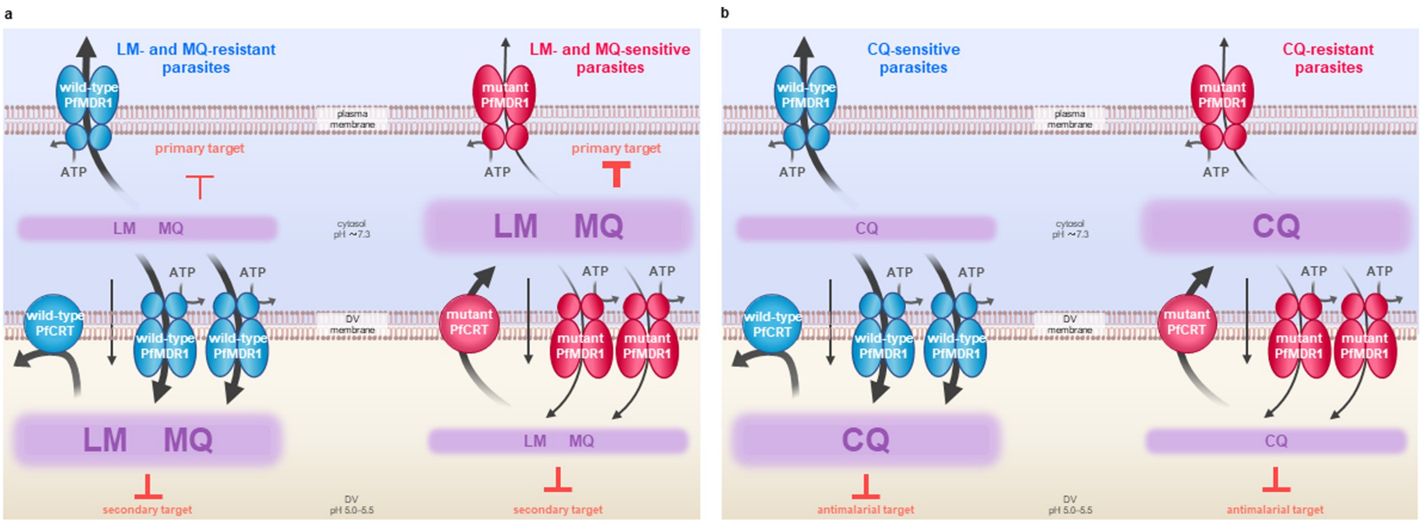

Fig 7. Roles of PfMDR1 and PfCRT in the parasite's susceptibility to lumefantrine, mefloquine, and chloroquine. Mechanistic explanations for how polymorphisms in *pfmdr1* and *pfcrt* alter the parasite's response to lumefantrine and mefloquine **(a)** and chloroquine **(b)**. Lumefantrine, mefloquine, and chloroquine are weak bases that enter the DV via 2 main routes: (1) simple diffusion of the neutral species across the membrane and subsequent protonation within the acidic DV lumen; and (2) ATP-driven import via PfMDR1. Wild-type PfMDR1 has a high capacity for drug transport and this activity, together with the inability of wild-type PfCRT to efflux lumefantrine, mefloquine, or chloroquine from the DV, causes these drugs to sequester within the DV. Overexpression of PfMDR1 results in a further increase in the rate of drug transport from the cytosol into the DV and thus greater accumulation of lumefantrine, mefloquine, and chloroquine in the DV (as well as concomitant reductions in their cytosolic concentrations). In parasites carrying a mutant PfMDR1 isoform (and/or only one *pfmdr1* copy) as well as a mutant isoform of PfCRT, there is a marked reduction in the DV accumulation of lumefantrine, mefloquine, and chloroquine as a result of (1) a decrease in the rate of drug import via PfMDR1; and (2) the PfCRT-mediated efflux of drugs from the DV back into the cytosol. The reduction in the concentration of chloroquine at its primary site of action allows the parasite to evade its killing effects, thereby causing chloroquine resistance. On the other hand, the concomitant increases in the cytosolic drug concentrations render these parasites more sensitive to lumefantrine and mefloquine, indicating that the primary targets of both drugs are located outside of the DV. CQ, chloroquine; DV, digestive vacuole; LM, lumefantrine; MQ, mefloquine; PfCRT, *Plasmodium falciparum* chloroquine resistance transporter; PfMDR1, *Plasmodium falciparum* multidrug resistance protein 1.

https://doi.org/10.1371/journal.pbio.3001616.g007

concentrations of these 3 drugs. By contrast, the overexpression of PfMDR1 would increase the rate of drug transport into the DV, leading to the heightened sequestration of lumefantrine, mefloquine, and chloroquine within the DV and a reduction in the cytosolic concentrations of these drugs. These findings, together with our previous demonstration of a positive correlation between the chloroquine transport capacities of field isoforms of PfCRT and the in vitro chloroquine responses of the corresponding parasites [7], reveal that the redistribution of drugs between the DV and the cytosol is the key mechanism by which polymorphisms in *pfmdr1* and *pfcrt* cause collateral drug sensitivity.

The detailed biochemical characterizations of PfMDR1 and PfCRT we have presented here enable the construction of a mechanistic model for collateral drug sensitivity in the malaria parasite (Fig 7 and S3 Text). Lumefantrine, mefloquine, and chloroquine enter the DV, and accumulate therein, via 2 main routes: (1) simple diffusion of the neutral species across the membrane and subsequent protonation within the acidic DV lumen; and (2) ATP-driven import via PfMDR1. Wild-type PfMDR1 has a relatively high capacity for drug transport and this activity, together with the inability of wild-type PfCRT to efflux lumefantrine, mefloquine, or chloroquine from the DV, causes these drugs to accumulate to high levels within the DV. Overexpression of PfMDR1 results in a further increase in the rate of drug transport from the cytosol into the DV and thus greater sequestration of lumefantrine, mefloquine, and chloroquine in the DV (as well as concomitant reductions in their cytosolic concentrations). Hence, parasites carrying wild-type *pfmdr1* (and/or multiple copies of *pfmdr1*) as well as wild-type *pfcrt* are chloroquine-sensitive because chloroquine accumulates to high levels at its primary site of antimalarial action—i.e., the detoxification of heme within the DV [96–98]. Given that these parasites exhibit reduced, rather than increased, susceptibilities to lumefantrine and mefloquine, our model indicates that these 2 drugs exert their primary antimalarial effects outside of the DV (mefloquine is thought to target the parasite's cytoplasmic 80S ribosome [50] and the primary target of lumefantrine remains unknown). In parasites carrying a mutant PfMDR1 isoform (and/or only one *pfmdr1* copy) as well as a mutant isoform of PfCRT, there is a marked reduction in the DV accumulation of lumefantrine, mefloquine, and chloroquine as a result of (1) a decrease in the rate of drug import via PfMDR1; and (2) the PfCRT-mediated efflux of drugs from the DV back into the cytosol. The reduction in the concentration of chloroquine at its primary site of action allows the parasite to evade its killing effects, thereby causing chloroquine resistance. On the other hand, the concomitant increases in the cytosolic drug concentrations render these parasites more sensitive to lumefantrine and mefloquine. The mechanistic model we have presented here concurs with previously proposed hypotheses of an interplay between PfMDR1 and PfCRT in modulating the parasite's susceptibility to these drugs [2–4,15,99,100]. Our model also suggests that the targets previously proposed for mefloquine and lumefantrine inside the DV (such as the detoxification of heme) play secondary roles, or perhaps no role, in the antimalarial activities of these drugs.

Our datasets also provide insights into why some pairings of PfMDR1 and PfCRT isoforms result in parasites with unexpectedly low or high susceptibilities to chloroquine [7]. Mutations in *pfcrt* are the primary determinant of chloroquine resistance and, according to the model we have proposed, the extent to which polymorphisms in *pfmdr1* contribute to a given chloroquine resistance phenotype will depend on several factors. These include (1) the rate of chloroquine efflux via the mutant PfCRT isoform expressed by the parasite; (2) the rate of chloroquine entry into the DV via simple diffusion (which is dependent on the concentration of chloroquine in the parasite cytosol and, in turn, the extracellular concentration of chloroquine); (3) the rate of chloroquine import via the PfMDR1 isoform(s) expressed by the parasite; and (4) the level of PfMDR1 expression at the DV membrane. For example, the combination of a mutant PfCRT isoform that mediates a high rate of chloroquine efflux (e.g., PfCRT^{Dd2}) and a mutant PfMDR1 isoform with a decreased capacity for chloroquine import could be expected to achieve a somewhat lower DV concentration of the drug (and thus perhaps a higher level of resistance) than would be brought about by the transport activity of PfCRT alone. However, the ability of PfMDR1 to influence the parasite's susceptibility to chloroquine is perhaps more evident when the mutant PfCRT has a relatively low capacity for chloroquine efflux (e.g., PfCRT^{7G8}). We have previously reported that 7G8 parasites exhibit a greater level of chloroquine resistance than what would be predicted given the low level of chloroquine transport mediated by PfCRT^{7G8} [7]. Here, our finding that PfMDR1^{NFCDY} (the isoform carried by 7G8 parasites) has a very low capacity for chloroquine transport provides a mechanistic explanation for this observation; the marked reduction in the rate of chloroquine import via PfMDR1^{NFCDY} helps offset the relatively low rate of chloroquine efflux via PfCRT^{7G8}, resulting in a lower DV concentration of chloroquine (and thus higher level of resistance) than would be achieved by PfCRT^{7G8} with wild-type PfMDR1 (or even with one of the other mutant PfMDR1 isoforms). Hence, our datasets suggest that PfMDR1^{NFCDY} has the potential to contribute to chloroquine resistance phenotypes to a greater extent than other PfMDR1 isoforms as a consequence of its very low capacity for chloroquine transport.

Several lines of evidence indicate that mutant isoforms of PfCRT play a key role in conferring quinine resistance [9,18,22,37,92], and we have previously used the *Xenopus* oocyte system to show that mutant isoforms of PfCRT have the ability to transport quinine out of the DV, whereas the wild-type protein lacks this activity [9,18] (see S4 Text for an extended analysis). Collectively, these findings indicate that PfCRT's role in quinine resistance is similar to its role in chloroquine resistance (Fig 7). That is, the efflux of quinine from the DV into the parasite cytosol via a mutant PfCRT isoform reduces the concentration of the drug at its DV target (the inhibition of heme detoxification and/or another aspect of hemoglobin digestion [101]), thereby reducing the susceptibility of the parasite to quinine. It might be predicted, therefore, that the role of PfMDR1 would likewise be similar in both chloroquine and quinine resistance. Indeed, our datasets showed that most of the mutant PfMDR1 isoforms have low capacities for quinine transport relative to the wild-type protein, and our observations are consistent with previous findings of associations between mutations in PfMDR1 and decreases in the parasite's susceptibility to quinine [70,102]. However, our analysis of the relationship between the quinine transport capacities of PfMDR1 and the quinine resistance indices for the corresponding parasites did not identify a correlation between these 2 factors. This is perhaps a reflection of a complex and multifactorial pathway to quinine resistance that may sometimes involve polymorphisms in *pfmdr1* and other times not. Indeed, when considered in context with a large body of previous research (see S4 Text for an extended discussion), our findings indicate that the role of PfMDR1 in quinine resistance is more complex and nuanced than simply either causing a decrease or an increase in the accumulation of the drug within the DV (i.e., the roles we have proposed for PfMDR1 in chloroquine resistance and mefloquine/lumefantrine resistance, respectively). Our analyses instead suggest that the complex and variable relationship between quinine susceptibility and polymorphisms in *pfcrt* and *pfmdr1* may center on 2 key factors: (1) the net flux of quinine across the DV membrane; and (2) the rate at which PfMDR1's natural substrates are transported into the DV (see S4 Text for an extended discussion).

The robust system we have established for the study of PfMDR1 in *Xenopus* oocytes provides the long-awaited means to undertake direct and detailed characterizations of its function and to make comparisons between different PfMDR1 isoforms and across different drugs. Our findings have delivered fundamental insights into PfMDR1 that have led to a greater understanding of its role in the phenomenon of multidrug resistance as well as the formulation of a mechanistic model for PfMDR1's contribution to collateral drug sensitivity in the malaria parasite. Together, the work presented here provides a valuable molecular basis for the rational design of approaches that maintain and extend the useful life span of current antimalarials by exploiting the opposing selection forces they exert upon PfCRT and PfMDR1. Looking ahead, our systems could be employed to address unresolved questions about PfMDR1 and PfCRT, such as the identity of the natural substrate(s) of PfMDR1, the functions and roles of the new PfMDR1 and PfCRT isoforms that continue to emerge in the field in response to changes in drug pressure, and the nature of the interactions of PfMDR1 and PfCRT with candidate antimalarials in the development pipeline.

Methods

Xenopus laevis frogs

Ethical approval of the work performed with female *X. laevis* frogs was obtained from the Australian National University Animal Experimentation Ethics Committee (Animal Ethics Protocol Numbers A2013/13 and A2019/26) in accordance with the Australian Code of Practice for the Care and Use of Animals for Scientific Purposes. The frogs were purchased from Nasco USA (catalog no. LM00535M) and were housed in the *Xenopus* Frog Facility (at the Australian National University Research School of Biology) in compliance with the relevant institutional and Australian Government regulations. *X. laevis* frogs are fully aquatic animals held in large tanks (8 to 20 frogs per tank). The water is percolated and filtered in a closed system, and the water temperature is maintained at 19 to 20˚C. The pH, hardness, ammonia, and other water parameters were checked daily and kept at levels reported to be necessary for the production of healthy oocytes [103,104].

Preparation of coding sequences and cRNA synthesis

The coding sequence of human P-gp was purchased from GenScript (catalog no. OHu23307; NM_000927; New Jersey USA) and inserted into the pGEM-He-Juel oocyte expression vector [105]. The PfMDR1^{NYSND} coding sequence was codon-harmonized to facilitate the correct folding, and thus the functional expression, of the transporter in *Xenopus* oocytes. This codon-harmonized sequence was custom synthesized and then inserted into the pGEM-He-Juel oocyte expression vector by GenScript. The remaining isoforms of PfMDR1, as well as the version of PfMDR1^{NYSND} carrying a double carboxyl-terminal HA tag (PfMDR1^{NYSND}-2xHA), were generated from the PfMDR1^{NYSND} template using site-directed mutagenesis [7] and the primers listed in S4 Table. The resulting PfMDR1 coding sequences were verified by sequencing (undertaken by the ACRF Biomolecular Resource Facility, Australian National University). Amino-terminally HA-tagged versions of these PfMDR1 variants, as well as the version of PfMDR1^{NYSND} that carries a triple HA tag at the carboxyl terminus (PfMDR1^{NYSND}-3xHA), were generated by GenScript.

The oocyte expression vectors containing PfNT1, PfCRT^{3D7}, PfCRT^{Dd2}, or PfCRT^{7G8} were made previously [6,7,106]. The PfCRT coding sequences were codon-harmonized and encode a version of PfCRT that is free of endosomal–lysosomal trafficking motifs, thereby resulting in the expression of the transporter at the plasma membrane of *Xenopus* oocytes [6,7].

The plasmids containing human P-gp, PfMDR1, PfCRT, or PfNT1 coding sequences were linearized with SalI (Thermo Fisher Scientific, Massachusetts, USA; catalog no. ER0642), and 5′-capped cRNA was synthesized using the mMESSAGE mMACHINE T7 transcription kit (Ambion, Texas, USA; catalog no. AM1344). The in vitro transcription reactions were conducted as per the manufacturer's instructions with the following minor modification for the synthesis of human P-gp and PfMDR1 cRNA: in a 40 μL reaction, 500 ng of linearized template plasmid was used, and 30 nmol GTP was added halfway into the 2-hour incubation. The resulting cRNA samples were purified with the MEGAclear kit (Ambion, catalog no. AM1908) and adjusted to the desired concentration using RNase-free elution buffer. The quality of the cRNA was assessed via agarose gel electrophoresis.

Isolation and microinjection of *Xenopus* oocytes

Adult female frogs were anaesthetized in a solution of ethyl 3-aminobenzoate methanesulfonate salt (Sigma-Aldrich, Missouri, USA; catalog no. A5040) and 1 mM $NaHCO_3$ (Sigma-Aldrich, catalog no. S5761) [8]. Sections of the ovary were removed from the frog using surgical grade forceps and scissors. The ovary sections were cut into pieces containing approximately 20 oocytes, transferred to a 100 mL Erlenmeyer flask, and then gently rinsed 5 times with "calcium-free oocyte ringer" buffer (OR2$^-$; 82.5 mM NaCl, 2.5 mM KCl, 1 mM $MgCl_2$, 1 mM Na_2HPO_4, 5 mM HEPES; pH 7.8). The collagenous membrane encasing the oocytes was degraded by incubating the ovary sections in 25 mL of OR2$^-$ buffer supplemented with 0.5 M Na_2HPO_4 (Sigma-Aldrich, catalog no. 342483), bovine serum albumin (250 mg/mL; Sigma-Aldrich, catalog no. A7030), and collagenase B (Roche, Basel, Switzerland; catalog no. 11088831001) for 12 to 13 hours at 16˚C on an orbital shaker. The speed of the orbital shaker was adjusted according to the volume of ovary sections in the flask, such that the ovary sections were circulating gently around the flask (shaker speeds that are too low will result in incomplete defolliculation, whereas speeds that are too high cause damage to the plasma membrane of the oocytes). The amount of collagenase B added to the solution was dependent on the amount of collagen surrounding the ovary sections, which was assessed by visual inspection under a dissecting microscope. The collagenase-treated oocytes were washed 10 times with OR2$^-$ buffer, 5 times with "calcium-containing oocyte ringer" (OR2$^+$) buffer (OR2$^-$ buffer supplemented with 1 mM $CaCl_2$ and 50 μg/mL penicillin and streptomycin), and then once with L-15 (Leibovitz) media with L-glutamine (used at 0.5×; Sigma-Aldrich, catalog no. L4386) supplemented with 10 mM HEPES and 50 μg/mL penicillin and streptomycin. Stage V and VI oocytes were microinjected with cRNA encoding a PfMDR1 isoform (10 ng per oocyte), a PfCRT isoform (20 ng per oocyte), human P-gp (10 ng per oocyte, these oocytes served as a positive control), or PfNT1 (20 ng per oocyte, these oocytes served as a negative control). In a subset of experiments that were performed to optimize the amount of cRNA required for human P-gp or PfMDR1 expression, oocytes were microinjected with cRNA amounts ranging from 2.5 to 50 ng. The oocytes were stored at 16 to 18˚C in L-15 media supplemented with 10 mM HEPES and 50 μg/mL penicillin and streptomycin.

Radiolabeled and unlabeled drugs used in the *Xenopus* oocyte transport assays

The radiolabeled drugs were purchased from either Pharmaron (Beijing, China; [^{3}H]chloroquine, 27 Ci/mmol; [^{3}H]dihydroartemisinin, 14 Ci/mmol), American Radiolabeled Chemicals (Missouri, USA; [^{3}H]lumefantrine, 10 Ci/mmol; [^{3}H]mefloquine, 20 Ci/mmol; [^{3}H]amodiaquine, 15 Ci/mmol; [^{3}H]piperaquine, 15 Ci/mmol; [^{3}H]quinine, 20 Ci/mmol; [^{3}H]quinidine, 20 Ci/mmol; [^{3}H]vinblastine sulfate, 20 Ci/mmol), Moravek (California, USA; [^{3}H]amantadine, 137 mCi/mmol), Cambridge Research Biochemicals (Billingham, UK; [^{3}H]VDPVNF, 20 Ci/mmol), or PerkinElmer (Massachusetts, USA; [^{3}H]hypoxanthine, 13.3 Ci/mmol). The structures and protonation states of these drugs are shown in S8 Fig and S2 Data, respectively. The unlabeled compounds were purchased from either Sigma-Aldrich (lumefantrine, mefloquine, chloroquine, quinine, quinacrine, rhodamine B, methylene blue, amantadine, nicardipine, vanadate, verapamil, PSC833, chlorpheniramine, saquinavir, histidine, and iron chelator IV) or GenScript (the peptides LH and VDPVNF). The structures of a subset of these compounds are shown in S8 Fig.

Measurements of drug transport via human P-gp and PfMDR1 in *Xenopus* oocytes

The human P-gp and PfMDR1 transport assays were performed 1 day post-cRNA injection and, unless specified otherwise, were conducted over 1.5 hours at 27.5˚C in ND96 buffer (96 mM NaCl, 2 mM KCl, 1 mM $MgCl_2$, 1.8 mM $CaCl_2$, 10 mM MES, and 10 mM Tris-base) that had been adjusted to pH 5.5 to mimic the pH of the DV lumen [107,108]. Since the ATPase domains of ABC transporters (such as PfMDR1 and human P-gp) are located in the cell's cytosol [36], both PfMDR1 and human P-gp are predicted to orientate in the oocyte plasma membrane with their ATPase domains in the oocyte cytosol. An established efflux assay [10] was therefore used to microinject the radiolabeled drug under study into the oocyte and measure its efflux via human P-gp or PfMDR1. In this assay, the transport of the substrate via human P-gp from the oocyte cytosol into the extracellular solution is analogous to the P-gp–mediated transport of a substrate from the cytosol of a human cell into the extracellular space. Likewise, for PfMDR1 the direction of transport is analogous to the PfMDR1-mediated transport of a substrate from the parasite's cytosol into the DV (S9 Fig). In all cases, 4 independent experiments were performed (on different days and using oocytes from different frogs) and within each experiment measurements were made from 10 oocytes per treatment.

The oocytes were microinjected with 35 nL of ND96 buffer (pH 8.0) supplemented with the [^{3}H]drug under study. The estimated intracellular concentrations (calculated on the basis that the aqueous volume of stage V andVI oocytes is 400 nL [109]) were as follows: [^{3}H]vinblastine sulfate, 4.4 μM; [^{3}H]lumefantrine, 2.2 μM; [^{3}H]chloroquine, 5.9 μM; [^{3}H]quinine, 4.4 μM;

[^{3}H] mefloquine, 4.4 μM; [^{3}H]amodiaquine, 3.1 μM; [^{3}H]piperaquine, 3.1 μM; [^{3}H]dihydroartemisinin, 3.1 μM; [^{3}H]quinidine, 4.4 μM; [^{3}H]amantadine, 30 μM. In the experiments measuring [^{3}H]dihydroartemisinin transport, 1 mM iron chelator IV was also microinjected into the oocyte to bind any free iron present in the oocyte (free iron could activate dihydroartemisinin, which, in turn, could damage the oocytes and thus interfere with measurements of transport; S10 Fig). Ten oocytes that had resealed at the injection site were transferred to a 5 mL polystyrene round-bottom tube (Corning, New York, USA; catalog no. 352008) and washed once with 3.5 mL of ND96 buffer (pH 5.5) before being transferred to separate wells of a white 96-well plate (PerkinElmer, catalog no. 6005299). This treatment determined the amount of radioactivity within the oocytes at the beginning of the assay (T = 0). Another 10 resealed oocytes were transferred to a 5-mL tube, washed once with 3.5 mL of ND96 buffer (pH 5.5), and suspended in 100 μL of ND96 buffer (pH 5.5) to commence the assay. The incubation was terminated by removing the reaction buffer with a pipette and washing the oocytes twice with 3.5 mL of ice-cold ND96 buffer (pH 5.5). Each oocyte was transferred to a separate well of a white 96-well plate, lysed by an overnight incubation at room temperature with 20 μL of 10% (w/v) SDS, and then combined with 150 μL of MicroScint-40 microscintillant (PerkinElmer, catalog no. 6013641). The plate was covered with a TopSeal-A (PerkinElmer, catalog no. 6050185), and the radioactivity within each well was measured with a MicroBeta^2 microplate liquid scintillation analyzer (PerkinElmer, catalog no. 2450–0010). Drug transport was calculated by subtracting the amount of radioactivity (measured in counts per min) present within the oocytes at the end of the incubation from that measured in the oocytes sampled immediately before the commencement of the assay.

The transport of methylene blue, quinacrine, and rhodamine B via PfMDR1 was measured using the intrinsic fluorescence of these compounds and a fluorescence-based transport assay. The oocytes were microinjected with 35 nL of ND96 buffer (pH 8.0) supplemented with the fluorescent compound under study. The estimated intracellular concentration (calculated on the basis that the aqueous volume of stage V and VI oocytes is 400 nL [109]) for quinacrine, rhodamine B, or methylene blue was 4 μM. Of the oocytes that had resealed at the injection site, 10 were transferred to a 5-mL polystyrene round bottom tube and washed once with 3.5 mL of ND96 buffer (pH 5.5) before being transferred to separate wells of a clear 96-well plate. This treatment determined the amount of fluorescence within the oocytes at the beginning of the assay (T = 0). Another 10 resealed oocytes were transferred to a 5-mL tube, washed once with 3.5 mL of ND96 buffer (pH 5.5), and suspended in 100 μL of ND96 buffer (pH 5.5) to commence the assay. The incubation was terminated by removing the reaction buffer with a pipette and washing the oocytes twice with 3.5 mL of ice-cold ND96 buffer (pH 5.5). Each oocyte was transferred to a separate well of a clear 96-well plate. In addition, the autofluorescence of oocytes that had not been microinjected with a drug was measured by transferring 10 oocytes to a 5-mL tube and washing them 3 times with 3.5 mL of ND96 buffer (pH 5.5) before transferring them to separate wells of a clear 96-well plate. The oocytes were lysed by an overnight incubation at room temperature with 20 μL of 10% (w/v) SDS. The fluorescence intensity in each well was measured using an Infinite M1000 PRO plate reader (Tecan, Mannedorf, Switzerland; catalog no. 30064852) at the following excitation and emission wavelengths: 440 nm and 510 nm for quinacrine; 546 nm and 568 nm for rhodamine B; 668 nm and 682 nm for methylene blue. Drug transport was calculated by first subtracting the autofluorescence measured from all treatments, and then subtracting the fluorescence present within the oocytes at the end of the incubation from that measured in the oocytes sampled immediately before the commencement of the assay.

A subset of assays measured the ability of unlabeled compounds to *cis*-inhibit [^{3}H]drug transport via human P-gp and PfMDR1. In these experiments, the oocytes were microinjected with 35 nL of the relevant [^{3}H]drug solution supplemented with the unlabeled test compound at a concentration that would achieve the desired intracellular concentration (0.1 to 30 μM). The test solutes included known inhibitors of human P-gp (nicardipine [46,54], PSC833 [55,56], vanadate [57,58], and verapamil [46,59]), and a compound that does not interact with human P-gp (the antiviral drug amantadine [46–48]). The abilities of unlabeled lumefantrine, mefloquine, and chloroquine (intracellular concentrations of 1 to 200 μM) to *cis*-inhibit [^{3}H] vinblastine transport via PfMDR1 were also assessed. The IC_{50} value of each inhibitor was determined in GraphPad Prism Version 8 by a least squares fit of the equation $y = y_{min} + [(y_{max} - y_{min})/(1 + ([\text{test compound}]/IC_{50})^c]$ to the data, where y is P-gp–or PfMDR1-mediated drug transport, y_{min} and y_{max} are the minimum and maximum values of y, and *c* is a fitted constant.

The ATP dependence of lumefantrine transport via PfMDR1 was determined by microinjecting the oocytes with [^{3}H]lumefantrine suspended in 35 nL of ND96 buffer (pH 8.0) containing different concentrations of ATP. Unfertilized stage V and VI oocytes typically contain approximately 2.3 mM ATP [110,111] and microinjection of the different ATP solutions is calculated to have raised the intracellular concentration by 0 to 2 mM.

Analyses of the kinetics of drug transport via PfMDR1 were undertaken by microinjecting the oocytes with ND96 buffer (pH 8.0) supplemented with the [^{3}H]drug under study and different concentrations of the unlabeled drug (to achieve intracellular concentrations between 0 and 100 μM). The kinetic parameters for drug transport via different isoforms of PfMDR1 were determined in GraphPad Prism Version 8 by a least squares fit of the Michaelis–Menten equation to the data.

The experiments measuring drug transport via human P-gp or PfMDR1 included ne and those expressing PfNT1 [60,61] (an unrelated transporter) as negative controls. The latter control verified that the integrity of the oocyte plasma membrane had not been compromised (i.e., that the membrane was not leaky) from the combined effects of the heterologous expression of a foreign protein and the second injection event. To confirm that PfNT1 was expressed at the oocyte surface, the uptake of [^{3}H]hypoxanthine (a known substrate of PfNT1) was measured in ne and those expressing PfNT1 on day 1 post-cRNA injection. Briefly, 10 oocytes were washed twice with 3.5 mL of ND96 buffer (pH 6.0), and the residual solution was removed by pipette. The assay commenced with the addition of 100 μL ND96 buffer (pH 6.0) containing 0.38 μM [^{3}H]hypoxanthine and the incubation period was 30 minutes. The assay was terminated by removing the reaction buffer and washing the oocytes twice with 3.5 mL of ice-cold ND96 buffer (pH 6.0). Each oocyte was transferred to a well of a white 96-well plate and the samples were processed, and the radioactivity measured, as described above.

Measurements of drug transport via PfCRT in *Xenopus* oocytes

Unless specified otherwise, the PfCRT transport assays were performed 2 to 3 days post-cRNA injection and were conducted over 1.5 hours at 27.5˚C. The orientation of PfCRT in the parasite's DV membrane is such that its amino terminus and carboxyl terminus extend into the cytosol, and hence, the orientation of the protein is predicted to be the same in the oocyte plasma membrane. Hence, the transport of a substrate via PfCRT from the acidic extracellular solution into the oocyte cytosol [6] is analogous to the PfCRT-mediated efflux of a substrate out of the parasite's acidic DV and into the cytosol [6] (S9 Fig). This is the direction in which mefloquine transport was measured in the PfCRT oocyte assays. Briefly, 10 oocytes were washed twice with 3.5 mL of ND96 buffer (pH 5.0), and the residual solution was removed by pipette. The assay commenced with the addition of 100 μL ND96 buffer (pH 5.0) containing 0.125 μM [^{3}H]mefloquine and 0.5 μM unlabeled mefloquine and, where specified, 100 μM of either a known inhibitor of the transporter (verapamil [6,18], chlorpheniramine [90], or saquinavir [10,91]) or a compound that does not interact with PfCRT (histidine or the dipeptide LH [9,10]). Four independent experiments were performed (on different days and using oocytes from different frogs), and within each experiment measurements were made from 10 oocytes per treatment.

Analyses of the kinetics of mefloquine transport via PfCRT were undertaken by measuring the uptake of [^{3}H]mefloquine (0.125 μM) in the presence of 0 to 50 μM unlabeled mefloquine. In all cases, the incubation was terminated by removing the reaction buffer and washing the oocytes twice with 3.5 mL of ice-cold ND96 buffer (pH 5.0). Each oocyte was transferred to a well of a white 96-well plate and the samples were processed, and the radioactivity measured, as described above. The component of transport attributable to PfCRT (i.e., PfCRT-mediated transport) was calculated by subtracting the level of [^{3}H]mefloquine accumulation detected in the negative control oocytes (ne) from that measured in oocytes expressing $PfCRT^{3D7}$, $PfCRT^{7G8}$, or $PfCRT^{Dd2}$. The kinetic parameters for mefloquine transport via PfCRT were determined in GraphPad Prism Version 8 by a least squares fit of the Michaelis–Menten equation to the data.

We have recently identified the native substrates of PfCRT as being host-derived peptides of 4 to 11 amino acid residues in length [10]. Moreover, we found that in addition to being H^+-dependent, peptide transport via PfCRT requires a second cosubstrate that remains to be identified, but which is naturally present in the *Xenopus* oocyte. The PfCRT-mediated transport of the hemoglobin peptide VDPVNF was therefore quantified by microinjecting [^{3}H]VDPVNF into the oocytes and measuring its efflux from the oocyte [10]. Moreover, after preliminary experiments revealed that [^{3}H]lumefantrine is likewise reliant on the presence of the second cosubstrate for transport via PfCRT ([^{3}H]lumefantrine uptake from the extracellular solution could not be detected in PfCRT-expressing oocytes), the transport of this drug was also measured using the efflux assay. Lumefantrine transport was measured by microinjecting oocytes with 25 nL of ND96 buffer (pH 5.5) supplemented with [^{3}H]lumefantrine and unlabeled lumefantrine (to achieve estimated intracellular concentrations of 1.6 μM and 1 μM, respectively). The measurements of [^{3}H]VDPVNF and [^{3}H]lumefantrine transport via PfCRT were conducted as described above for the PfMDR1 efflux assays. Four independent experiments were performed (on different days and using oocytes from different frogs), and within each experiment measurements were made from 10 oocytes per treatment.

Analyses of the kinetics of lumefantrine transport via PfCRT were undertaken by microinjecting the oocytes with [^{3}H]lumefantrine supplemented with different concentrations of unlabeled lumefantrine (to achieve estimated intracellular concentrations between 0 and 50 μM). The kinetic parameters for lumefantrine transport via PfCRT were determined in GraphPad Prism Version 8 by a least squares fit of the Michaelis–Menten equation to the data.

The ability of unlabeled verapamil, chlorpheniramine, saquinavir, histidine, or LH to *cis*-inhibit [^{3}H]lumefantrine transport was assessed by supplementing the solution containing [^{3}H]lumefantrine and unlabeled lumefantrine with the unlabeled test compound (to achieve an intracellular concentration of 100 μM).

The ability of unlabeled mefloquine or lumefantrine to *cis*-inhibit [^{3}H]VDPVNF transport was assessed by microinjecting oocytes with 25 nL of ND96 buffer (pH 5.5) supplemented with [^{3}H]VDPVNF and unlabeled VDPVNF (to achieve estimated intracellular concentrations of 1.4 μM and 200 μM, respectively) as well as the unlabeled drug at a concentration that would achieve the desired intracellular concentration (10 to 250 μM). The IC_{50} values were determined in GraphPad Prism Version 8 by a least squares fit of the equation $y = y_{min} + [(y_{max} - y_{min})/(1 + ([\text{test compound}]/IC_{50})^c]$ to the data, where y is PfCRT-mediated VDPVNF transport, y_{min} and y_{max} are the minimum and maximum values of y, and *c* is a fitted constant.

Western blot analyses

Semiquantitative measurements of the level of HA-tagged PfMDR1 protein in the oocyte membrane 1 day post-cRNA injection were performed using an established method for obtaining preparations of oocyte membrane proteins [7]. The pellet containing the membrane protein fraction was solubilized in a solution comprising 10 mM dithiothreitol, 1.5% (v/v) SDS, 10% (v/v) β-mercaptoethanol, 9 mM Tris-HCl (pH 7.6), 4.5 mM NaCl, 0.45% (v/v) Triton X-100, and 27.5% (v/v) NuPage LDS sample buffer (Life Technologies, California, USA; catalog no. NP0007). The proteins present in the oocyte membrane preparations were separated in a NuPage 3 to 8% Tris-Acetate polyacrylamide gel (Thermo Fisher Scientific, catalog no. EA03752) using Tris-Acetate SDS running buffer, and then transferred to a 0.45 μM nitrocellulose blotting membrane (Bio-Rad, California, USA; catalog no. 1620115). The membranes were probed with mouse anti-HA antibody (1:5,000; Sigma-Aldrich, catalog no. H9658) followed by horseradish peroxidase-conjugated horse anti-mouse antibody (1:3,000; Cell Signaling Technologies, Massachusetts, USA; catalog. no 7076S). The band for each PfMDR1 isoform was detected with SuperSignal West Pico Chemiluminescent reagent (Thermo Fisher Scientific, catalog no. 34578), quantified using the ImageJ software [112], and expressed as a percentage of the band intensity measured for PfMDR1^{NYSND}. Total protein staining was used to evaluate sample loading and efficiency of transfer [7,113]. Briefly, the nitrocellulose membranes were stained with Ponceau S for 5 minutes, then de-stained using ultrapure water. The stained protein bands were visualized using the Bio-Rad ChemiDoc MP Imaging System, and densitometric analyses were performed in Image Lab version 6.0.1 software (Bio-Rad) to quantify the summed intensity of all of the protein bands between 70 and 180 kDa (the region in which PfMDR1 is detected) within each lane. At least 4 independent experiments were performed (using oocytes from different frogs), and within each experiment, measurements were averaged from 2 separate replicates.

Immunofluorescence assays

An immunofluorescence assay was used to localize HA-tagged PfMDR1 in oocytes 1 to 2 days post-cRNA injection using a method adapted from Richards and colleagues [9]. Unless otherwise specified, all incubation and wash steps were conducted at room temperature with gentle shaking or rotation. All incubations were performed using a volume of 500 μL, and all wash steps were performed using a volume of 1 mL. Six oocytes of each oocyte type were fixed with 4% (v/v) paraformaldehyde in PBS for 30 minutes. Oocytes were then washed 3 times for 10 minutes each in PBS and then permeabilized by incubation in 100% methanol at −20˚C for 20 minutes without shaking. Another three 10-minute washes in PBS were performed before the oocytes were incubated for 2 hours in a blocking solution (4% (w/v) BSA, 2% (v/v) normal goat serum, and 0.1% (v/v) Triton X-100 in PBS). The solution was replaced with a second blocking solution (4% (w/v) BSA and 2% (v/v) normal goat serum in PBS) and incubated overnight at 4˚C. The following day, the oocytes were incubated for an additional 4 hours at room temperature in the same blocking solution before incubation in a solution containing mouse anti-HA antibody (1:100; in a solution of PBS containing 1.5% (w/v) BSA and 0.01% (v/v) Triton X-100; Sigma-Aldrich, catalog no. H9568) for 4 hours at room temperature and then overnight at 4˚C. The following day, the oocytes were washed 3 times for 10 minutes each in PBS supplemented with 1.5% (w/v) BSA. All of the remaining steps were performed in the dark at room temperature. The oocytes were incubated for 4 hours in a solution containing the Alexa Fluor 488 donkey anti-mouse antibody (1:500; in a solution of PBS containing 4% (w/v) BSA and 2% (v/v) normal goat serum; Molecular Probes, Oregon, USA; catalog no. A21202). The oocytes were then washed 3 times for 10 minutes each in PBS, fixed with 3.7% (v/v) paraformaldehyde in PBS for 30 minutes, and washed twice for 15 minutes each in PBS. The oocytes were dehydrated by a series of 15-minute incubations in solutions of increasing ethanol content: 30% (v/v) ethanol in PBS, 50% (v/v) ethanol in PBS, 70% (v/v) ethanol in ultrapure water, 90% (v/v) ethanol in ultrapure water, and 100% ethanol (3 incubations in 100% ethanol were performed). The dehydrated oocytes were embedded in acrylic resin using the Technovit 7100 plastic embedding system (Kulzer, Indiana, USA; catalog no. 64709003). Slices of 2 μm were obtained using a microtome with a glass knife, and the slices were dried on microscope slides. A drop of ProLong Gold Antifade Mountant (Life Technologies, catalog no. P36934) was placed on a #1.5 coverslip, which was then placed over the oocyte slices on each slide and sealed using clear nail polish. Images were captured using a Leica Sp5 inverted confocal laser microscope (Leica Microsystems, Wetzlar, Germany) using a 63× objective. Excitation was achieved with a 488-nm argon laser, and the emissions were captured using a 500- to 550-nm filter. Images were acquired using the Leica Application Suite Advanced Fluorescence Version 3.6 software (Leica Microsystems). At least 2 independent experiments were performed (on oocytes from different frogs) for each oocyte type, within which slices were examined from at least 5 oocytes.

Orientation of PfMDR1 in the plasma membrane of *Xenopus* oocytes

To determine the orientation of PfMDR1 at the surface of *Xenopus* oocytes, an immunofluorescence assay was developed and performed on oocytes 1 day post-cRNA injection. This method used live oocytes that were not fixed or permeabilized, thus preventing the penetration of antibody into the oocyte cytosol. Hence, under these conditions, the antibody can only bind to cognate extracellular epitopes. All incubation steps were performed at 16 to 18˚C in a volume of 500 μL with gentle shaking. The experiment included the following oocyte types: ne (the negative control), oocytes expressing HA_{EL2}-AmDAT (the positive control), and oocytes expressing either 3xHA-PfMDR1^{NYSND} or PfMDR1^{NYSND}-3xHA. Six oocytes from each type were incubated for 6 hours in a blocking solution (3% (w/v) BSA and 1% (v/v) normal goat serum in OR2^{+} buffer). This was followed by a 2-hour incubation with the mouse anti-HA antibody (1:250 in a solution of 1.5% (w/v) BSA in OR2^{+} buffer; Sigma-Aldrich catalog no. H9568). The samples were washed 3 times for 10 minutes each with OR2^{+} buffer and then incubated for 2 hours with the Alexa Fluor 488 donkey anti-mouse antibody (1:500 in a solution of 1.5% (w/v) BSA in OR2^{+} buffer; Molecular Probes, catalog no. A21202). The oocytes were then rinsed 3 times (10 minutes each) with OR2^{+} buffer. Imaging was performed using a Leica M205 FA fluorescence stereomicroscope and Leica Application Suite Version 4.12 software (Leica Microsystems). Excitation was achieved using a 488 nm laser and the emissions were captured using a 500- to 550-nm filter. At least 2 independent experiments were performed (using oocytes from different frogs) for each oocyte type.

Culture of parasitized erythrocytes

The use of human blood for this work was approved by the ANU Human Research Ethics Committee (Human Ethics Approval Number 2017/351). The asexual intraerythrocytic stages of 3 *P*. *falciparum pfcrt* transfectant lines and 3 *P*. *falciparum* strains were studied. The 3 *pfcrt* transfectant lines were the chloroquine-sensitive line C2^{GC03} (a recombinant control that retains the wild-type *pfcrt* allele, PfCRT^{3D7}) and the chloroquine-resistant lines C6^{7G8} and C4^{Dd2} (in which the wild-type *pfcrt* allele of the "GC03" line has been replaced with the mutant allele from the 7G8 or Dd2 strain, respectively [17]). A PCR error in the generation of the C6^{7G8} line introduced an additional mutation (I351M) [22], which is not found in the sequence of PfCRT^{7G8}. The strains included 3D7 and HB3, which are chloroquine-sensitive parasites that carry $PfCRT^{3D7}$, but express either $PfMDR1^{NYSND}$ or $PfMDR1^{NFSDD}$, respectively. The chloroquine-resistant strain was Dd2, which expresses $PfCRT^{Dd2}$ and $PfMDR1^{FYSND}$ and/or $PfMDR1^{YYSND}$. The parasite cultures were maintained at 4% hematocrit and synchronized with 5% (w/v) sorbitol [114]. The *pfcrt* transfectant lines were maintained in the presence of the selection agents blasticidin (5 μM; Sigma-Aldrich, catalog no. 30891) and WR99210 (5 nM; MedChemExpress, catalog no. HY-116387). These selection agents were not present during the experiments.

Two cell line authentication methods were used to verify the identities of the 6 parasite cultures. The first evaluated the chloroquine resistance phenotype of each culture by performing proliferation assays, thereby yielding chloroquine IC_{50}s for each parasite line or strain. The results were verified by comparing them to previously published data [9,10,20,21] (see the *P. falciparum* proliferation assays section for details). Mycoplasma detection assays were also performed periodically on each of the 6 parasite cultures via PCR with a primer mix that amplifies ribosomal DNA from various mycoplasma strains [115]. No mycoplasma infections were detected in any of the parasite cultures throughout the course of this study.

P. falciparum H^+-efflux assays

Parasite cultures were enriched for trophozoite-stage parasites by magnetic separation and were cultured with uninfected erythrocytes loaded with the membrane-impermeant pH-sensitive fluorescent indicator fluorescein-dextran (10,000 MW; Life Technologies, catalog no. D1821). This dye is taken up into the parasite's DV as they grow inside the erythrocyte. Following a complete asexual cycle (approximately 48 hours) mature trophozoite-stage parasites were isolated from erythrocytes using 0.05% (w/v) saponin and suspended in a saline solution (125 mM NaCl, 5 mM KCl, 1 mM $MgCl_2$, 20 mM glucose, and 25 mM HEPES; pH 7.1) at a density of 1×10^7 cells/mL. The fluorometry experiments were performed as outlined previously [21]. Briefly, the pH of the DV was monitored at 37˚C using a Cary Eclipse fluorescence spectrophotometer (Agilent Technologies, California, USA) (excitation wavelengths 490 nm and 450 nm; emission wavelength 520 nm). The drugs were added to the parasite suspension (2.5 μM of either chloroquine, saquinavir, mefloquine, or lumefantrine), and the solution was incubated for 4 minutes (chloroquine, saquinavir, and mefloquine) or 8 minutes (lumefantrine) to allow the drugs to accumulate to a high concentration within the DV. This was followed by the addition of the V-type H^+-ATPase inhibitor concanamycin A (100 nM; Sigma-Aldrich, catalog no. 27689). Half-times for the rate of DV alkalinization were determined in GraphPad Prism Version 8 by a least squares fit of the equation $F = F_0 + F_{max}/[1 + (t/t_{1/2})^c]$ where F is the fluorescence ratio, F_0 is the initial fluorescence ratio (averaged over 20 seconds immediately prior to opening the chamber of the fluorometer and adding concanamycin A), t is time, $t_{1/2}$ is the half-time for DV alkalinization, F_{max} is the maximal change in fluorescence ratio, and *c* is a fitted constant [20]. The rate of PfCRT-mediated DV alkalinization was calculated by subtracting the rate of DV alkalinization of the solvent control from that of each treatment within each parasite line. In all cases, 4 independent experiments were performed on different days.

P. falciparum proliferation assays

The parasite proliferation assays were performed in clear 96-well plates using a fluorescent DNA-intercalating dye as described previously [116,117]. Briefly, synchronous ring-stage parasite cultures (approximately 1% hematocrit and 1% parasitemia) were incubated with increasing concentrations of quinine or chloroquine for 72 hours at 37˚C and under reduced O_2 conditions. The assay was terminated by freezing and thawing the samples, after which 100 μL from each well was transferred to another 96-well plate. This was followed by the addition of 100 μL of SYBR Safe DNA Gel Stain (0.2 μL/mL; Molecular Probes, catalog no. S33102) in a lysis buffer (20 mM Tris-HCl, 5 mM EDTA, 0.008% (w/v) saponin, and 0.08% (v/v) Triton X-100; pH 7.5) to each well. Fluorescence was measured using a Tecan Infinite M1000 PRO microplate reader (excitation wavelength 490 nm; emission wavelength 520 nm). For each 96-well plate, the fluorescence values for the wells containing the highest concentration of the compound were averaged, and this value was then subtracted from the fluorescence values obtained for each well. The level of parasite proliferation in the presence of each compound concentration was expressed as a percentage of the proliferation measured in the absence of the compound. The IC_{50}s were determined in GraphPad Prism Version 8 by a least squares fit of the equation $y = a/[1 + ([\text{compound}]/IC_{50})^c]$ to the data, where y is the percent parasite proliferation, *a* is the maximum change in the percent parasite proliferation, and *c* is a fitted constant. In all cases, 4 independent experiments were performed (on different days), and within each experiment, measurements were averaged from 3 replicates.

Construction of the MDR1 alignment and generation of the PfMDR1 homology model

Proteins belonging to the MDR1 family were retrieved from the NCBI database using a Basic Local Alignment Search Tool (BLAST) search with PfMDR1 (PF3D7_0523000) as the query sequence. A representative selection of 61 of these proteins, including those for which structures have been determined, were aligned using the ClustalW program [118], and the resulting alignment was manually edited in MacVector Version 12.7.5. Generating an alignment that includes a large number of related proteins is likely to enhance confidence in the alignment of PfMDR1 to a template structure compared with using a simple pairwise alignment. Using this large multiple sequence alignment, we identified 2 proteins related to PfMDR1 with known structures and significant sequence identity: *C. elegans* P-gp in the inward-open state [68] (PDB accession code 4F4C, 32.6% sequence identity) and human P-gp in the outward-open state [69] (PDB accession code 6C0V, 33.2% sequence identity). Using the automodel protocol of MODELLER Version 9.17 [119], 100 models of PfMDR1 were built from each template, and the best model was chosen according to the lowest discrete optimized protein energy (DOPE) [120] value calculated by MODELLER Version 9.17. Molecular figures were made using the Visual Molecular Dynamics (VMD) modeling program [121].

Molecular dynamics simulations of quinine in the binding pocket of the inward open PfMDR1 homology model were conducted using the NAMD Version 2.13 simulation code [122]. First, CGENFF force field [123] parameters for quinine were generated using the automated ParamChem CGENFF tool [124,125]. Seven independent simulations were conducted, with random starting positions and orientations of quinine within the large aqueous cavity of PfMDR1. Within the structure of PfMDR1, atoms further than 17 Å from the center of the binding pocket (defined by the midpoint of the backbones of L327 and F1072 that are on opposing sides of the cavity) were harmonically restrained while atoms within this range were not restrained. Protein restraints were decreased from 1 kcal/mol/$Å^2$ to 0.001 kcal/mol/$Å^2$ over 8 steps (values were 1, 0.5, 0.2, 0.1, 0.05, 0.02, 0.01, and 0.001) with the system energy minimized for 100 steps before 100 ps of dynamics at each step. Once this equilibration phase was complete, simulations were continued for 30 ns with the final harmonic restraint on the protein maintained. The central cavity of PfMDR1 was solvated with TIP3P water molecules that were restrained to stay within a sphere (radius of 20 Å) at the center of the binding pocket, using a spherical harmonic boundary potential applied to the water molecule's oxygen atoms with a force constant of 20 kcal/mol/$Å^2$. The CHARMM36 force field with CMAP correction [126] was used for the protein, and the simulations were performed at a temperature of 300 K using a Langevin thermostat. All bonds to hydrogen were kept fixed, allowing the use of 2 fs timesteps.

Correlations between in vitro drug resistance indices and the rate of drug transport via PfMDR1

IC_{50}s for lumefantrine, mefloquine, chloroquine, and quinine were collated from the relevant literature (see S3 Table for references). The inclusion criteria that were applied to previously published studies were: (1) that an IC_{50} for one or more of the parasite strains of interest (i.e., HB3, Dd2, K1, GB4, or 7G8) be reported, and (2) that the IC_{50} for the 3D7 control strain be performed pairwise. For lumefantrine, mefloquine, and quinine, 4 to 10 studies fitted these criteria and were thus incorporated into the analyses. Several of the studies that measured chloroquine IC_{50}s did not include pairwise measurements with the 3D7; instead, pairwise measurements with either HB3 or GC03 parasites were made (both of these strains express $PfCRT^{3D7}$ and $PfMDR1^{NFSDD}$, and their chloroquine IC_{50}s are typically very similar to 3D7 in pairwise studies). Since these studies measured chloroquine IC_{50}s for infrequently investigated parasite strains such as GB4, it was important to include them in our analyses. Therefore, the inclusion criteria for the chloroquine studies were altered to include those that had measured chloroquine IC_{50}s in either HB3 or GC03 parasites as the control strains, regardless of whether the 3D7 strain was included. The in vitro resistance indices for each study were calculated by dividing the IC_{50} of each strain by the IC_{50} of the control strain (3D7 for lumefantrine, mefloquine, and quinine; HB3 or GC03 for chloroquine). The indices across multiple studies were then averaged and the standard error of the mean calculated (or the range/2 for resistance indices that were calculated from only 2 studies). For each drug, the resistance indices were plotted against the experimentally determined transport activities of the PfMDR1 isoforms in *Xenopus* oocytes (S1 Data).

Quantification and statistical analyses

The statistical tests, data collection, and analyses were performed using ImageJ Version 1.8.0, GraphPad Prism Version 8, Leica Application Suite Advanced Fluorescence software Version 3.6, Leica Application Suite software Version 4.12, Image Lab version 6.0.1 software (Bio-Rad), MODELLER Version 9.17, VMD, NAMD Version 2.13, and MarvinSketch software Version 18.10. Statistical comparisons were made using 1-way ANOVAs in conjunction with Tukey multiple comparisons test. All errors cited in the text and shown in the figures represent the SEM or the range/2. Where not shown, error bars fall within the symbols. Significance was defined as $P < 0.05$. The key statistical details for each dataset are included in the figure legends.

Supporting information

S1 Fig. PfNT1 transports [^{3}H]hypoxanthine when expressed in *Xenopus* oocytes. Oocytes expressing PfNT1 were used as a negative control in the experiments measuring [^{3}H]drug efflux from oocytes expressing human P-gp or PfMDR1 and in the experiments measuring [^{3}H]lumefantrine or [^{3}H]VDPVNF efflux from oocytes expressing PfCRT. This control demonstrated that the heterologous expression of a transporter in *Xenopus* oocytes does not affect the ability of the oocyte membrane to reseal following the microinjection of a [^{3}H]drug or [^{3}H]VDPVNF. To confirm that PfNT1 was expressed and functional at the oocyte plasma membrane, the uptake of hypoxanthine (a known substrate of PfNT1) was measured in oocytes expressing the transporter, as well as in nonexpressing (ne) oocytes. The low level of [^{3}H]hypoxanthine accumulation in ne is due to the simple diffusion of the unprotonated species. The data are the mean of $n = 4$ independent experiments, each yielding similar results

and overlaid as individual data points, and the error is the SEM. The asterisks denote a significant difference from ne; $^{***}P < 0.001$ (1-way ANOVA). The data underlying this figure is supplied in S3 Data. ne, nonexpressing oocytes; PfCRT, *Plasmodium falciparum* chloroquine resistance transporter; PfNT1, *Plasmodium falciparum* nucleoside transporter 1; PfMDR1, *Plasmodium falciparum* multidrug resistance protein 1; P-gp, P-glycoprotein.
(TIF)

S2 Fig. Known inhibitors of human P-gp inhibit the transport of lumefantrine via PfMDR1. (a) Schematic showing the *cis*-inhibition of [^{3}H]drug transport via human P-gp or PfMDR1 by known P-gp inhibitors in the *Xenopus* oocyte system. **(b)** The IC_{50} values of nicardipine, PSC833, vanadate, and verapamil against [^{3}H]vinblastine transport via human P-gp and [^{3}H]lumefantrine transport via PfMDR1. The data are the mean of $n = 4$ independent experiments, and the error is the SEM. The data underlying this figure is supplied in S3 Data. PfMDR1, *Plasmodium falciparum* multidrug resistance protein 1; P-gp, P-glycoprotein.
(TIF)

S3 Fig. Predicted topologies of PfMDR1 and PfCRT. (a) PfMDR1 consists of 1,419 amino acid residues that are arranged into 12 TMDs and 2 NBDs. The length of the loops shown surrounding the NBDs are approximate. **(b)** PfCRT consists of 424 amino acid residues that are arranged into 10 TMDs. All loops are representative of the true loop length. The positions of the mutations in the isoforms of PfMDR1 and PfCRT used in this study are indicated by pink circles and the box attached to each polymorphic residue lists the (non-wild type) amino acid (s) that occur at that position. NBD, nucleotide-binding domain; PfCRT, *Plasmodium falciparum* chloroquine resistance transporter; PfMDR1, *Plasmodium falciparum* multidrug resistance protein 1; TMD, transmembrane domain.
(TIF)

S4 Fig. PfMDR1 is expressed at the oocyte surface and is orientated with its termini in the cytosol. (a) Immunofluorescence microscopy images confirmed that the expression of each of the 3xHA-tagged PfMDR1 isoforms resulted in a fluorescent band external to the pigment layer, indicating that the proteins were expressed in the oocyte plasma membrane. The band was not present in ne. Oocytes expressing a HA-tagged version of the *Apis mellifera* dopamine transporter (HA_{EL2}-AmDAT) at the plasma membrane serve as a positive control [113]. The length of the scale bar is 50 μm. The images are representative of at least 2 independent experiments (performed using oocytes from different frogs), within which images were obtained from a minimum of 3 oocytes per oocyte type. **(b)** Immunofluorescence microscopy was used to determine the orientation of PfMDR1 in the plasma membrane of live oocytes using an anti-HA antibody and a fluorescent secondary antibody. The anti-HA antibody will bind to extracellular HA-tags and cannot access those that are intracellular. Hence, only proteins with extracellular HA-tags will be detected by the anti-HA antibody. The fluorescent signal in oocytes expressing HA_{EL2}-AmDAT is at its strongest at the periphery of the oocyte, indicating that AmDAT is orientated in the oocyte membrane such that the HA-tagged loop is extracellular. There was no fluorescent signal in the ne (the negative control) or in oocytes expressing 3xHA-PfMDR1^{NYSND} or PfMDR1^{NYSND}-3xHA (see S1 Text). This indicates that the amino terminus and carboxyl terminus of PfMDR1 are located in the cytosol of the oocyte. The length of the scale bar is 1 mm. The images are representative of 3 independent experiments, within which images were obtained from a minimum of 3 oocytes per oocyte type. HA, hemagglutinin; ne, nonexpressing oocytes; PfMDR1, *Plasmodium falciparum* multidrug resistance protein 1.
(TIFF)

S5 Fig. Measurement of protein levels and [^{3}H]lumefantrine transport activities of HA-tagged PfMDR1 isoforms in *Xenopus* oocytes. (a) Analysis of the PfMDR1 levels in different dilutions of a membrane protein preparation from 3xHA-PfMDR1^{NYSND}-expressing oocytes revealed a sigmoidal relationship between the relative quantity of membrane protein and the intensity of the corresponding PfMDR1 band (r^2 = 0.99). **(b)** A sigmoidal relationship was observed between the intensity of the 3xHA-PfMDR1^{NYSND} protein band and the amount of 3xHA-PfMDR1^{NYSND} cRNA microinjected into oocytes (r^2 = 0.99). The relationship is approximately linear between 2.5 and 10 ng of cRNA. **(c)** A sigmoidal relationship was observed between the level of [^{3}H]lumefantrine transport and the quantity of 3xHA-PfMDR1-^{NYSND} cRNA microinjected into the oocyte (r^2 = 0.99). This relationship is linear between 1 and 10 ng of cRNA, with [^{3}H]lumefantrine transport saturating above this range. **(d)** Combining the plots in panels **b** and **c** revealed that in oocytes microinjected with 2.5 to 10 ng of 3xHA-PfMDR1^{3D7} cRNA, the intensity of the 3xHA-PfMDR1^{NYSND} protein band strongly correlates with the level of 3xHA-PfMDR1^{NYSND}-mediated [^{3}H]lumefantrine transport (r^2 = 0.9904). **(e)** Semiquantification of PfMDR1 protein levels in the membranes of oocytes expressing either 3xHA-PfMDR1^{NYSND}, PfMDR1^{NYSND}-2xHA, or PfMDR1^{NYSND}-3xHA revealed that, relative to 3xHA-PfMDR1^{NYSND}, the addition of HA-tags to the carboxyl terminus of the protein significantly reduced PfMDR1 levels. **(f)** Oocytes expressing PfMDR1^{NYSND}-2xHA or PfMDR1^{NYSND}-3xHA also displayed significantly lower levels of [^{3}H]lumefantrine transport relative to those expressing 3xHA-PfMDR1^{NYSND}. **(g)** Densitometric analyses of total protein indicated that there were no significant differences between sample lanes in the western blot experiments that gave rise to Fig 1G. In each experiment, the protein on the nitrocellulose membrane was stained with Ponceau S and the intensity between 70 and 180 kDa was measured within each lane. **(h)** 3xHA-PfMDR1^{NYSND} and 3xHA-PfMDR1^{NFCDY} had slightly reduced lumefantrine transport activities relative to the respective untagged proteins. The data are the mean of 4 to 9 independent experiments (each yielding similar results and overlaid as individual data points in panels **e**–**h**), and the error is the SEM. Where not visible, the error bars fall within the symbols. The asterisks denote a significant difference from the 3xHA-PfMDR1^{NYSND} control or the PfMDR1^{NYSND} control; $^*P < 0.05$, $^{***}P < 0.001$, ns, not significant (1-way ANOVA). The data underlying this figure is supplied in S3 Data. ne, nonexpressing oocytes; PfMDR1, *Plasmodium falciparum* multidrug resistance protein 1.
(TIFF)

S6 Fig. Interaction between quinine and the 1042D residue in PfMDR1^{NFSDD}. The movement of the quinine molecule during the 7 molecular dynamics simulations is indicated by the distance between the protonated cyclic amine ring of quinine and the carboxylate oxygen atom on the 1042D side chain over the duration of the simulation. Seven simulations were performed, each represented by a different colored line. Quinine moves close to D1042 in 4 of the 7 simulations (denoted by the yellow, blue, navy, and green lines), forming stable, long-lasting hydrogen bonds in 2 of these simulations (denoted by the navy and green lines). PfMDR1, *Plasmodium falciparum* multidrug resistance protein 1.
(TIF)

S7 Fig. Transport of lumefantrine and mefloquine via PfCRT in *Xenopus* oocytes. (a, c) The transport of [^{3}H]lumefantrine (a) and [^{3}H]mefloquine (c) via PfCRT^{Dd2} was approximately linear with time for at least 2 hours. **(b, d)** The transport of [^{3}H]lumefantrine (b) and [^{3}H]mefloquine (d) via PfCRT^{Dd2} and PfCRT^{7G8} was reduced by known inhibitors of the transporter (verapamil, chlorpheniramine, and saquinavir) and was unaffected by histidine and LH (metabolites that do not interact with PfCRT). The data are the mean of n = 4

independent experiments, each yielding similar results and overlaid as individual data points in panels **b** and **d**, and the error is the SEM. Where not visible, the error bars fall within the symbols. The asterisks denote a significant difference from the PfCRT^{Dd2} control (red asterisks) or the PfCRT^{7G8} control (orange asterisks): $^{**}P < 0.01$, $^{***}P < 0.001$ (1-way ANOVA). The data underlying this figure is supplied in S3 Data. PfCRT, *Plasmodium falciparum* chloroquine resistance transporter.
(TIF)

S8 Fig. Structures of a subset of compounds used in this study. The pK_a values for the protonatable nitrogen(s) within each compound are indicated. The structures and pK_a values were collated from the literature [127] or generated in the MarvinSketch software (ChemAxon). pK_a, the negative logarithm to the base 10 of the acid dissociation constant.
(TIF)

S9 Fig. Direction of drug transport via PfMDR1 and PfCRT in situ versus in *Xenopus* oocytes. PfMDR1 orientates in the DV membrane such that its amino terminus and carboxyl terminus, as well as its NBDs, are located in the parasite cytosol [36]. It was expected that PfMDR1 would adopt the same orientation in the oocyte plasma membrane (i.e., with its termini and NBDs extending into the oocyte cytosol) due to the "positive inside rule" [128,129]. This orientation was confirmed using immunofluorescence microscopy and live oocytes expressing HA-tagged versions of PfMDR1 (S4 Fig). PfCRT also orientates in the DV membrane with its amino terminus and carboxyl terminus in the parasite cytosol [130] and is predicted, on the basis of the "positive inside rule," to adopt the same orientation in the oocyte plasma membrane (i.e., with its amino terminus and carboxyl terminus in the oocyte cytosol). **(a)** In the malaria parasite, PfMDR1 mediates the transport of drugs from the parasite cytosol (pH approximately 7.3) into the acidic environment of the DV (pH 5.0 to 5.5), where the weak base drugs will become protonated [94]. In the *Xenopus* oocyte system, the drug under study is microinjected into the oocyte cytosol (pH approximately 7.2) and is transported via PfMDR1 into the extracellular solution (pH 5.5). Thus, in both cases, the direction of PfMDR1-mediated drug transport is from the cell cytosol into the acidic DV lumen or the acidic extracellular solution. **(b)** Weak base drugs also accumulate in the parasite DV via simple diffusion of the neutral species, which becomes protonated upon entering the acidic lumen of this organelle. In parasites that express chloroquine resistance-conferring isoforms of PfCRT, the transporter mediates the transport of the protonated drug from the DV into the parasite cytosol. In the *Xenopus* oocyte expression system, the drug under study is typically added to the acidic extracellular solution and mutant isoforms of PfCRT transport the protonated drug into the oocyte cytosol. Therefore, in both scenarios, the direction of PfCRT-mediated drug transport is from the acidic DV lumen/acidic extracellular solution into the cell cytosol. That said, in the case of lumefantrine, the drug was microinjected into the oocyte and its transport from the cytosol into the extracellular solution was measured. This modified protocol was used because lumefantrine transport via PfCRT appears to be reliant on the (as yet unidentified) second cosubstrate of the transporter [10]. The endogenous substrates of PfCRT, such as the hemoglobin-derived hexapeptide VDPVNF, are translocated with H^+ and a second cosubstrate that is naturally present within the oocyte cytosol [10]. It should be noted, however, that PfCRT is a carrier [6,10,131], which means it can mediate the transport of a substrate in either direction across the membrane (assuming the necessary cosubstrates are present), with the net direction of transport determined by the prevailing electrochemical gradients of the substrates. In the parasite DV, these gradients will result in lumefantrine being cotransported with H^+ (and the unidentified second cosubstrate) from the DV lumen into the parasite cytosol. DV, digestive vacuole; NBD, nucleotide-binding domain; PfCRT, *Plasmodium falciparum* chloroquine

resistance transporter; PfMDR1, *Plasmodium falciparum* multidrug resistance protein 1.
(TIF)

S10 Fig. Iron chelator IV does not affect drug transport via PfMDR1. Measurements of [^{3}H]dihydroartemisinin transport via PfMDR1 were made in the presence of the iron chelator IV to bind any free iron present in the oocyte. Free iron could activate dihydroartemisinin, thereby damaging the oocytes and interfering with measurements of transport. The effect of iron chelator IV (estimated intracellular concentration of 1 mM) on [^{3}H]lumefantrine transport was measured in ne and oocytes expressing either PfNT1, PfMDR1^{NYSND}, or PfMDR1^{NFCDY}. The data are the mean of $n = 4$ independent experiments (each yielding similar results and overlaid as individual data points), and the error is the SEM. Where not visible, the error bars fall within the symbols. Statistical analyses were performed relative to the PfMDR1^{NYSND} control (blue) or the PfMDR1^{NFCDY} (dark pink) control; ns, not significant (1-way ANOVA). The data underlying this figure is supplied in S3 Data. ne, nonexpressing oocytes; PfMDR1, *Plasmodium falciparum* multidrug resistance protein 1; PfNT1, *Plasmodium falciparum* nucleoside transporter 1.
(TIF)

S1 Table. Amino acid mutations in the PfMDR1 isoforms included for study. PfMDR1, *Plasmodium falciparum* multidrug resistance protein 1.
(PDF)

S2 Table. Amino acid mutations in the PfCRT isoforms included for study. PfCRT, *Plasmodium falciparum* chloroquine resistance transporter.
(PDF)

S3 Table. In vitro resistance indices of *P. falciparum* strains for lumefantrine, mefloquine, chloroquine, and quinine.
(PDF)

S4 Table. Generation of PfMDR1 coding sequences for expression in *Xenopus* oocytes. PfMDR1, *Plasmodium falciparum* multidrug resistance protein 1.
(PDF)

S1 Text. Effects of amino-terminal or carboxyl-terminal epitope tags on the expression and function of PfMDR1 in *Xenopus* oocytes. PfMDR1, *Plasmodium falciparum* multidrug resistance protein 1.
(PDF)

S2 Text. Direct measurement of the transport of fluorescent compounds via PfMDR1. PfMDR1, *Plasmodium falciparum* multidrug resistance protein 1.
(PDF)

S3 Text. Roles of PfMDR1 in modulating the parasite's response to a range of antimalarial drugs. PfMDR1, *Plasmodium falciparum* multidrug resistance protein 1.
(PDF)

S4 Text. Quinine resistance in the malaria parasite is a multifactorial phenomenon.
(PDF)

S1 File. Alignment of MDR1 proteins used to generate the PfMDR1 homology model. PfMDR1, *Plasmodium falciparum* multidrug resistance protein 1.
(PDF)

S1 Data. Rates of PfMDR1-mediated drug transport. PfMDR1, *Plasmodium falciparum* multidrug resistance protein 1.
(XLSX)

S2 Data. Protonated drug proportions.
(XLSX)

S3 Data. Source data file containing the underlying data presented in Figs 1–6, Table 1, and S1, S2, S5, S7, and S10 Figs.
(XLSX)

Acknowledgments

We thank Prof. David Fidock for providing the transfectant *P. falciparum* lines, Jamie Robertson for generating the PfMDR1^{FYSND} construct, Prof. Richard Callaghan for helpful discussions regarding the manuscript, the Canberra Branch of the Australian Red Cross Service for the provision of blood, the Imaging and Cytometry facility (Australian National University) for facilities and technical assistance, and Microscopy Australia at the Centre for Advanced Microscopy (funded by the Australian National University and the Federal Government) for facilities as well as scientific and technical assistance.

Author Contributions

Conceptualization: Sarah Heckmatt Shafik, Sashika Natasha Richards, Rowena Elizabeth Martin.

Formal analysis: Sarah Heckmatt Shafik, Sashika Natasha Richards, Ben Corry, Rowena Elizabeth Martin.

Funding acquisition: Rowena Elizabeth Martin.

Investigation: Sarah Heckmatt Shafik, Sashika Natasha Richards, Ben Corry, Rowena Elizabeth Martin.

Methodology: Sarah Heckmatt Shafik, Sashika Natasha Richards, Ben Corry, Rowena Elizabeth Martin.

Project administration: Rowena Elizabeth Martin.

Resources: Sarah Heckmatt Shafik, Sashika Natasha Richards, Ben Corry.

Supervision: Rowena Elizabeth Martin.

Visualization: Sarah Heckmatt Shafik, Sashika Natasha Richards, Ben Corry, Rowena Elizabeth Martin.

Writing – original draft: Sarah Heckmatt Shafik, Sashika Natasha Richards, Ben Corry, Rowena Elizabeth Martin.

Writing – review & editing: Sarah Heckmatt Shafik, Sashika Natasha Richards, Ben Corry, Rowena Elizabeth Martin.

References

1. Martin RE. The transportome of the malaria parasite. Biol Rev. 2020; 95:305–32. https://doi.org/10.1111/brv.12565 PMID: 31701663
2. Sisowath C, Petersen I, Veiga MI, Martensson A, Premji Z, Bjorkman A, et al. *In vivo* selection of *Plasmodium falciparum* parasites carrying the chloroquine-susceptible *pfcrt* K76 allele after treatment with

artemether-lumefantrine in Africa. J Infect Dis. 2009; 199:750–7. https://doi.org/10.1086/596738 PMID: 19210165

3. Otienoburu SD, Maiga-Ascofare O, Schramm B, Jullien V, Jones JJ, Zolia YM, et al. Selection of *Plasmodium falciparum pfcrt* and *pfmdr1* polymorphisms after treatment with artesunate-amodiaquine fixed dose combination or artemether-lumefantrine in Liberia. Malar J. 2016; 15:452. https://doi.org/10.1186/s12936-016-1503-3 PMID: 27596849
4. Sisowath C, Strömberg J, Mårtensson A, Msellem M, Obondo C, Björkman A, et al. *In vivo* selection of *Plasmodium falciparum pfmdr1* 86N coding alleles by artemether-lumefantrine (Coartem). J Infect Dis. 2005; 191:1014–7. https://doi.org/10.1086/427997 PMID: 15717281
5. Zhang M, Wang C, Otto TD, Oberstaller J, Liao X, Adapa SR, et al. Uncovering the essential genes of the human malaria parasite *Plasmodium falciparum* by saturation mutagenesis. Science (New York, NY). 2018; 360: eaap7847. https://doi.org/10.1126/science.aap7847 PMID: 29724925
6. Martin RE, Marchetti RV, Cowan AI, Howitt SM, Broer S, Kirk K. Chloroquine transport via the malaria parasite's chloroquine resistance transporter. Science (New York, NY). 2009; 325:1680–2. https://doi.org/10.1126/science.1175667 PMID: 19779197
7. Summers RL, Dave A, Dolstra TJ, Bellanca S, Marchetti RV, Nash MN, et al. Diverse mutational pathways converge on saturable chloroquine transport via the malaria parasite's chloroquine resistance transporter. Proc Natl Acad Sci U S A. 2014; 111:E1759–67. https://doi.org/10.1073/pnas.1322965111 PMID: 24728833
8. van Schalkwyk DA, Nash MN, Shafik SH, Summers RL, Lehane AM, Smith PJ, et al. Verapamil-sensitive transport of quinacrine and methylene blue via the *Plasmodium falciparum* chloroquine resistance transporter reduces the parasite's susceptibility to these tricyclic drugs. J Infect Dis. 2016; 213:800–10. https://doi.org/10.1093/infdis/jiv509 PMID: 26503982
9. Richards SN, Nash MN, Baker ES, Webster MW, Lehane AM, Shafik SH, et al. Molecular mechanisms for drug hypersensitivity induced by the malaria parasite's chloroquine resistance transporter. PLoS Pathog. 2016; 12:e1005725. https://doi.org/10.1371/journal.ppat.1005725 PMID: 27441371
10. Shafik SH, Cobbold SA, Barkat K, Richards SN, Lancaster NS, Llinás M, et al. The natural function of the malaria parasite's chloroquine resistance transporter. Nat Commun. 2020; 11:3922. https://doi.org/10.1038/s41467-020-17781-6 PMID: 32764664
11. Papakrivos J, Sa JM, Wellems TE. Functional characterization of the *Plasmodium falciparum* chloroquine-resistance transporter (PfCRT) in transformed *Dictyostelium discoideum* vesicles. PLoS ONE. 2012; 7:e39569. https://doi.org/10.1371/journal.pone.0039569 PMID: 22724026
12. Callaghan PS, Siriwardana A, Hassett MR, Roepe PD. *Plasmodium falciparum* chloroquine resistance transporter (PfCRT) isoforms PH1 and PH2 perturb vacuolar physiology. Malar J. 2016; 15:186. https://doi.org/10.1186/s12936-016-1238-1 PMID: 27036417
13. Callaghan PS, Hassett MR, Roepe PD. Functional comparison of 45 naturally occurring isoforms of the *Plasmodium falciparum* chloroquine resistance transporter (PfCRT). Biochemistry. 2015; 54:5083–94. https://doi.org/10.1021/acs.biochem.5b00412 PMID: 26208441
14. Baro NK, Pooput C, Roepe PD. Analysis of chloroquine resistance transporter (CRT) isoforms and orthologues in *S. cerevisiae* yeast. Biochemistry. 2011; 50:6701–10. https://doi.org/10.1021/bi200922g PMID: 21744797
15. Summers RL, Nash MN, Martin RE. Know your enemy: understanding the role of PfCRT in drug resistance could lead to new antimalarial tactics. Cell Mol Life Sci. 2012; 69:1967–95. https://doi.org/10.1007/s00018-011-0906-0 PMID: 22286067
16. Fidock DA, Nomura T, Talley AK, Cooper RA, Dzekunov SM, Ferdig MT, et al. Mutations in the *P. falciparum* digestive vacuole transmembrane protein PfCRT and evidence for their role in chloroquine resistance. Mol Cell. 2000; 6:861–71. https://doi.org/10.1016/s1097-2765(05)00077-8 PMID: 11090624
17. Sidhu AB, Verdier-Pinard D, Fidock DA. Chloroquine resistance in *Plasmodium falciparum* malaria parasites conferred by *pfcrt* mutations. Science (New York, NY). 2002; 298:210–3. https://doi.org/10.1126/science.1074045 PMID: 12364805
18. Bellanca S, Summers RL, Meyrath M, Dave A, Nash MN, Dittmer M, et al. Multiple drugs compete for transport via the *Plasmodium falciparum* chloroquine resistance transporter at distinct but interdependent sites. J Biol Chem. 2014; 289:36336–51. https://doi.org/10.1074/jbc.M114.614206 PMID: 25378409
19. Kim J, Tan YZ, Wicht KJ, Erramilli SK, Dhingra SK, Okombo J, et al. Structure and drug resistance of the *Plasmodium falciparum* transporter PfCRT. Nature. 2019; 576:315–20. https://doi.org/10.1038/s41586-019-1795-x PMID: 31776516

20. Lehane AM, Hayward R, Saliba KJ, Kirk K. A verapamil-sensitive chloroquine-associated H^+ leak from the digestive vacuole in chloroquine-resistant malaria parasites. J Cell Sci. 2008; 121:1624–32. https://doi.org/10.1242/jcs.016758 PMID: 18445688

21. Lehane AM, Kirk K. Chloroquine resistance-conferring mutations in *pfcrt* give rise to a chloroquine-associated H^+ leak from the malaria parasite's digestive vacuole. Antimicrob Agents Chemother. 2008; 52:4374–80. https://doi.org/10.1128/AAC.00666-08 PMID: 18852275

22. Lehane AM, Kirk K. Efflux of a range of antimalarial drugs and 'chloroquine resistance reversers' from the digestive vacuole in malaria parasites with mutant PfCRT. Mol Microbiol. 2010; 77:1039–51. https://doi.org/10.1111/j.1365-2958.2010.07272.x PMID: 20598081

23. Duraisingh MT, Jones P, Sambou I, von Seidlein L, Pinder M, Warhurst DC. The tyrosine-86 allele of the *pfmdr1* gene of *Plasmodium falciparum* is associated with increased sensitivity to the anti-malarials mefloquine and artemisinin. Mol Biochem Parasitol. 2000; 108:13–23. https://doi.org/10.1016/s0166-6851(00)00201-2 PMID: 10802315

24. Duraisingh MT, Roper C, Walliker D, Warhurst DC. Increased sensitivity to the antimalarials mefloquine and artemisinin is conferred by mutations in the *pfmdr1* gene of *Plasmodium falciparum*. Mol Microbiol. 2000; 36:955–61. https://doi.org/10.1046/j.1365-2958.2000.01914.x PMID: 10844681

25. Eyase FL, Akala HM, Ingasia L, Cheruiyot A, Omondi A, Okudo C, et al. The role of *Pfmdr1* and *Pfcrt* in changing chloroquine, amodiaquine, mefloquine and lumefantrine susceptibility in western-Kenya *P. falciparum* samples during 2008–2011. PLoS ONE. 2013; 8:e64299. https://doi.org/10.1371/journal.pone.0064299 PMID: 23675533

26. Foote SJ, Kyle DE, Martin RK, Oduola AM, Forsyth K, Kemp DJ, et al. Several alleles of the multidrug-resistance gene are closely linked to chloroquine resistance in *Plasmodium falciparum*. Nature. 1990; 345:255–8. https://doi.org/10.1038/345255a0 PMID: 2185424

27. Nsobya SL, Kiggundu M, Nanyunja S, Joloba M, Greenhouse B, Rosenthal PJ. *In vitro* sensitivities of *Plasmodium falciparum* to different antimalarial drugs in Uganda. Antimicrob Agents Chemother. 2010; 54:1200–6. https://doi.org/10.1128/AAC.01412-09 PMID: 20065051

28. Wurtz N, Fall B, Pascual A, Fall M, Baret E, Camara C, et al. Role of *Pfmdr1* in *in vitro Plasmodium falciparum* susceptibility to chloroquine, quinine, monodesethylamodiaquine, mefloquine, lumefantrine, and dihydroartemisinin. Antimicrob Agents Chemother. 2014; 58:7032–40. https://doi.org/10.1128/AAC.03494-14 PMID: 25199781

29. Sidhu AB, Valderramos SG, Fidock DA. *pfmdr1* mutations contribute to quinine resistance and enhance mefloquine and artemisinin sensitivity in *Plasmodium falciparum*. Mol Microbiol. 2005; 57:913–26. https://doi.org/10.1111/j.1365-2958.2005.04729.x PMID: 16091034

30. Cowman AF, Galatis D, Thompson JK. Selection for mefloquine resistance in *Plasmodium falciparum* is linked to amplification of the *pfmdr1* gene and cross-resistance to halofantrine and quinine. Proc Natl Acad Sci U S A. 1994; 91:1143–7. https://doi.org/10.1073/pnas.91.3.1143 PMID: 8302844

31. Peel SA, Bright P, Yount B, Handy J, Baric RS. A strong association between mefloquine and halofantrine resistance and amplification, overexpression, and mutation in the P-glycoprotein gene homolog (*pfmdr*) of *Plasmodium falciparum in vitro*. Am J Trop Med Hyg. 1994; 51:648–58. https://doi.org/10.4269/ajtmh.1994.51.648 PMID: 7985758

32. Price RN, Uhlemann AC, Brockman A, McGready R, Ashley E, Phaipun L, et al. Mefloquine resistance in *Plasmodium falciparum* and increased *pfmdr1* gene copy number. Lancet (London, England). 2004; 364:438–47. https://doi.org/10.1016/S0140-6736(04)16767-6 PMID: 15288742

33. Sondo P, Derra K, Diallo Nakanabo S, Tarnagda Z, Kazienga A, Zampa O, et al. Artesunate-amodiaquine and artemether-lumefantrine therapies and selection of *Pfcrt* and *Pfmdr1* alleles in Nanoro, Burkina Faso. PLoS ONE. 2016; 11:e0151565. https://doi.org/10.1371/journal.pone.0151565 PMID: 27031231

34. Windle ST, Lane KD, Gadalla NB, Liu A, Mu J, Caleon RL, et al. Evidence for linkage of *pfmdr1*, *pfcrt*, and *pfk13* polymorphisms to lumefantrine and mefloquine susceptibilities in a *Plasmodium falciparum* cross. Int J Parasitol. 2020; 14:208–17.

35. Yeka A, Kigozi R, Conrad MD, Lugemwa M, Okui P, Katureebe C, et al. Artesunate/amodiaquine versus artemether/lumefantrine for the treatment of uncomplicated malaria in Uganda: A randomized trial. J Infect Dis. 2016; 213:1134–42. https://doi.org/10.1093/infdis/jiv551 PMID: 26597254

36. Karcz SR, Galatis D, Cowman AF. Nucleotide binding properties of a P-glycoprotein homologue from *Plasmodium falciparum*. Mol Biochem Parasitol. 1993; 58:269–76. https://doi.org/10.1016/0166-6851(93)90048-3 PMID: 8097560

37. Sanchez CP, Rotmann A, Stein WD, Lanzer M. Polymorphisms within PfMDR1 alter the substrate specificity for anti-malarial drugs in *Plasmodium falciparum*. Mol Microbiol. 2008; 70:786–98. https://doi.org/10.1111/j.1365-2958.2008.06413.x PMID: 18713316

38. van Es HH, Karcz S, Chu F, Cowman AF, Vidal S, Gros P, et al. Expression of the plasmodial *pfmdr1* gene in mammalian cells is associated with increased susceptibility to chloroquine. Mol Cell Biol. 1994; 14:2419–28. https://doi.org/10.1128/mcb.14.4.2419-2428.1994 PMID: 7511206

39. Amoah LE, Lekostaj JK, Roepe PD. Heterologous expression and ATPase activity of mutant versus wild type PfMDR1 protein. Biochemistry. 2007; 46:6060–73. https://doi.org/10.1021/bi7002026 PMID: 17469853

40. Pleeter P, Lekostaj JK, Roepe PD. Purified *Plasmodium falciparum* multi-drug resistance protein (PfMDR 1) binds a high affinity chloroquine analogue. Mol Biochem Parasitol. 2010; 173:158–61. https://doi.org/10.1016/j.molbiopara.2010.05.012 PMID: 20546803

41. Volkman SK, Cowman AF, Wirth DF. Functional complementation of the *ste6* gene of *Saccharomyces cerevisiae* with the *pfmdr1* gene of *Plasmodium falciparum*. Proc Natl Acad Sci U S A. 1995; 92:8921–5. https://doi.org/10.1073/pnas.92.19.8921 PMID: 7568044

42. Ruetz S, Delling U, Brault M, Schurr E, Gros P. The *pfmdr1* gene of *Plasmodium falciparum* confers cellular resistance to antimalarial drugs in yeast cells. Proc Natl Acad Sci U S A. 1996; 93:9942–7. https://doi.org/10.1073/pnas.93.18.9942 PMID: 8790436

43. Shalinsky DR, Jekunen AP, Alcaraz JE, Christen RD, Kim S, Khatibi S, et al. Regulation of initial vinblastine influx by P-glycoprotein. Br J Cancer. 1993; 67:30–6. https://doi.org/10.1038/bjc.1993.6 PMID: 8094005

44. Eytan GD, Regev R, Oren G, Hurwitz CD, Assaraf YG. Efficiency of P-glycoprotein-mediated exclusion of rhodamine dyes from multidrug-resistant cells is determined by their passive transmembrane movement rate. Eur J Biochem. 1997; 15:104–12. https://doi.org/10.1111/j.1432-1033.1997.00104.x PMID: 9310367

45. Senarathna SM, Page-Sharp M, Crowe A. The interactions of P-glycoprotein with antimalarial drugs, including substrate affinity, inhibition and regulation. PLoS ONE. 2016; 11:e0152677. https://doi.org/10.1371/journal.pone.0152677 PMID: 27045516

46. Polli JW, Wring SA, Humphreys JE, Huang L, Morgan JB, Webster LO, et al. Rational use of *in vitro* P-glycoprotein assays in drug discovery. J Pharmacol Exp Ther. 2001; 299:620–8. PMID: 11602674

47. Suzuki T, Fukami T, Tomono K. Possible involvement of cationic-drug sensitive transport systems in the blood-to-brain influx and brain-to-blood efflux of amantadine across the blood-brain barrier. Biopharm Drug Dispos. 2015; 36:126–37. https://doi.org/10.1002/bdd.1926 PMID: 25410756

48. Doan KMM, Humphreys JE, Webster LO, Wring SA, Shampine LJ, Serabjit-Singh CJ, et al. Passive permeability and P-glycoprotein-mediated efflux differentiate central nervous system (CNS) and non-CNS marketed drugs. J Pharmacol Exp Ther. 2002; 303:1029–37. https://doi.org/10.1124/jpet.102.039255 PMID: 12438524

49. Mwai L, Diriye A, Masseno V, Muriithi S, Feltwell T, Musyoki J, et al. Genome wide adaptations of *Plasmodium falciparum* in response to lumefantrine selective drug pressure. PLoS ONE. 2012; 7:e31623. https://doi.org/10.1371/journal.pone.0031623 PMID: 22384044

50. Wong W, Bai XC, Sleebs BE, Triglia T, Brown A, Thompson JK, et al. Mefloquine targets the *Plasmodium falciparum* 80S ribosome to inhibit protein synthesis. Nat Microbiol. 2017; 2:17031. https://doi.org/10.1038/nmicrobiol.2017.31 PMID: 28288098

51. Solomonov I, Osipova M, Feldman Y, Baehtz C, Kjaer K, Robinson IK, et al. Crystal nucleation, growth, and morphology of the synthetic malaria pigment β-hematin and the effect thereon by quinoline additives: The malaria pigment as a target of various antimalarial drugs. J Am Chem Soc. 2007; 129:2615–27. https://doi.org/10.1021/ja0674183 PMID: 17290993

52. Buller R, Peterson ML, Almarsson Ö, Leiserowitz L. Quinoline binding site on malaria pigment crystal: A rational pathway for antimalaria drug design. Cryst Growth Des. 2002; 2:553–62.

53. Bergeron MJ, Boggavarapu R, Meury M, Ucurum Z, Caron L, Isenring P, et al. Frog oocytes to unveil the structure and supramolecular organization of human transport proteins. PLoS ONE. 2011; 6:e21901. https://doi.org/10.1371/journal.pone.0021901 PMID: 21760919

54. Safa AR. Photoaffinity labeling of the multidrug-resistance-related P-glycoprotein with photoactive analogs of verapamil. Proc Natl Acad Sci U S A. 1988; 85:7187–91. https://doi.org/10.1073/pnas.85.19.7187 PMID: 2902625

55. Boesch D, Gavériaux C, Jachez B, Pourtier-Manzanedo A, Bollinger P, Loor F. *In vivo* circumvention of P-glycoprotein-mediated multidrug resistance of tumor cells with SDZ PSC 833. Cancer Res. 1991; 51:4226–33. PMID: 1678313

56. Twentyman PR, Bleehen NM. Resistance modification by PSC-833, a novel non-immunosuppressive cyclosporin. Eur J Cancer. 1991; 27:1639–42. https://doi.org/10.1016/0277-5379(91)90435-g PMID: 1816768

57. Urbatsch IL, Sankaran B, Weber J, Senior AE. P-glycoprotein is stably inhibited by vanadate-induced trapping of nucleotide at a single catalytic site. J Biol Chem. 1995; 270:19383–90. https://doi.org/10.1074/jbc.270.33.19383 PMID: 7642618

58. Urbatsch IL, Beaudet L, Carrier I, Gros P. Mutations in either nucleotide-binding site of P-glycoprotein (Mdr3) prevent vanadate trapping of nucleotide at both sites. Biochemistry. 1998; 37:4592–602. https://doi.org/10.1021/bi9728001 PMID: 9521779

59. Beck WT, Cirtain MC, Glover CJ, Felsted RL, Safa AR. Effects of indole alkaloids on multidrug resistance and labeling of P-glycoprotein by a photoaffinity analog of vinblastine. Biochem Biophys Res Commun. 1988; 153:959–66. https://doi.org/10.1016/s0006-291x(88)81321-4 PMID: 2898941

60. Carter NS, Ben Mamoun C, Liu W, Silva EO, Landfear SM, Goldberg DE, et al. Isolation and functional characterization of the PfNT1 nucleoside transporter gene from *Plasmodium falciparum*. J Biol Chem. 2000; 275:10683–91. https://doi.org/10.1074/jbc.275.14.10683 PMID: 10744765

61. Parker MD, Hyde RJ, Yao SY, McRobert L, Cass CE, Young JD, et al. Identification of a nucleoside/nucleobase transporter from *Plasmodium falciparum*, a novel target for anti-malarial chemotherapy. Biochem J. 2000; 349:67–75. https://doi.org/10.1042/0264-6021:3490067 PMID: 10861212

62. Urbatsch IL, Gimi K, Wilke-Mounts S, Senior AE. Investigation of the role of glutamine-471 and glutamine-1114 in the two catalytic sites of P-glycoprotein. Biochemistry. 2000; 39:11921–7. https://doi.org/10.1021/bi001220s PMID: 11009605

63. Zolnerciks JK, Wooding C, Linton KJ. Evidence for a Sav1866-like architecture for the human multidrug transporter P-glycoprotein. FASEB J. 2007; 21:3937–48. https://doi.org/10.1096/fj.07-8610com PMID: 17627029

64. Zolnerciks JK, Akkaya BG, Snippe M, Chiba P, Seelig A, Linton KJ. The Q loops of the human multidrug resistance transporter ABCB1 are necessary to couple drug binding to the ATP catalytic cycle. FASEB J. 2014; 28:4335–46. https://doi.org/10.1096/fj.13-245639 PMID: 25016028

65. Loo TW, Clarke DM. Attachment of a 'molecular spring' restores drug-stimulated ATPase activity to P-glycoprotein lacking both Q loop glutamines. Biochem Biophys Res Commun. 2017; 483:366–70. https://doi.org/10.1016/j.bbrc.2016.12.137 PMID: 28025146

66. Patel SK, George LB, Prasanth Kumar S, Highland HN, Jasrai YT, Pandya HA, et al. A computational approach towards the understanding of *Plasmodium falciparum* multidrug resistance protein 1. ISRN Bioinform. 2013; 2013:437168. https://doi.org/10.1155/2013/437168 PMID: 25937947

67. Ferreira PE, Holmgren G, Veiga MI, Uhlén P, Kaneko A, Gil JP. PfMDR1: mechanisms of transport modulation by functional polymorphisms. PLoS ONE. 2011; 6:e23875. https://doi.org/10.1371/journal.pone.0023875 PMID: 21912647

68. Jin MS, Oldham ML, Zhang Q, Chen J. Crystal structure of the multidrug transporter P-glycoprotein from *Caenorhabditis elegans*. Nature. 2012; 490:566–9. https://doi.org/10.1038/nature11448 PMID: 23000902

69. Kim Y, Chen J. Molecular structure of human P-glycoprotein in the ATP-bound, outward-facing conformation. Science (New York, NY). 2018; 359:915–9. https://doi.org/10.1126/science.aar7389 PMID: 29371429

70. Reed MB, Saliba KJ, Caruana SR, Kirk K, Cowman AF. Pgh1 modulates sensitivity and resistance to multiple antimalarials in *Plasmodium falciparum*. Nature. 2000; 403:906–9. https://doi.org/10.1038/35002615 PMID: 10706290

71. Johnson DJ, Fidock DA, Mungthin M, Lakshmanan V, Sidhu AB, Bray PG, et al. Evidence for a central role for PfCRT in conferring *Plasmodium falciparum* resistance to diverse antimalarial agents. Mol Cell. 2004; 15:867–77. https://doi.org/10.1016/j.molcel.2004.09.012 PMID: 15383277

72. Lakshmanan V, Bray PG, Verdier-Pinard D, Johnson DJ, Horrocks P, Muhle RA, et al. A critical role for PfCRT K76T in *Plasmodium falciparum* verapamil-reversible chloroquine resistance. EMBO J. 2005; 24:2294–305. https://doi.org/10.1038/sj.emboj.7600681 PMID: 15944738

73. Baniecki ML, Wirth DF, Clardy J. High-throughput *Plasmodium falciparum* growth assay for malaria drug discovery. Antimicrob Agents Chemother. 2007; 51:716–23. https://doi.org/10.1128/AAC.01144-06 PMID: 17116676

74. Van Tyne D, Park DJ, Schaffner SF, Neafsey DE, Angelino E, Cortese JF, et al. Identification and functional validation of the novel antimalarial resistance locus PF10_0355 in *Plasmodium falciparum*. PLoS Genet. 2011; 7:e1001383. https://doi.org/10.1371/journal.pgen.1001383 PMID: 21533027

75. Yuan J, Cheng KC, Johnson RL, Huang R, Pattaradilokrat S, Liu A, et al. Chemical genomic profiling for antimalarial therapies, response signatures, and molecular targets. Science (New York, NY). 2011; 333:724–9.

76. Chugh M, Scheurer C, Sax S, Bilsland E, van Schalkwyk DA, Wicht KJ, et al. Identification and deconvolution of cross-resistance signals from antimalarial compounds using multidrug-resistant

Plasmodium falciparum strains. Antimicrob Agents Chemother. 2015; 59:1110–8. https://doi.org/10.1128/AAC.03265-14 PMID: 25487796

77. Eastman RT, Khine P, Huang R, Thomas CJ, Su XZ. PfCRT and PfMDR1 modulate interactions of artemisinin derivatives and ion channel blockers. Sci Rep. 2016; 6:25379. https://doi.org/10.1038/srep25379 PMID: 27147113
78. Mehlotra RK, Fujioka H, Roepe PD, Janneh O, Ursos LM, Jacobs-Lorena V, et al. Evolution of a unique *Plasmodium falciparum* chloroquine-resistance phenotype in association with *pfcrt* polymorphism in Papua New Guinea and South America. Proc Natl Acad Sci U S A. 2001; 98:12689–94. https://doi.org/10.1073/pnas.221440898 PMID: 11675500
79. Mu J, Ferdig MT, Feng X, Joy DA, Duan J, Furuya T, et al. Multiple transporters associated with malaria parasite responses to chloroquine and quinine. Mol Microbiol. 2003; 49:977–89. https://doi.org/10.1046/j.1365-2958.2003.03627.x PMID: 12890022
80. Sá JM, Twu O, Hayton K, Reyes S, Fay MP, Ringwald P, et al. Geographic patterns of *Plasmodium falciparum* drug resistance distinguished by differential responses to amodiaquine and chloroquine. Proc Natl Acad Sci U S A. 2009; 106:18883–9. https://doi.org/10.1073/pnas.0911317106 PMID: 19884511
81. Mu J, Myers RA, Jiang H, Liu S, Ricklefs S, Waisberg M, et al. *Plasmodium falciparum* genome-wide scans for positive selection, recombination hot spots and resistance to antimalarial drugs. Nat Genet. 2010; 42:268–71. https://doi.org/10.1038/ng.528 PMID: 20101240
82. Valderramos SG, Valderramos JC, Musset L, Purcell LA, Mercereau-Puijalon O, Legrand E, et al. Identification of a mutant PfCRT-mediated chloroquine tolerance phenotype in *Plasmodium falciparum*. PLoS Pathog. 2010; 6:e1000887. https://doi.org/10.1371/journal.ppat.1000887 PMID: 20485514
83. Sanchez CP, Mayer S, Nurhasanah A, Stein WD, Lanzer M. Genetic linkage analyses redefine the roles of PfCRT and PfMDR1 in drug accumulation and susceptibility in *Plasmodium falciparum*. Mol Microbiol. 2011; 82:865–78. https://doi.org/10.1111/j.1365-2958.2011.07855.x PMID: 21999470
84. Griffin CE, Hoke JM, Samarakoon U, Duan J, Mu J, Ferdig MT, et al. Mutation in the *Plasmodium falciparum* CRT protein determines the stereospecific activity of antimalarial cinchona alkaloids. Antimicrob Agents Chemother. 2012; 56:5356–64. https://doi.org/10.1128/AAC.05667-11 PMID: 22869567
85. Reiling SJ, Rohrbach P. Monitoring PfMDR1 transport in *Plasmodium falciparum*. Malar J. 2015; 14:270. https://doi.org/10.1186/s12936-015-0791-3 PMID: 26169590
86. Ross LS, Dhingra SK, Mok S, Yeo T, Wicht KJ, Kumpornsin K, et al. Emerging Southeast Asian PfCRT mutations confer *Plasmodium falciparum* resistance to the first-line antimalarial piperaquine. Nat Commun. 2018; 9:3314. https://doi.org/10.1038/s41467-018-05652-0 PMID: 30115924
87. Friedrich O, Reiling SJ, Wunderlich J, Rohrbach P. Assessment of *Plasmodium falciparum* PfMDR1 transport rates using Fluo-4. J Cell Mol Med. 2014; 18:1851–62. https://doi.org/10.1111/jcmm.12313 PMID: 24889967
88. Preechapornkul P, Imwong M, Chotivanich K, Pongtavornpinyo W, Dondorp AM, Day NP, et al. *Plasmodium falciparum pfmdr1* amplification, mefloquine resistance, and parasite fitness. Antimicrob Agents Chemother. 2009; 53:1509–15. https://doi.org/10.1128/AAC.00241-08 PMID: 19164150
89. Sidhu ABS, Uhlemann A-C, Valderramos SG, Valderramos J-C, Krishna S, Fidock DA. Decreasing *pfmdr1* copy number in *Plasmodium falciparum* malaria heightens susceptibility to mefloquine, lumefantrine, halofantrine, quinine, and artemisinin. J Infect Dis. 2006; 194:528–35. https://doi.org/10.1086/507115 PMID: 16845638
90. Deane KJ, Summers RL, Lehane AM, Martin RE, Barrow RA. Chlorpheniramine analogues reverse chloroquine resistance in *Plasmodium falciparum* by inhibiting PfCRT. ACS Med Chem Lett. 2014; 5:576–81. https://doi.org/10.1021/ml5000228 PMID: 24900883
91. Martin RE, Butterworth AS, Gardiner DL, Kirk K, McCarthy JS, Skinner-Adams TS. Saquinavir inhibits the malaria parasite's chloroquine resistance transporter. Antimicrob Agents Chemother. 2012; 56:2283–9. https://doi.org/10.1128/AAC.00166-12 PMID: 22354298
92. Hrycyna CA, Summers RL, Lehane AM, Pires MM, Namanja H, Bohn K, et al. Quinine dimers are potent inhibitors of the *Plasmodium falciparum* chloroquine resistance transporter and are active against quinoline-resistant *P. falciparum*. ACS Chem Biol. 2014; 9:722–30. https://doi.org/10.1021/cb4008953 PMID: 24369685
93. Cowman AF, Karcz S, Galatis D, Culvenor JG. A P-glycoprotein homologue of *Plasmodium falciparum* is localized on the digestive vacuole. J Cell Biol. 1991; 113:1033–42. https://doi.org/10.1083/jcb.113.5.1033 PMID: 1674943
94. Rohrbach P, Sanchez CP, Hayton K, Friedrich O, Patel J, Sidhu AB, et al. Genetic linkage of *pfmdr1* with food vacuolar solute import in *Plasmodium falciparum*. EMBO J. 2006; 25:3000–11. https://doi.org/10.1038/sj.emboj.7601203 PMID: 16794577

95. Cowell AN, Istvan ES, Lukens AK, Gomez-Lorenzo MG, Vanaerschot M, Sakata-Kato T, et al. Mapping the malaria parasite druggable genome by using *in vitro* evolution and chemogenomics. Science (New York, NY). 2018; 359:191–9. https://doi.org/10.1126/science.aan4472 PMID: 29326268

96. Sullivan DJ Jr, Gluzman IY, Russell DG, Goldberg DE. On the molecular mechanism of chloroquine's antimalarial action. Proc Natl Acad Sci U S A. 1996; 93:11865–70. https://doi.org/10.1073/pnas.93.21.11865 PMID: 8876229

97. Zhang Y, Hempelmann E. Lysis of malarial parasites and erythrocytes by ferriprotoporphyrin IX-chloroquine and the inhibition of this effect by proteins. Biochem Pharmacol. 1987; 36:1267–73. https://doi.org/10.1016/0006-2952(87)90080-3 PMID: 3297071

98. Fitch CD, Chevli R, Banyal HS, Phillips G, Pfaller MA, Krogstad DJ. Lysis of *Plasmodium falciparum* by ferriprotoporphyrin IX and a chloroquine-ferriprotoporphyrin IX complex. Antimicrob Agents Chemother. 1982; 21:819–22. https://doi.org/10.1128/AAC.21.5.819 PMID: 7049079

99. Veiga MI, Dhingra SK, Henrich PP, Straimer J, Gnadig N, Uhlemann AC, et al. Globally prevalent PfMDR1 mutations modulate *Plasmodium falciparum* susceptibility to artemisinin-based combination therapies. Nat Commun. 2016; 7:11553. https://doi.org/10.1038/ncomms11553 PMID: 27189525

100. Martin RE, Shafik SH, Richards SN. Mechanisms of resistance to the partner drugs of artemisinin in the malaria parasite. Curr Opin Pharmacol. 2018; 42:71–80. https://doi.org/10.1016/j.coph.2018.07.010 PMID: 30142480

101. Bohorquez E, Chua M, Meshnick S. Quinine localizes to a non-acidic compartment within the food vacuole of the malaria parasite *Plasmodium falciparum*. Malar J. 2012; 11:350. https://doi.org/10.1186/1475-2875-11-350 PMID: 23088166

102. Calçada C, Silva M, Baptista V, Thathy V, Silva-Pedrosa R, Granja D, et al. Expansion of a specific *Plasmodium falciparum* PfMDR1 haplotype in Southeast Asia with increased substrate transport. MBio. 2020; 11:e02093–20. https://doi.org/10.1128/mBio.02093-20 PMID: 33262257

103. Godfrey EW, Sanders GE. Effect of water hardness on oocyte quality and embryo development in the African clawed frog (*Xenopus laevis*). Comp Med. 2004; 54:170–5. PMID: 15134362

104. Schultz TW, Dawson DA. Housing and husbandry of *Xenopus* for oocyte production. Lab Anim (NY). 2003; 32:34–9. https://doi.org/10.1038/laban0203-34 PMID: 12545183

105. Bröer S, Rahman B, Pellegri G, Pellerin L, Martin JL, Verleysdonk S, et al. Comparison of lactate transport in astroglial cells and monocarboxylate transporter 1 (MCT 1) expressing *Xenopus laevis* oocytes. Expression of two different monocarboxylate transporters in astroglial cells and neurons. J Biol Chem. 1997; 272:30096–102. https://doi.org/10.1074/jbc.272.48.30096 PMID: 9374487

106. Saliba KJ, Martin RE, Bröer A, Henry RI, Siobhan McCarthy C, Downie MJ, et al. Sodium-dependent uptake of inorganic phosphate by the intracellular malaria parasite. Nature. 2006; 443:582–5. https://doi.org/10.1038/nature05149 PMID: 17006451

107. Hayward R, Saliba KJ, Kirk K. The pH of the digestive vacuole of *Plasmodium falciparum* is not associated with chloroquine resistance. J Cell Sci. 2006; 119:1016–25. https://doi.org/10.1242/jcs.02795 PMID: 16492710

108. Klonis N, Tan O, Jackson K, Goldberg D, Klemba M, Tilley L. Evaluation of pH during cytostomal endocytosis and vacuolar catabolism of haemoglobin in *Plasmodium falciparum*. Biochem J. 2007; 407:343–54. https://doi.org/10.1042/BJ20070934 PMID: 17696875

109. Taylor MA, Smith LD. Accumulation of free amino acids in growing *Xenopus laevis* oocytes. Dev Biol. 1987; 124:287–90. https://doi.org/10.1016/0012-1606(87)90480-5 PMID: 2889640

110. Newmeyer DD, Lucocq JM, Bürglin TR, De Robertis EM. Assembly *in vitro* of nuclei active in nuclear protein transport: ATP is required for nucleoplasmin accumulation. EMBO J. 1986; 5:501–10. PMID: 3709518

111. Gribble F, Loussouarn G, Tucker S, Zhao C, Nichols C, Ashcroft F. A novel method for measurement of submembrane ATP concentration. J Biol Chem. 2000; 275:30046–9. https://doi.org/10.1074/jbc.M001010200 PMID: 10866996

112. Schneider CA, Rasband WS, Eliceiri KW. NIH Image to ImageJ: 25 years of image analysis. Nat Methods. 2012; 9:671–5. https://doi.org/10.1038/nmeth.2089 PMID: 22930834

113. Zhang V, Kucharski R, Landers C, Richards SN, Bröer S, Martin RE, et al. Characterization of a dopamine transporter and Its splice variant reveals novel features of dopaminergic regulation in the honey bee. Front Physiol. 2019; 10. https://doi.org/10.3389/fphys.2019.01375 PMID: 31736791

114. Allen RJ, Kirk K. *Plasmodium falciparum* culture: the benefits of shaking. Mol Biochem Parasitol. 2010; 169:63–5. https://doi.org/10.1016/j.molbiopara.2009.09.005 PMID: 19766147

115. Drexler HG, Uphoff CC. Mycoplasma contamination of cell cultures: incidence, sources, effects, detection, elimination, prevention. Cytotechnology. 2002; 39:75–90. https://doi.org/10.1023/A:1022913015916 PMID: 19003295

116. Smilkstein M, Sriwilaijaroen N, Kelly JX, Wilairat P, Riscoe M. Simple and inexpensive fluorescence-based technique for high-throughput antimalarial drug screening. Antimicrob Agents Chemother. 2004; 48:1803–6. https://doi.org/10.1128/AAC.48.5.1803-1806.2004 PMID: 15105138

117. Spry C, Macuamule C, Lin Z, Virga KG, Lee RE, Strauss E, et al. Pantothenamides are potent, on-target inhibitors of *Plasmodium falciparum* growth when serum pantetheinase is inactivated. PLoS ONE. 2013; 8:e54974. https://doi.org/10.1371/journal.pone.0054974 PMID: 23405100

118. Thompson JD, Higgins DG, Gibson TJ. CLUSTAL W: improving the sensitivity of progressive multiple sequence alignment through sequence weighting, position-specific gap penalties and weight matrix choice. Nucleic Acids Res. 1994; 22:4673–80. https://doi.org/10.1093/nar/22.22.4673 PMID: 7984417

119. Sali A, Blundell T. Comparative protein modelling by satisfaction of spatial restraints. Protein Struct Distance Anal. 1994; 64.

120. Shen MY, Sali A. Statistical potential for assessment and prediction of protein structures. Protein Sci. 2006; 15:2507–24. https://doi.org/10.1110/ps.062416606 PMID: 17075131

121. Humphrey W, Dalke A, Schulten K. VMD: Visual molecular dynamics. J Mol Graph. 1996; 14:33–8. https://doi.org/10.1016/0263-7855(96)00018-5 PMID: 8744570

122. Vermaas J, Hardy D, Stone J, Tajkhorshid E, Kohlmeyer A. TopoGromacs: Automated topology conversion from CHARMM to Gromacs within VMD. J Chem Inf Model. 2016; 56. https://doi.org/10.1021/acs.jcim.6b00103 PMID: 27196035

123. Vanommeslaeghe K, Hatcher E, Acharya C, Kundu S, Zhong S, Shim J, et al. CHARMM general force field: A force field for drug-like molecules compatible with the CHARMM all-atom additive biological force fields. J Comput Chem. 2010; 31:671–90. https://doi.org/10.1002/jcc.21367 PMID: 19575467

124. Vanommeslaeghe K, Raman EP, MacKerell AD Jr. Automation of the CHARMM General Force Field (CGenFF) II: assignment of bonded parameters and partial atomic charges. J Chem Inf Model. 2012; 52:3155–68. https://doi.org/10.1021/ci3003649 PMID: 23145473

125. Vanommeslaeghe K, MacKerell AD Jr. Automation of the CHARMM General Force Field (CGenFF) I: bond perception and atom typing. J Chem Inf Model. 2012; 52:3144–54. https://doi.org/10.1021/ci300363c PMID: 23146088

126. Best RB, Zhu X, Shim J, Lopes PE, Mittal J, Feig M, et al. Optimization of the additive CHARMM all-atom protein force field targeting improved sampling of the backbone φ, ψ and side-chain $\chi(1)$ and $\chi(2)$ dihedral angles. J Chem Theory Comput. 2012; 8:3257–73. https://doi.org/10.1021/ct300400x PMID: 23341755

127. Foley M, Tilley L. Quinoline antimalarials: mechanisms of action and resistance and prospects for new agents. Pharmacol Therapeut. 1998; 79:55–87. https://doi.org/10.1016/s0163-7258(98)00012-6 PMID: 9719345

128. vonHeijne G. Control of topology and mode of assembly of a polytopic membrane protein by positively charged residues. Nature. 1989; 341:456–8. https://doi.org/10.1038/341456a0 PMID: 2677744

129. von Heijne G. Membrane-protein topology. Nat Rev Mol Cell Biol. 2006; 7:909–18. https://doi.org/10.1038/nrm2063 PMID: 17139331

130. Kuhn Y, Sanchez CP, Ayoub D, Saridaki T, Van Dorsselaer A, Lanzer M. Trafficking of the phosphoprotein PfCRT to the digestive vacuolar membrane in *Plasmodium falciparum*. Traffic. 2010; 11:236–49. https://doi.org/10.1111/j.1600-0854.2009.01018.x PMID: 20015114

131. Summers RL, Martin RE. Functional characteristics of the malaria parasite's "chloroquine resistance transporter": implications for chemotherapy. Virulence. 2010; 1:304–8. https://doi.org/10.4161/viru.1.4.12012 PMID: 21178460